1-1-2018

Segmented Filamentous Bacteria Critically Regulates Commensal Gut Microbiota Osteoimmune Response Effects During Post-Natal Skeletal Development

Nicole Ann Poulides
Medical University of South Carolina

Segmented Filamentous Bacteria Critically Regulates Commensal Gut Microbiota Osteoimmune Response Effects During Post-Natal Skeletal Development

by

Nicole Ann Poulides

A dissertation submitted to the faculty of the Medical University of South Carolina in partial fulfillment of the requirements for the degree of Masters in Biomedical Sciences in the College of Graduate Studies

Department of Microbiology and Immunology

2018

Approved by:

Chairman, Advisory Committee

Chad Novince

Bei Liu

Caroline Westwater

Chenthamarakshan Vasu

DEDICATION

To my husband, Nick.

To my step-daughter, Amelia.

To my parents, Mike and Lori.

To my sister, Megan.

TABLE OF CONTENTS

LIST OF TABLES

Table

LIST OF FIGURES

Figure

Appendix

ABSTRACT

NICOLE ANN POULIDES. Segmented Filamentous Bacteria Critically Regulates Commensal Gut Microbiota Osteoimmune Response Effects during Post-Natal Skeletal Development. (Under the direction of CHAD NOVINCE).

Problem: The role of individual commensal microbes within the commensal gut microbiota on regulating osteoimmune effects in the growing/developing skeleton is currently unidentified. Discerning a specific commensal gut microbe's impact on osteoimmune processes is important because this knowledge could be employed to optimize skeletal growth in adolescents.

Approach: To investigate this, two specific pathogen free murine models were used because of their one reported microbial difference: murine pathogen free (MPF) mice are colonized by segmented filamentous bacteria (SFB) vs. excluded flora (EF) mice, which are void of SFB. The mice were sacrificed at 9 weeks to investigate SFB's effects on the adolescent skeleton. Micro-CT and histomorphometry were used to investigate tibia bone architecture, osteoclast, and growth plate differences. Nanostring and qRT-PCR were used to investigate gene expression levels of osteoblast, osteoclast, and inflammatory immune response genes. Flow cytometry was used to assess the frequencies of T and B-cells in the mesenteric lymph nodes (mLNs), spleen, and marrow.

Results: Bone mineral density, bone volume per tissue volume, and trabecular number were all decreased in MPF vs. EF mice proximal tibia. The number of osteoclasts per bone perimeter and the osteoclast master regulator *Nfatc1* expression were increased in MPF vs. EF mice. Pattern recognition receptor related genes for the TLR4 signaling

response were increased in MPF vs. EF marrow. There was no difference in the helper T-cell frequencies in the marrow.

Conclusion: The results suggest alterations of gut commensal microbiota, even a single gut microbe, SFB, within health models for the gut commensal microbiota, can lead to decreased trabecular bone area per tissue area, bone volume per tissue volume, bone mineral density, and trabecular number as well as increased osteoclast number per bone perimeter. A healthy microbial composition with SFB can have similar implications in osteoclastogenesis, causing decreases in trabecular parameters as seen in SPF / Conventionalized vs. germfree studies caused by immunomodulation.

CHAPTER 1: INTRODUCTION

1.1 Problem Statement

The commensal gut microbiota is a critical regulator of health and disease, having effects on processes like intestinal function, metabolism, behavior, and skeletogenesis [1]. Important to this proposal, the gut microbiota regulates osteoimmune processes during normal skeletal growth/development [1]. Studies utilizing the specific pathogen free (SPF) vs. germfree (GF) mouse model have discerned that the commensal gut microbiota suppresses osteoblastogenesis and enhances osteoclastogenesis, which impairs skeletal bone mass [2-4]. The commensal gut microbiota suppresses the bone marrow stromal cell (BMSC) potential to differentiate / function as osteoblastic cells, but also enhances osteoclast precursor cell potential to differentiate into osteoclastic cells [2-4]. Increased pro-inflammatory cytokines (i.e. TNFα, IL6, IL17), which suppress osteoblastogenesis / enhance osteoclastogenesis, correlate with decreased bone parameters in SPF vs. GF mice [2, 4, 5]. We recently showed that the commensal gut microbiota increases the frequency of T_H17 cells / $CD4^+Il17^+$ cells in the bone marrow of SPF vs. GF mice, which highlights that T_H17 / Il17 mediated immunity may critically regulate gut microbiota effects on skeletogenesis [2].

Segmented filamentous bacteria (SFB) is a commensal gut bacterium that has strong immunomodulatory effects like inducing IgA production and T_H17 cell differentiation [6-8]. Studies have found intestinal T_H17 cells in mice colonized with SFB to have a localized antigen specific response to SFB [9, 10]. Murine models for

inflammatory diseases have suggested SFB to have a systemic effect on immune responses [11-13].

The role of specific commensal microbes on commensal gut microbiota osteoimmunoregulatory effects in the growing / developing skeleton is currently unknown. Investigations discerning the impact of specific commensal gut microbes on osteoimmune processes are important since this knowledge could be employed to optimize skeletal growth. The development of pre-biotics / pro-biotics targeting specific commensal gut microbes, such as SFB, could be utilized as non-invasive therapeutic interventions supporting normal skeletal growth and development.

1.2 Hypothesis

SFB influences commensal gut microbiota regulation of osteoimmune processes in post-natal skeletal development.

Specific Aims

Aim 1: Investigate SFB's role in commensal gut microbiota effects on bone modeling / growth during post-natal skeletal development.

Aim 2: Determine the impact of SFB on commensal gut microbiota osteoimmune response effects.

1.3 Background and Significance

General background on commensal gut microbiota / SFB regulation of host immune response

The gut microbiota, which is the collection of diverse microbes colonizing the gut, significantly regulates the development of host immunity [14]. The immune system is composed of the innate and adaptive immune responses. Innate immune responses

shape the commensal communities of resident microbes, which support a mutualistic relationship in which the host benefits from the microbiota's metabolic activities [15]. When recognition of the commensal microbiota by the innate immune system is lost, the once mutualistic relationship between the microbiota and the host becomes harmful, often with health consequences [16, 17]. The microbiota has been reported to influence all stages of myeloid cell functions and maturation, as well as tissue-specific functions of innate lymphoid cells [18-20]. The commensals regulate intestinal homeostasis through pattern-recognition receptors (PRRs), such as nucleotide-binding oligomerization domain-containing protein (NOD1), which has been shown to mediate commensal microbiota-induced lymphoid tissue genesis [20].

Microbial associated molecular patterns (MAMPs), recognized by PRRs, are an important component of innate immunity [21, 22]. The toll-like receptor (TLR) family recognize specific extracellular microbial cell components, flagellin, and microbial nucleic acids [23]. MAMPs function as distinct molecular ligands having high affinity for corresponding PRRs, which are expressed by innate immune cells (e.g. neutrophils, monocytes, macrophages, dendritic cells, natural killer cells), adaptive immune cells (e.g. T-lymphocytes, B-lymphocytes), and extracellular matrix cells (e.g. epithelial cells, fibroblasts, cementoblasts, osteoblasts) [23]. Signaling via TLR activation activates transcription factors, like nuclear factor (NF) κB (NFκB), inducing expression of pro-inflammatory cytokines and chemotactic factors [23].

Important to the current study, TLR4 recognizes lipopolysaccharides (LPS), a predominant structural component in the cell walls of Gram-negative bacteria. There are two TLR4 signaling pathways that both result in NFκB activation and inflammatory cytokine production: MyD88-dependent signaling occurs when TLR4 is activated on the

plasma membrane of the cell, and MyD88-independent signaling occurs when TLR4 is activated in an endosome [24-27].

Bacterial LPS associates with LPS binding protein (LBP), an acute phase protein that circulates in the blood, and then the complex binds CD14 [28, 29]. Next, the LPS is transferred to MD2 (LY96*)* which associates with the extracellular part of TLR4 [29]. This association causes an immune response that activates NFκB, inducing the expression of pro-inflammatory cytokine genes such as *Il1β* and *Il18* [28-30]. Studies in mice have found activation of TLR4 expressed on osteoblasts leads to the expression of pro-inflammatory / catabolic cytokines which decreased osteoblast differentiation and increased osteoclast maturation / function [31-38].

Table 1: Helper T-cell transcription factors and cytokines

$CD4^+$ T-cell	Transcription factor	Cytokine
T_H1	T-BET, STAT4	IFNγ, TNF
T_H2	GATA3, STAT6	IL4, IL5, IL13
T_H9	IRF4, PU.1	IL9
T_H17	RORγt, STAT3	IL17, IL22
T_H22	AHR	IL22
T_{REG}	FOXP3, STAT5	IL10, TGFβ

Slower to respond to MAMPs are adaptive immune cells. Adaptive immunity is different from innate immunity in that it is highly specific to antigens and has immunological memory. The adaptive immune cells differentiate from pluripotent hematopoietic stem cells in the bone marrow into the two main immune cells involved in adaptive immunity, T-cells or B-cells [39, 40]. T-cells differentiate and mature in the thymus [41-43]. B-cells mature in the bone marrow [44]. Some mature T-cells and B-cells return to the marrow and reside there.

Important to this study are the different characterized $CD4^+$ helper T-cell subsets that can be defined by transcription factor expression and cytokine secretion (Table 1) [45]. To broadly define the different T helper cell subsets: T_H1 cells mediate the cellular immune response, T_H2 cells potentiate the humoral response, T_H17 cells maintain mucosal barrier functions but have been implicated in many different autoimmune and inflammatory diseases, T_H22 cells are involved in tissue inflammation, T_H9 cells are involved in skin homeostasis and tissue inflammation, and T_{REG} cells are keepers of immune homeostasis [46].

Studies utilizing the SPF vs. GF mouse model have found altered helper $CD4^+$ T-cell populations in GF mice, including: reduced T_{REG} cells, decreased T_H17 cells, altered T_H1 / T_H2 ratios, and enhanced T_H2 cell responses [12]. Reports have shown that helper $CD4^+$ T-cell mediated immunity is influenced by the commensal gut microbiota, as well as by SFB specifically [4, 8, 12, 47, 48].

SFB is a Gram-positive, commensal bacterium that adheres to the epithelial cells in the ileum and colonizes the ileum post-weaning through post-natal development in most species, including humans and mice [49]. Investigations with SFB mono-associated mice reported SFB colonization to modulate immunity by augmenting the following: IgA production, intestinal epithelial lymphocyte recruitment, and intestinal epithelial cell major histocompatibility complex (MHC) II expression [7, 50]. Furthermore, SFB mono-associated vs. GF mice have increased T_H1, T_H2, T_H17, and T_{REG} cells and increased *Ifnγ, Tnf, Il17,* and *Il10* expression in the ileum lamina propria [8]. While mono-associated animal models discern the effects of individual microbes on immunity, it is more translatable to investigate the impact of specific commensal microbes in conjunction with the complex gut microbiota.

Studies in SPF mice from Jackson (SFB^-) and Taconic (SFB^+) found SFB to be associated with alterations in innate and adaptive immunity. Investigations in Taconic SPF (SFB^+) mice vs. Jackson SPF (SFB^-) mice found SFB to be associated with an increase in induction of T_H17 cell differentiation in the ileum and increased frequencies of T_H1, T_H2, and T_{REG} cells [6, 8, 9]. It has since been demonstrated that SFB colonization depends on not only the vendor but also the barrier location within each vendor [49].

Taconic has addressed barrier location differences in SFB colonization by separating out SPF colonies based on stricter microbial guidelines. Taconic currently has available the following SPF mouse models, which are listed from most to least restricted colonization: germ free (GF), defined flora (DF), excluded flora (EF), opportunistic free (OF), restricted flora (RF), and murine pathogen free (MPF). Taconic's more precise categorization of murine SPF health models minimizes differences in commensal gut microbiota composition, which limits confounding variables in gut microbiota research studies.

General background on osteoimmunology and post-natal skeletal growth / development

Osteoimmunology is the study of interactions between the skeleton and the immune system. Osteoimmunology studies have revealed that innate immunity, adaptive immune cells, and the endocrine system regulate bone modeling (growth) and remodeling (turnover) [51-55]. Bone modeling directs longitudinal skeletal growth and bone mass accrual in the developing skeleton, whereas remodeling has implications for the maintenance of bone mass in the mature adult skeleton. The current research will focus on osteoimmune processes that influence bone modeling during post-natal skeletal development. The bone cells that critically regulate bone modeling and skeletal growth / development are osteoblasts and osteoclasts [52-54, 56].

Osteoblasts are mesenchymal-derived bone-forming cells, which secrete and mineralize the bone matrix. Osteoblast function can be characterized by the secretion of collagen type 1 (COL1A1) and the bone mineral matrix proteins osteocalcin (OCN) and osteopontin (OPN) [57-59]. Bone mineral matrix formation begins with formation of the organic matrix via osteoblasts secreting collagen type 1, OCN, OPN, and proteoglycans [60]. Then matrix vesicles are released from the osteoblasts into the organic matrix which ends in calcification of the mineral matrix [60-63]. Insulin-like growth factor (IGF1) is an osteoblast signaling factor that upregulates osterix (*Sp7*) mediated osteoblast maturation and function [58, 64].

Osteoclasts are monocyte-myeloid derived bone resorbing cells. Osteoclast precursor cells are increased in the presence of inflammatory cytokines, but inflammatory cytokine stimulation alone is not sufficient for promoting osteoclast differentiation [65-67]. Osteoclast differentiation is dependent on macrophage colony stimulating factor (M-CSF) and the receptor activator of NFκB ligand (RANKL) signaling [56]. M-CSF drives cells down the osteoclast lineage and induces expression of the RANKL receptor, RANK [68]. RANKL signaling drives osteoclast differentiation, maturation, and function [69, 70].

In the bone marrow environment, RANKL is derived from stromal cells, osteoblasts, and T-cells [71]. Osteoprotegerin (OPG), the RANK decoy receptor, is expressed in the marrow environment by stromal cells, osteoblasts, dendritic cells, B-cells, and T-cells. [72-76]. When OPG binds RANKL, RANK-mediated osteoclast differentiation and function are inhibited [71].

The binding of RANKL to RANK causes the activation of NFκB, which augments the nuclear factor for activated T-cells, cytoplasmic 1 (NFATC1) [77]. This leads to NFATC1 transcription of genes that regulate osteoclast differentiation, maturation, and

function [77]. Inflammatory cytokines like IL1β, IL6, IL7, IL17A, and tumor necrosis factor alpha (TNF) have been shown to promote osteoclastogenesis indirectly via regulation of RANKL-signaling [78]. The cytokine IL1β upregulates the expression of RANKL and the expression of pro-inflammatory cytokines which promote osteoclastogenesis / inhibit osteoblastogenesis [79-83]. Along with these pro-osteoclastogenic effects, IL1β enhances the pro-resorptive effects of TNF [84, 85]. Like IL1β, IL7 and IL17A influence osteoclastogenesis by increasing RANKL / TNF producing T-cells and mesenchymal cells, and the expression of other inflammatory cytokines [86, 87]. The $CD4^+$ T_H17 derived, pro-inflammatory cytokine IL17A signals to stromal / osteoblastic cells, leading to an increase in pro-resorptive cytokines like IL6 and RANKL [88-91].

The Novince lab recently published a study investigating the commensal gut microbiota's modulation of T_H17 / IL17 in the healthy skeleton, which found up-regulated T_H17 / IL17 in marrow and a decreased bone mass phenotype in SPF compared to GF mice [2]. T_H17 cells and IL17A are suggested to be pro-osteoclastogenic because they induce RANKL expression on mesenchymal stem cells and osteoblasts [52]. Osteoclastogenesis is regulated by RANKL binding to RANK and activating osteoclasts, which increases osteoclast fusion, differentiation, and function.

<u>Commensal gut microbiota impact on osteoimmunology and skeletal growth / development</u>

Skeletal growth and homeostasis are affected by immune cells interacting with bone cells [52, 53, 55, 92, 93]. Inflammation suppresses osteoblast mediated bone formation and enhances osteoclast mediated bone resorption [53, 85, 94]. Studies using C57BL/6 GF vs. SPF and C57BL/6 GF vs. conventional (Conv) mice found that the commensal gut microbiota negatively affects bone mass accrual in growing mice [2, 4]. This is proposed to be due to increased osteoclast differentiation / function, secondary to

gut microbiota induction RANKL-signaling and pro-inflammatory mediators [2, 4]. The RANKL / OPG ratio was increased in the marrow of SPF vs. GF mice [2]. The commensal gut microbiota has been shown to upregulate *Il1β and Tnf* expression in marrow, and increase TNF levels in serum [2, 4]. The pro-inflammatory cytokine TNF synergistically enhances RANKL-mediated osteoclastogenesis [2].

Investigations in C57BL/6 mice have demonstrated that the commensal gut microbiota suppress osteoblast proliferation, differentiation, and function [2, 3]. Based on findings that *Igf1* expression was reduced in skeletal tissues and IGF1 levels were decreased in serum, gut microbiota anti-osteoblastic effects in C57BL/6 mice have been attributed to suppressed IGF1-mediated osteoblastogenesis [2, 3]. However, investigations utilizing BALB/c or CB6F1 (hybrid BALB/c and C57BL/6) mice have reported increased skeletal growth in the presence of the gut microbiota through increased serum IGF1 from the liver [95, 96]. The conflicting findings of these studies suggest that gut microbiota's actions on osteoblastogenesis and skeletal growth are dependent on endogenous genetic factors modulating IGF1.

Long bone growth occurs through the process of endochondral bone formation, which is centered in the growth plate. Differences in long bone length are attributed to alterations in the chondrocyte zones within the growth plate. The growth plate zones are determined by differences in chondrocyte differentiation [97]. The chondrocytes at the epiphyseal end of the growth plate are resting and thought of as a type of stem cell [97, 98]. When the stem cells reach the proliferating zone they organize into columns, divide, and make extracellular matrix proteins [97]. Next, chondrocytes lose the ability to divide and begin to differentiate and enlarge [97]. This is known as the hypertrophic zone [97]. Differentiated hypertrophic chondrocytes continue secreting matrix proteins and at the same time their intracellular calcium concentration is increasing [97]. Then the

chondrocytes mineralize longitudinal septa in the surrounding matrix, and blood vessels invade the matrix [97]. The blood vessels allow for the osteoclast and osteoblast precursors to reach the longitudinal septa [97]. Most of the septa is then resorbed in the metaphyseal zone, creating the frameworks for the osteoblasts to mineralize cartilage, leading to primary spongiosa production [97, 99, 100].

SFB impact on osteoimmunology and skeletal growth/development

SFB is a Gram-positive bacteria commensal gut microbe which potently modulates gut microbiota induction of IgA and T_H17 cell mediate immunity [6-8]. The T_H17 cells of mice colonized with SFB have been reported to have a localized antigen specific response to SFB [9, 10]. Inflammatory disease murine models have revealed SFB to systemically affect immune responses [11-13]. In GF mice predisposed to arthritis, the level of T_H17 cells is very low and the arthritis is dampened [11]. Once these GF mice are colonized with SFB, there is a drastic increase in T_H17 cells and quick onset of arthritis [11]. The GF murine model for experimental autoimmune encephalomyelitis (EAE) when colonized with SFB have increased T_H17 cells in the spinal cord equivalent to that of SPF EAE mice [12].

The commensal gut microbiota has been shown to be a critical regulator of osteoimmune processes in the healthy developing skeleton [2-4]. The influence of specific commensal gut microbes on commensal gut microbiota immunomodulatory actions impacting physiologic skeletal growth / development is unknown. This investigation of differences in healthy microbiota, like SFB, and the effects on commensal gut microbiota osteoimmunomodulatory actions in the post-pubertal growing skeleton will discern whether specific commensal microbes impact healthy skeletal development. Studying a specific commensal gut microbe's effects on osteoimmune response effects could provide novel insight for non-invasive interventions in the gut

microbiota, targeted towards optimizing peak bone mass accrual during healthy skeletal growth / development.

CHAPTER 2: MATERIALS AND METHODS

Animal Model

Nine-week-old, female, C57BL/6T murine-pathogen-free (MPF) mice (*specific-pathogen-free mice colonized by segmented filamentous bacteria) and excluded-flora (EF) mice (*specific-pathogen-free mice devoid of segmented filamentous bacteria) were purchased from Taconic, and euthanized 48 hours following arrival to a specific-pathogen-free (SPF) vivarium at Medical University of South Carolina (MUSC). Mice were euthanized via cardiac blood draw following ketamine and xylazine intraperitoneal anesthesia. At the time of sacrifice animal body weights and tissue weights were recorded. Animal procedures were approved by the MUSC Institutional Animal Care and Use Committee and carried out in accordance with the approved guidelines.

Micro-CT

Tibiae were fixed in 10% phosphate-buffered-formalin and stored in 70% ethanol. Specimens were scanned with Scanco Medical μCT 40 Scanner, using the following acquisition parameters: X-ray tube potential = 55 kVp; X-ray intensity = 145 μA; Integration time = 200 ms; Isotropic voxel size = 6 μm^3. Calibrated three-dimensional images were reconstructed. Tibia trabecular bone morphology was analyzed using Analyze 12.0 Bone Microarchitecture Analysis software. For trabecular analysis, transverse CT slices were analyzed beginning 300 μm distal to the proximal growth plate and extending 1000 μm distally; fixed threshold of 1750 Hounsfield Units was used to discriminate mineralized tissue. Tibia length and cortical bone morphology were analyzed using Analyze 12.0 Bone Microarchitecture Analysis software. For cortical analysis, transverse CT slices were analyzed in a 1000 μm segment of the mid-

diaphysis; fixed threshold of 2500 Hounsfield Units was used to discriminate mineralized tissue. Data are reported in accordance with standardized nomenclature [101].

Histomorphometry

Tibiae were fixed in 10% phosphate-buffered-formalin for 24 hours at room temperature. Tibiae were decalcified in 10% ethylenediaminetetraacetic acid (EDTA) for 21 days at room temperature. Proximal tibiae were embedded in paraffin, and 5 μm serial frontal sections were cut and stained. Safranin O-fast green stain and tartrate resistant acid phosphatase (TRAP) with a hematoxylin counter stain were performed. Trabecular bone area per tissue area (BA/TA) analysis was carried out in the secondary spongiosa of TRAP / hematoxylin stained proximal tibia sections [2, 102]. Growth plate chondrocyte zone analysis was performed in Safranin O-fast green stained proximal tibia sections. Five measurements of the proliferative zone and the hypertrophic zone were carried out in the central two-thirds of the growth plate of each sample [102]. Osteoclast cellular endpoints were evaluated in TRAP / hematoxylin stained proximal tibia sections. Analyses were limited to the secondary spongiosa, beginning 250 μm distal to the growth plate and extended 1000 μm distally (50 μm from endocortical surfaces) [2, 102]. Data were collected semi-automatically via an Olympus BX61 microscope and Visiopharm software. Data are reported in accordance with standardized nomenclature [101].

Quantitative Real-Time PCR (qRT-PCR) and Nanostring

RNA extraction (QIAgen QIAcube method): Ribonucleic acid (RNA) extractions of spleen and ileum were performed using the RNeasy Mini (QIAgen) extraction kit, following manufacturer's protocol. Whole spleen and ileum were flash frozen upon collection and stored at -80°C. Tissues stored at -80°C were pulverized with mortar and

pestle in liquid nitrogen. Pulverized tissues were then poured into and homogenized in the supplied buffer RLT at 600 µL for every 30 mg frozen tissue. Tissue lysate was then centrifuged at full speed for 3 minutes in a microcentrifuge and the lysate was transferred, without disturbing the pellet, to a clean 2 mL microcentrifuge tube. The QIAcube was then loaded with the microcentrifuge tube containing the lysate, RNeasy mini spin column and 1.5 mL collection tube in the rotor adaptor, 70% ethanol, buffer RW1, buffer RPE, and RNase free water. *In the QIAcube:* an equal volume of 70% ethanol was added to the lysate and homogenized. The sample was then transferred to an RNeasy mini spin column in a 2 mL collection tube, centrifuged for 15 seconds at 10,000 rpm, and the flow through was discarded. Buffer RW1 was added to the RNeasy spin column, centrifuged for 15 seconds at 10,000 rpm, and the flow through was discarded. Buffer RPE was added to the RNeasy spin column and centrifuged for 2 minutes at 10,000 rpm. The RNeasy spin column was then moved to a new 1.5 mL collection tube, 50 µL of RNase-free water was added directly to the column and centrifuged for 1 minute at 10,000 rpm to elute the RNA.

RNA Extraction (TRIzol Method): RNA extractions of the right femur and tibia bone marrow were performed using TRIzol (Invitrogen) extraction method, following manufacturer's protocol. Marrow from right femur and tibia was flushed with 3 mL of TRIzol and a 25G 5/8 syringe homogenized and stored at -80°C. Samples were thawed, homogenized, and incubated for 5 minutes at 15-30°C. Chloroform (600 µL) was added to the samples. They were homogenized for 15 seconds by hand and incubated for 2-3 minutes at 15-30°C. The samples were then centrifuged at 9,500 RCF for 15 minutes at 4°C to complete the phase separation. The upper aqueous phase of each sample was transferred to a fresh tube. Isopropyl alcohol (1.5 mL) was added to each sample and then mixed via inverting tubes 10 times. Samples were incubated at 15-30°C for 10

minutes, then centrifuged for 10 minutes at 9,500 RCF at 4°C, completing the RNA precipitation. The supernatant was poured off/decanted, 75% ethanol (3 mL) was added to each sample, vortexed briefly and centrifuged for 5 minutes at 9,500 RCF at 4°C to wash the RNA. The supernatant was poured off/decanted and the RNA pellet was homogenized and re-dissolved in RNase free water.

Quantify RNA: Total RNA was quantified via NanoDrop 1000 (Thermo Scientific). RNA was read on a spectrophotometer at wavelength 260 nm to detect RNA, and 280 nm to determine sample purity.

cDNA Synthesis: Complementary deoxyribonucleic acid (cDNA) was synthesized from RNA isolates using Taqman Random Hexamers and Reverse Transcription Reagents, according to Applied Biosystems manufacturer's protocol. To summarize, cDNA synthesis reactions were set up using 4 µL 10X RT buffer, 8.8 µL $MgCl_2$ solution, 8 µL dNTP solution, 2 µL random hexamers, 0.8 µL RNase inhibitor, 1.04 µL reverse transcriptase, 1 µg/µL worth of RNA as determined by spectrophotometer, and RNase-free water to a final volume of 40 µL. Samples were then subjected to thermocycling on a MyCycler Thermocycler system (Bio-Rad); 25°C for 10 min; 48° for 30 min, 95° for 5 min; 4° holding. cDNA was then used for qRT-PCR reactions with different cytokine primers.

Table 2: qRT-PCR primers.

Gene	ThermoFisher primer used
IFNγ	Mm01168134_m1
IL4	Mm00445259_m1
IL17	Mm00439618_m1
IL10	Mm00439614_m1
IL9	Mm00434305_m1
IL22	Mm01226711_g1
BGLAP	Mm00649782_gH
IGF1	Mm00439560_m1
GAPDH	Mm99999915_g1

Primers: Primers were used for the following cytokines. All primers were ordered from ThermoFisher Scientific. Purchased primers arrived in solution at concentration of 200 µM.

qRT-PCR gene expression analysis: Synthesized cDNA was amplified via the StepOnePlus System (Applied Biosystems) protocol, using TaqMan Universal PCR Master Mix and TaqMan gene expression primer probes. A 20 µL PCR reaction was performed using 10 µL of Taqman MM (2x), 1 µL of primer probes (20x), 2 µL of sample cDNA (10x), and 7 µL of RNase free water. PCR samples were then subjected to a 40-cycle thermocycler protocol using the StepOnePlus System (Applied Biosystems); 50°C for 2 minutes, 95°C for 10 minutes, followed by 40 cycles of 95°C for 15 seconds, 60°C for 1 minute, ending with a hold at 4°C. Relative quantification of mRNA was performed via the comparative CT method (ΔΔCT); *Gapdh* was utilized as an internal control gene [2].

NanoString gene expression analysis: nCounter PanCancer Immune Profiling for Mouse gene expression panel (NanoString Technologies) was applied to assess gene expression in bone marrow RNA isolates. Hybridization was carried out and products were run on the nCounter preparation station, according to the manufacturer's protocol final step executed by LCOHR. Data collected by the nCounter digital analyzer was evaluated via nSolver Analysis Software v2.6 (NanoString Technologies). Data were normalized to the geometric means of spiked-in positive controls and internal control genes. Absolute quantification of RNA reported as normalized RNA counts [2].

Flow Cytometry Analysis

Live Cell Analysis: Femur bone marrow, spleen, and mesenteric lymph node (mLN) cells were isolated, washed, and counted. Cells were resuspended at 100,000

cells/50 µL. Cells were treated with FcR-block (Miltenyi Biotec) and stains were performed. Dead cells were excluded via propidium iodide viability dye (Miltenyi Biotec). Data was acquired by the MACSQuant System (Miltenyi Biotec). Analyses were performed via FlowJo VX software (TreeStar). Analysis was limited to 10,000 events.

T-cell hematopoiesis: anti-CD3-PE-Vio770 (Miltenyi Biotec, clone REA641), anti-CD4-VB (Miltenyi Biotec, clone REA604), anti-CD8-PE (Miltenyi Biotec, clone REA601), anti-CD62L-FITC (Miltenyi Biotec, clone REA828), anti-CD69-APC (Miltenyi Biotec, clone H1.2F3), anti-γδTCR-APC-Vio770 (Miltenyi Biotec, clone REA727).

- Helper T-cells: $CD3^+CD8^-CD4^+$ (% $CD3^+$ cells)
- Activated Helper T-cells: $CD3^+CD8^-CD4^+CD62L^-CD69^+$ (% $CD3^+CD4^+$ cells)
- Naïve Helper T-cells: $CD3^+CD8^-CD4^+CD62L^+CD69^-$ (% $CD3^+CD4^+$ cells)
- Cytotoxic T-cells: $CD3^+CD8^+CD4^-$ (% $CD3^+$ cells)
- Activated Cytotoxic T-cells: $CD3^+CD4^-CD8^+CD62L^-CD69^+$ (% $CD3^+CD8^+$ cells)
- Naïve Cytotoxic T-cells: $CD3^+CD4^-CD8^+CD62L^+CD69^-$ (% $CD3^+CD8^+$ cells)
- Gamma-Delta T-cells: $CD3^+CD4^-CD8^-\gamma\delta^+$ (% $CD3^+$ cells)

Spleen / mLN B-cells: anti-B220-VB (Miltenyi Biotec, clone REA755), anti-CD19-APC (Miltenyi Biotec, clone REA749), anti-IgM-PC (Miltenyi Biotec, clone X-54), anti-IgD-FITC (Miltenyi Biotec, clone REA772).

- Total B-Cells: $B220^+CD19^+$ (% live cells)
- Activated B-Cells: $B220^+CD19^+IgM^+IgD^+$ (% $B220^+CD19^+$ cells)

- Memory B-Cells: $B220^{+}CD19^{+}IgM^{+}IgD^{-}$ (% $B220^{+}CD19^{+}$ cells)
- Follicular B-Cells: $B220^{+}CD19^{+}IgM^{lo}IgD^{+}$ (% $B220^{+}CD19^{+}$ cells)
- Marginal Zone B-Cells: $B220^{+}CD19^{+}IgM^{+}IgD^{lo}$ (% $B220^{+}CD19^{+}$ cells)

Marrow B-cells: anti-B220-VB (Miltenyi Biotec, clone REA755), anti-CD19-APC (Miltenyi Biotec, clone REA749), anti-IgM-PC (Miltenyi Biotec, clone X-54), anti-BP-1 (Miltenyi Biotec, clone 6C3).

- Total B-Cells: $B220^{+}CD19^{+}$ (% live cells)
- Pro B-Cells: $B220^{+}CD19^{+}CD249^{-}IgM^{-}$ (% $B220^{+}CD19^{+}$ cells)
- Pre B-Cells: $B220^{+}CD19^{+}CD249^{+}IgM^{-}$ (% $B220^{+}CD19^{+}$ cells)
- Immature B-Cells: $B220^{+}CD19^{+}CD249^{-}IgM^{+}$ (% $B220^{+}CD19^{+}$ cells)

Transcription Factor Analysis: Femur bone marrow, spleen, and mLN cells were isolated, washed, and counted. Cells were re-suspended at 100,000 cells / 50 µL. Cells were treated with FcR-block (Miltenyi Biotec). Cells were plated with a surface dye panel and incubated for 30 minutes, and intracellular stains were carried out following the fixation-permeabilization buffer manufacturer's protocol (eBioscience).

Fixation/Permeabilization: Cells were washed with phosphate-buffered saline (PBS) buffer, centrifuged for 5 minutes at 1,500 RPM at 4°C, then the supernatant was aspirated. This was repeated for 3 washes with no aspiration at the end of the 3rd. Diluted VioB viability dye was added to the cells and incubated in the fridge for 30 minutes. Cells were washed twice via FACS buffer added, centrifuged for 5 minutes at 1,500 RPM at 4°C, and supernatant was aspirated. Then the fixation permeabilization solution, 1 part eBioscience fixation / permeabilization concentrate plus 3 parts eBioscience fixation / permeabilization diluent, was added to cells and plates were placed in the fridge to incubate overnight. The next morning, two washes were done with

permeabilization buffer, centrifuged for 5 minutes at 1,500 RPM at 4°C, and supernatant was aspirated. Samples were resuspended in permeabilization buffer. The cells were incubated for 30 minutes at room temperature in the dark with intracellular antibodies. Two more washes were done with permeabilization buffer, centrifuged for 5 minutes at 1,500 RPM at 4°C, followed by aspiration. The samples were resuspended in FACS buffer. Dead cells were excluded via eFlour 780 viability dye (eBioscience). Data was acquired by the MACSQuant System. Analyses were performed via FlowJo VX software. Analysis was limited to 10,000 events.

T_{REG} cells: anti-CD3-PE-Vio770 (Miltenyi Biotec, clone REA641), anti-CD4-FITC (Miltenyi Biotec, clone REA604), anti-CD25-PE-vio770 (Miltenyi Biotec, clone 7D4), anti-FoxP3-PE (Miltenyi Biotec, clone REA788), anti-RORγt-APC (Miltenyi Biotec, clone REA278).

- T_{REG} Cells: $CD3^+CD4^+CD25^+FOXP3^+ROR\gamma t^-$ (% $CD3^+CD4^+$ cells)

T_H1 cells: anti-CD3-PE-Vio770 (Miltenyi Biotec, clone REA641), anti-CD4-FITC (Miltenyi Biotec, clone REA604), anti-CD183-PE (Miltenyi Biotec, clone CXCR3-173), anti-T-bet-APC (Miltenyi Biotec, clone REA102).

- T_H1 Cells: $CD3^+CD4^+CD183^+T\text{-}BET^+$ (% $CD3^+CD4^+$ cells)

T_H2 / T_H9 cells: anti-CD3-APC-Vio770 (Miltenyi Biotec, clone REA641), anti-CD4-FITC (Miltenyi Biotec, clone REA604), anti-CD184-PE-Vio770 (Miltenyi Biotec, clone REA107), anti-GATA3-PE (Miltenyi Biotec, clone REA174), anti-IRF4-APC (Miltenyi Biotec, clone REA201).

- T_H2 Cells: $CD3^+CD4^+CD184^+GATA3^+IRF4^-$ (% $CD3^+CD4^+$ cells)
- T_H9 Cells: $CD3^+CD4^+CD184^+GATA3^-IRF4^+$ (% $CD3^+CD4^+$ cells)

T_H17 / T_H22 cells: anti-CD3-APC-Vio770 (Miltenyi Biotec, clone REA641), anti-CD4-FITC (Miltenyi Biotec, clone REA604), anti-CD196-PE (Miltenyi Biotec, clone REA277), anti-RORγt-APC (Miltenyi Biotec, clone REA278), anti-AHR-PE-Vio770 (eBioscience, clone 4MEJJ).

- T_H17 Cells: $CD3^+CD4^+CD196^+ROR\gamma t^+AHR^-$ (% $CD3^+CD4^+$ cells)
- T_H22 Cells: $CD3^+CD4^+CD196^+ROR\gamma t^-AHR^+$ (% $CD3^+CD4^+$ cells)

Intracellular Cytokine Analysis: Femoral bone marrow cells were isolated and plated. Whole marrow cultures were maintained undisturbed for 6-hours; cultures were subsequently stimulated with 6 mL eBioscience Cell Stimulation Cocktail [phorbol 12-myristate 13-acetate (40.5 μM), lonomycin (670 μM), brefeldin A (5.3 mM), monensin (1 mM) in ethanol (500X), plus protein transport inhibitors] added to 3 mL culture medium for 6 hours. Cells were harvested, washed, and counted. Cells were re-suspended at 100,000 cells / 50 μL. Surface stains were performed, and intracellular cytokine stains were carried out. Data was acquired by the MACSQuant System. Analyses were performed via FlowJo VX software. Analysis was limited to 10,000 events.

T_H17 stimulation: anti-CD3-APC-Vio770 (Miltenyi Biotech, clone REA641), anti-CD4-VB (Miltenyi Biotech, clone REA604), anti-CD8-PE-Vio770 (Miltenyi Biotech, clone REA601), anti-IL17-FITC (Miltenyi Biotech, clone REA660).

- T_H17 cells: $CD3^+CD4^+CD8^-IL17^+$ (% $CD3^+CD4^+CD8^-$ cells)

T_H1 / T_H2 / T_{REG} stimulation: anti-CD3-APC-Vio770 (Miltenyi Biotech, clone REA641), anti-CD4-VB (Miltenyi Biotech, clone REA604), anti-CD8-PE-Vio770 (Miltenyi Biotech, clone REA601), anti-IFNγ-FITC (Miltenyi Biotech, clone REA638), anti-IL4-PE (Miltenyi Biotech, clone BVD4-1D11), anti IL10-APC (Miltenyi Biotech, clone JES5-16E3).

- T_H1 Cells: $CD3^+CD4^+CD8^-IFN\gamma^+IL4^-IL10^-$ (% $CD3^+CD4^+CD8^-$ cells)
- T_H2 Cells: $CD3^+CD4^+CD8^-IFN\gamma^-IL4^+IL10^-$ (% $CD3^+CD4^+CD8^-$ cells)
- T_{REG} Cells: $CD3^+CD4^+CD8^-IFN\gamma^-IL4^-IL10^+$ (% $CD3^+CD4^+CD8^-$ cells)

CHAPTER 3: RESULTS

3.1 Aim 1 Results

Previous studies in our research lab have found an association between the presence of a healthy gut microbiota and trabecular bone parameters in the young adult murine skeleton. These studies used SPF vs. GF mice to investigate commensal gut microbiota osteoimmune effects on osteoblastogenesis and osteoclastogenesis in the young adult skeleton [2]. In SPF mice colonized with commensal microbiota, a decrease in specific trabecular bone parameters was found via micro-CT analysis. Histomorphometric analysis showed an increase in osteoclast size, osteoclast perimeter per bone perimeter, and in the eroded bone perimeter in SPF mice [2].

Aim 1: Investigate SFB's role in commensal gut microbiota effects on bone modeling/growth during post-natal skeletal development.

Somatic growth differences were assessed by measuring animal body weight and tibia length. Body weight was increased in MPF vs. EF mice (Fig. 1a). Tibia length measurements demonstrated that MPF mice had longer tibiae than EF mice (Fig. 1b).

The decreased tibia length in EF vs. MPF mice (Fig. 1b) implies that different microbial compositions impair endochondral bone formation. Alterations in endochondral bone formation were assessed via histomorphometric analysis of proximal tibia growth plate chondrocyte zones (Fig. 1c-f). The hypertrophic chondrocyte zone height was increased in EF vs. MPF mice (Fig. 1d), which suggests reduced tibia length is due to delayed linear bone growth.

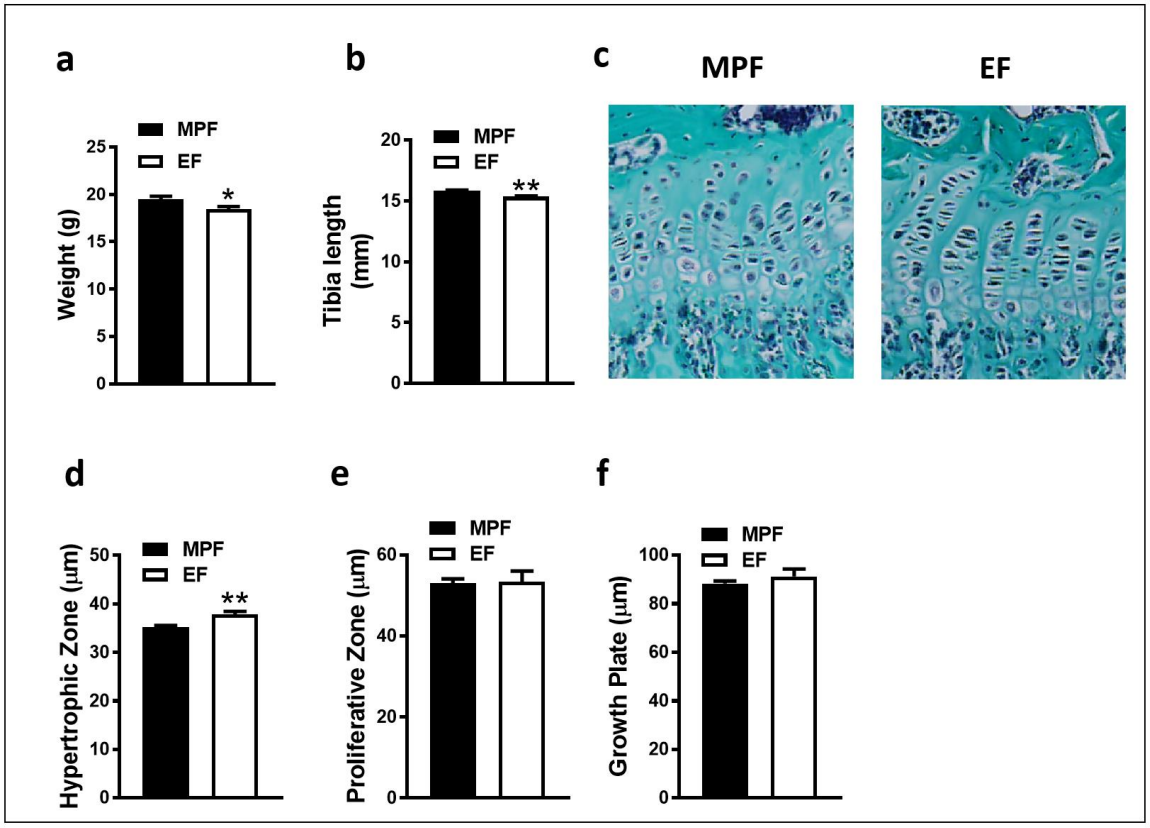

Figure 1: Somatic growth and endochondral bone formation analysis. Nine-week-old female MPF vs. EF mice were weighed, euthanized, and tibia harvested for histology analysis. (a) Animal weight (n=5/gp), (b) tibia length (n=4/gp), (c-f) proximal tibia growth plate analysis (n=5/gp); (c) Representative images of Safranin-O-Fast Green stained growth plate in proximal tibia; (d) Hypertrophic chondrocyte zone height; (e) Proliferating chondrocyte zone height; (f) Total growth plate height. Data reported as mean $\pm$ SEM. *p<0.05 vs. MPF. **p<0.01 vs. MPF.

Histomorphometric (Fig. 2a,b) and micro-CT analysis (Fig. 2c-h) were carried out in the proximal tibia trabecular bone. Histomorphometric analysis revealed decreased trabecular bone area per tissue area in MPF vs. EF mice (Fig. 2a,b). Micro-CT analysis validated histomorphometric outcomes, demonstrating a reduced trabecular bone phenotype in MPF vs. EF mice. Trabecular bone mineral density (Fig. 2d) and bone

volume per tissue volume (Fig. 2e) were decreased in the proximal tibia of MPF vs. EF mice. The decreased trabecular bone mass phenotype in MPF mice was attributed to reduced trabecular number (Fig. 2f). Trabecular thickness (Fig. 2g) and trabecular separation (Fig. 2h) were similar in MPF vs. EF mice.

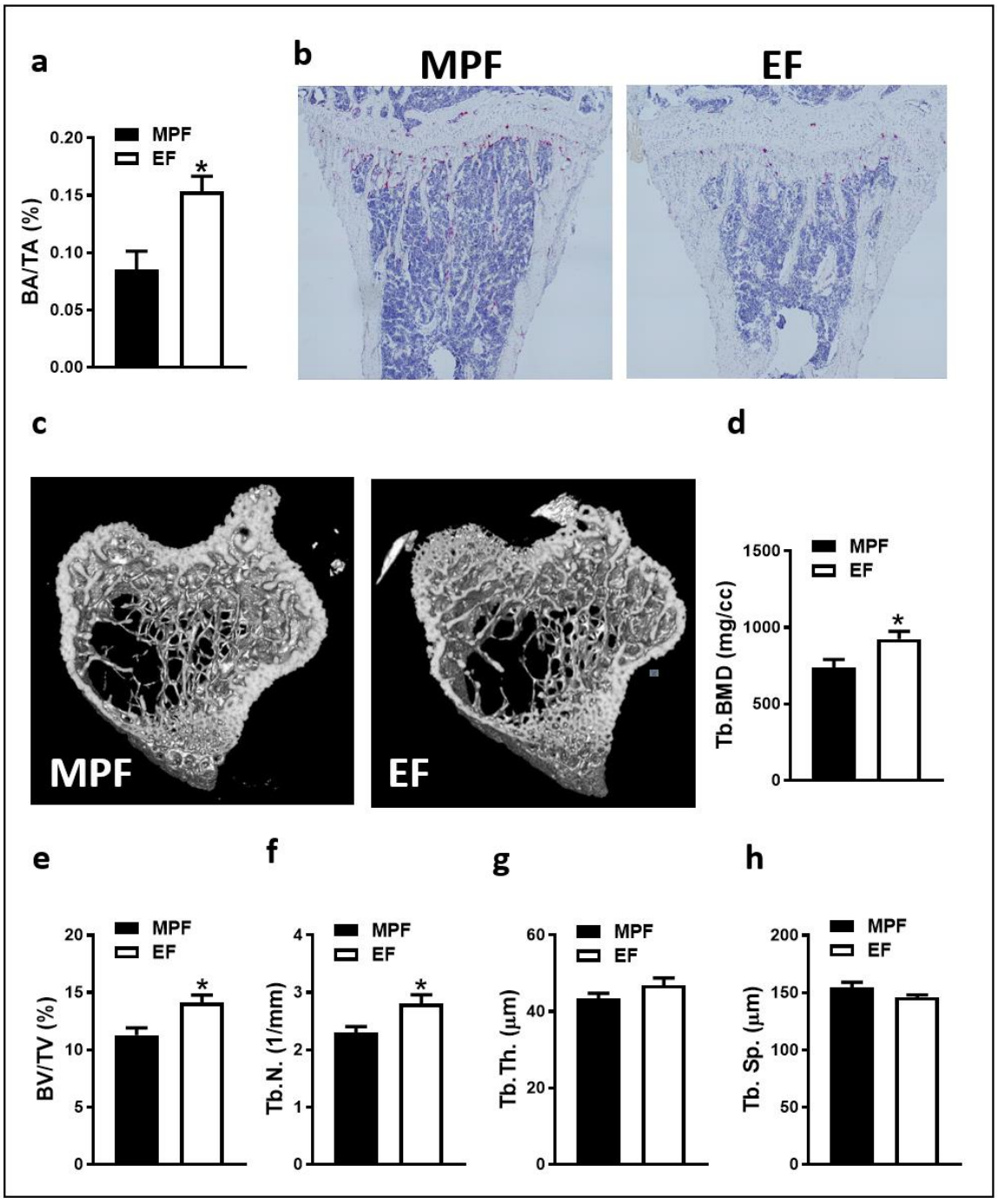

Figure 2: Proximal tibia trabecular bone analysis. Nine-week-old female MPF vs. EF mice were weighed, euthanized, and tibia harvested for histomorphometric and micro-CT analysis. (a, b) Histomorphometric analysis of proximal tibia trabecular bone (n = 5 / gp). (a) BA / TA = bone area fraction. (b) Representative images of tartrate resistant acid

phosphatase (TRAP) / hematoxylin counterstained proximal tibia sections. (c-h) Micro-CT analysis of proximal tibia trabecular bone (n = 4/gp). (c) Representative reconstructed cross-sectional images, extending 360 μm distally from where analysis was initiated. (d) Tb.BMD = trabecular bone mineral density. (e) BV/TV = trabecular bone volume fraction. (f) Tb.N = trabecular number. (g) Tb.Th = trabecular thickness. (h) Tb.Sp = trabecular separation. Data are reported as mean ± SEM. *$p<0.05$ vs. MPF.

Micro-CT analysis was carried out in the tibia mid-diaphysis to assess cortical bone parameters (Fig. 3). There was a trend towards an increase in cortical area per total area (Fig. 3d) and cortical thickness (Fig. 3e) in MPF vs. EF mice.

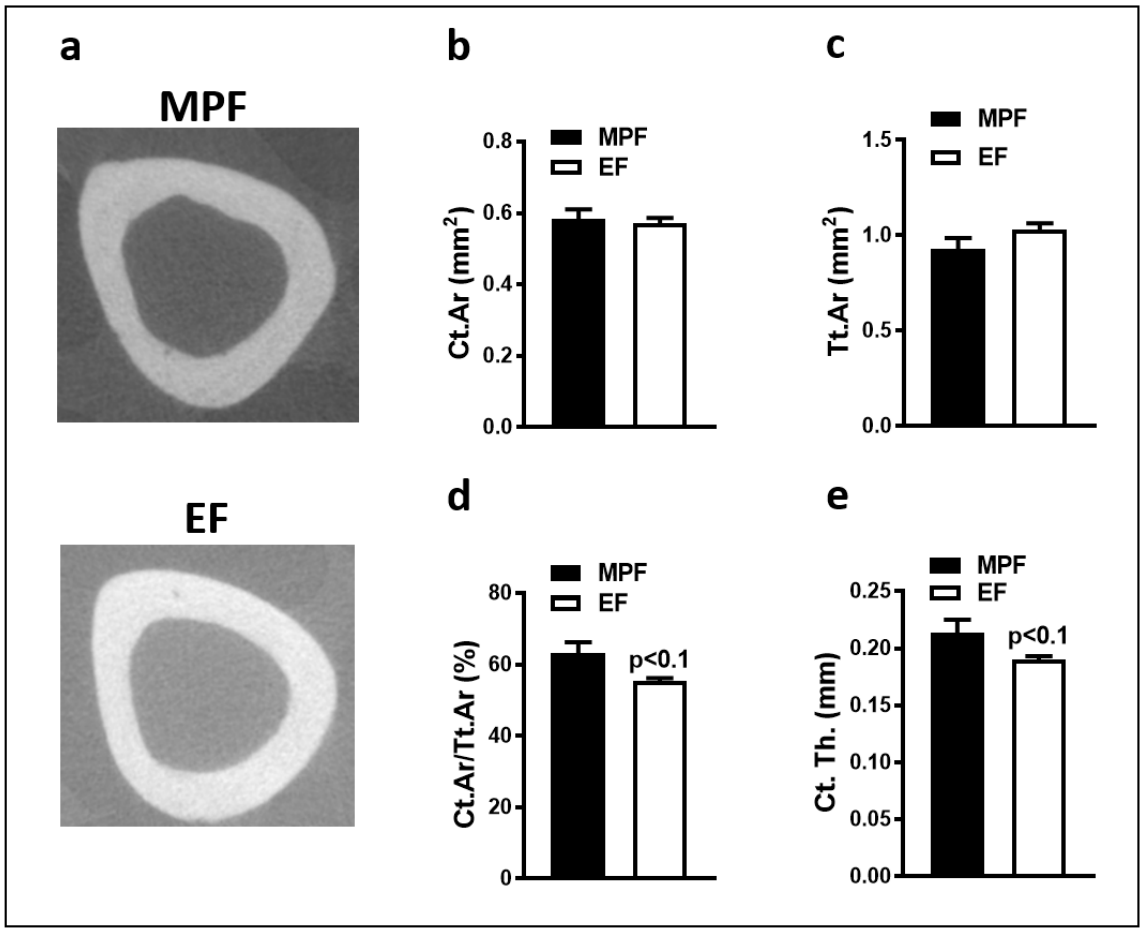

Figure 3: Tibia mid-diaphysis cortical bone analysis. Nine-week-old female MPF vs. EF mice were weighed, euthanized, and tibia harvested for micro-CT analysis. (a-e) Micro-CT analysis of tibia mid-diaphysis cortical bone (n = 4 / gp). (a) Representative reconstructed cross-sectional images taken in the middle of the region of interest in the mid-diaphysis of the tibia. (b) Ct.Ar = cortical area. (c) Tt.Ar = total area. (d) Ct.Ar / Tt.Ar = cortical bone volume fraction. (e) Ct.Th = cortical thickness. Data reported as mean ± SEM. *p<0.05 vs. MPF.

Histomorphometric analysis of tartrate-resistant acid phosphatase (TRAP) stained proximal tibia sections was performed to investigate alterations in commensal microbes like, SFB, and the effects on osteoclastogenesis (Fig. 4). MPF vs. EF mice had

an increased number of osteoclasts lining the trabecular bone perimeter (Fig. 4b), which suggests that enhanced osteoclast mediated bone resorption contributes to the decreased trabecular bone phenotype found in MPF mice (Fig. 2).

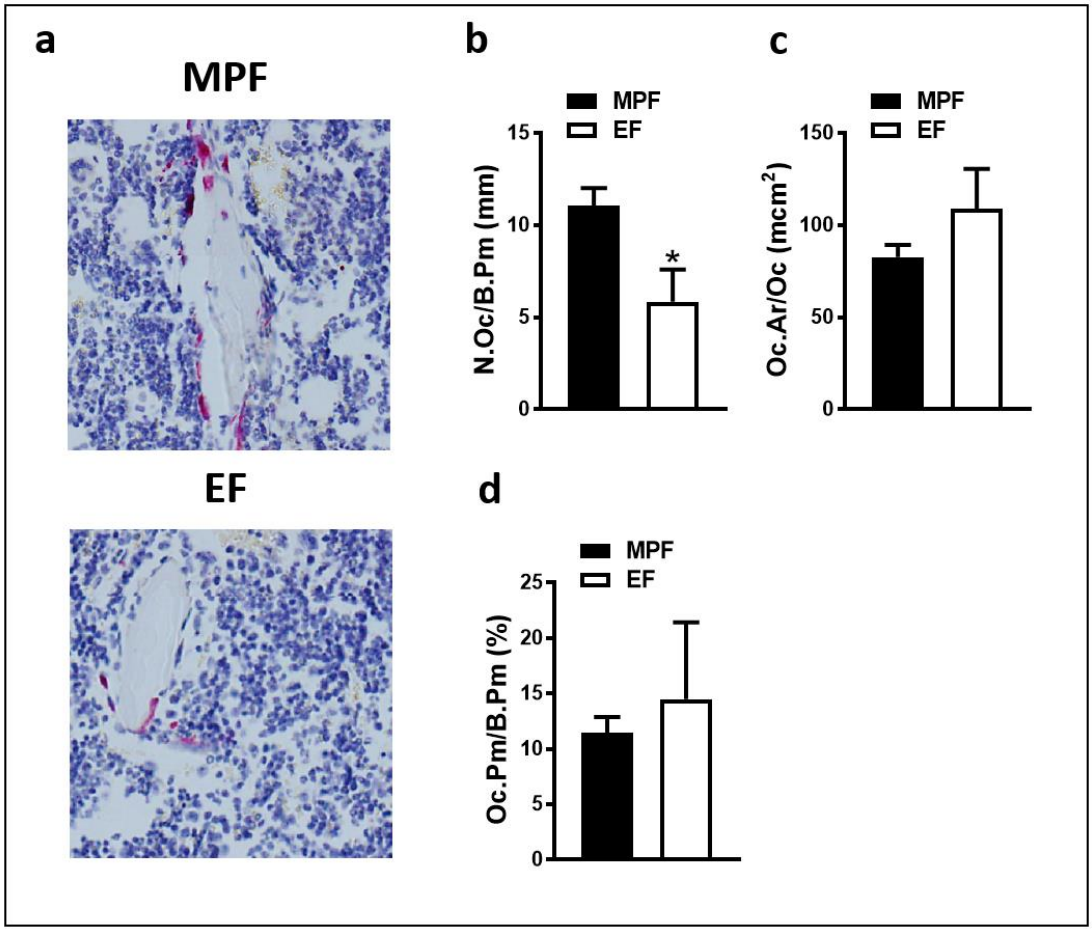

Figure 4: Osteoclast histomorphometric analysis. Nine-week-old female MPF vs. EF mice were weighed, euthanized, and tibia harvested for histomorphometric analysis. Histomorphometric analysis of osteoclast cellular endpoints were performed in the trabecular bone secondary spongiosa of tartrate-resistant acid phosphatase (TRAP) stained proximal tibia sections; TRAP + cell lining bone with ≥ 3 nuclei designated an osteoclast. (a) Representative images of TRAP-stained secondary spongiosa. (b) N.Oc / B.Pm = osteoclast number per bone perimeter. (c) Oc.Ar / Oc = average osteoclast area.

(d) Oc.Pm / B.Pm = osteoclast perimeter per bone perimeter. Data are reported as mean ± SEM. *p<0.05 vs. MPF.

Genes involved in osteoimmune processes, inflammation, and bacterial recognition were quantified via the nCounter method (Fig. 5) to elucidate mechanisms driving the pro-osteoclastic phenotype found in marrow of MPF vs. EF mice (Fig. 4). Osteoclast transcription factors and critical osteoclast signaling factors were assessed to discern alterations in osteoclast differentiation and maturation. *Nfatc1* expression was elevated (Fig. 5a) in MPF vs. EF marrow [103-106]. NFATc1 is known as the osteoclast differentiation master regulator, and drives expression of essential osteoclast genes like TRAP, Cathepsin K, and calcitonin receptor [77, 107-110]. The increased number of osteoclasts per bone perimeter (Fig. 4b) and up-regulated *Nfatc1* expression in the marrow of MPF vs. EF mice (Fig. 5a) reveal that complex microbial compositions harboring SFB, enhances osteoclastogenesis.

The *Tnfsf11 (Rankl)* / *Tnfrsf11b (Opg)* axis was evaluated (Fig. 5a) to determine whether alterations in critical osteoclastic signaling factors mediate the pro-osteoclastic phenotype in MPF vs. EF mice. RANKL, which signals at the RANK receptor on pre-osteoclast/osteoclast cells, is required for osteoclast differentiation and function [72-76]. Since OPG functions as the RANK decoy receptor, evaluation of the RANKL / OPG ratio is imperative when assessing potential alterations in RANKL-mediated osteoclastogenesis. The gene expression of *Opg* (*Tnfrsf11b*) and *Rankl* (*Tnfsf11*) (Fig. 5a) were similar in MPF vs. EF mice, which implies that the different commensal gut microbiota do not impact RANKL-induced osteoclastogenesis.

Pro-inflammatory cytokines have synergistic effects on RANKL-signaling, which potently enhances RANKL-mediated osteoclastogenesis. Taking into consideration that

there were no differences in the *Tnfsf11 (Rankl) / Tnfrsf11b (Opg)* axis (Fig. 5a), we investigated alterations in pro-inflammatory cytokines known to enhance RANKL-induced osteoclastogenesis (Fig. 5b). Inflammatory cytokine gene expression analysis in the marrow of MPF vs. EF mice revealed that *Il18* expression was increased in MPF mice (Fig. 5b). Because IL18 is released in response to TLR4 signaling, the expression of components of the TLR4 signaling pathway were assessed. Augmented expression of TLR4 signaling components, *Lbp, Ly96,* and *Tlr4,* (Fig. 5c) was found in the marrow of MPF vs. EF mice.

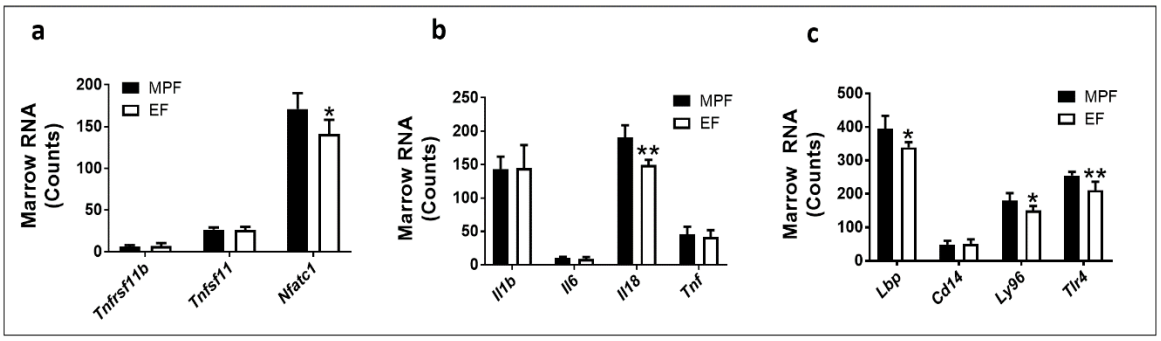

Figure 5: Osteoclastogenic, pro-inflammatory cytokine, and MAMP response gene analysis. Nine-week-old female MPF vs. EF mice were weighed, euthanized, and bone marrow isolated for gene expression analysis. Nanostring gene expression analysis (n=5/gp): (a) osteoclastogenesis; (b) pro-inflammatory cytokines; (c) bacterial recognition. Data were normalized to the geometric means of spiked-in positive controls and internal control genes *(Ppia, Eif2b4, Tubb5*, and *Alas1)*. Absolute quantification of RNA expressed as normalized RNA counts. Data are reported as mean ± SEM. * $p<0.05$ vs. MPF. ** $p<0.01$ vs. MPF.

Because bone modeling is mediated by dual osteoclast and osteoblast actions, alterations in osteoblastogenesis were evaluated. Gene expressions studies were performed in bone marrow, via nCounter and qRT-PCR, to discern complex commensal

gut microbial compositions, with differing SFB colonization statuses, impact on osteoblastogenesis (Fig. 6). Collagen type 1 alpha 1 chain (*Col1a1*) was investigated as a marker for early osteoblast activity (Fig. 6a). The bone mineral matrix proteins, osteopontin (*Spp1*) (Fig. 6a) and osteocalcin (*Bglap / Ocn*) (Fig. 6b), were assessed as markers of more mature osteoblast activity. *Col1a1* (Fig. 6a) was decreased, whereas *Spp1* (Fig. 6a) and *Bglap* (Fig. 6b) were similar in the marrow of MPF vs. EF mice. To elucidate differences in osteoblast processes, the critical osteoblastic signaling factor *Igf1* was investigated (Fig. 6b). There was a significant increase in *Igf1* expression (Fig. 6b) in the marrow of MPF vs. EF mice.

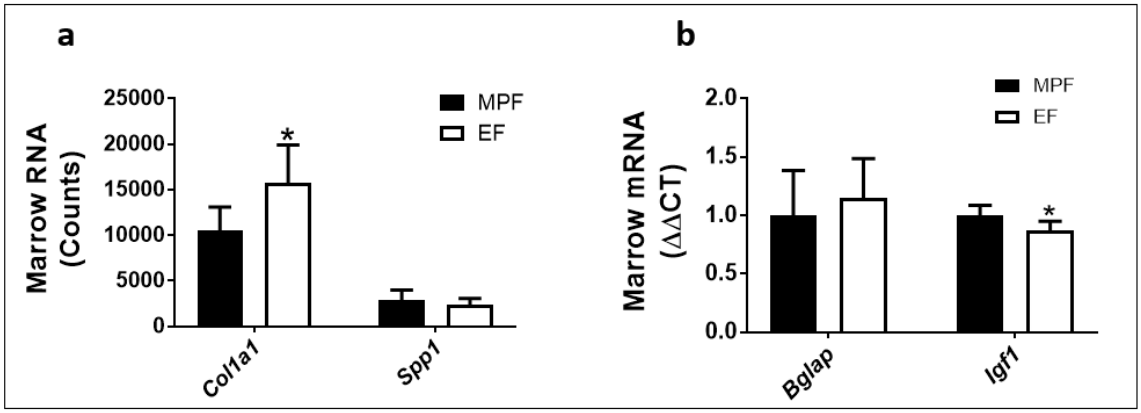

Figure 6: Bone marrow osteogenic gene expression. Nine-week-old female MPF vs. EF mice were weighed, euthanized, and bone marrow isolated for gene expression analysis. (a) Nanostring gene expression analysis (n=5/gp): *Col1a1* assessed as early osteoblast activity marker; *Spp1* assessed as a mature osteoblast activity marker. Data were normalized to the geometric means of spiked-in positive controls and internal control genes *(Ppia, Eif2b4, Tubb5*, and *Alas1)*. Absolute quantification of RNA expressed as normalized RNA counts. (b) qRT-PCR gene expression analysis (n=5/gp): *Bglap* assessed as a mature osteoblast activity marker; *Igf1* assessed as critical osteoblastic signaling factor. Relative quantification of mRNA was performed via the

comparative C_T method (ΔΔCT); GAPDH was utilized as an internal control gene. Data are reported as mean ± SEM. *p<0.05 vs. MPF.

3.3 Aim 2 Results

Studies on the commensal microbiota's impact on immunity have shown how important the different niches of microbes, especially the gut commensals, are in educating and developing the immune system. A potent inducer of T_H17 cells in the gut is the commensal bacteria, segmented filamentous bacteria (SFB) [6]. T_H17 cell mucosal defenses are up-regulated with SFB adherence to the small intestine epithelial cells [6, 8]. Both GF mice and mice treated with antibiotics have decreased T_H17 cells, but when colonized with SFB, T_H17 cells increase within 2 weeks [8, 111]. Colonization with SFB induces T_H17 protective effects against *Citrobacter rodentium* in the intestine [6]. However, effects of SFB colonization are not always protective and beneficial. In autoimmune diseases, like inflammatory bowel disease and autoimmune arthritis, SFB colonization exacerbates the disease state via systemic T_H17 cell induction [11, 112, 113]. Experimental autoimmune encephalomyelitis (EAE) GF mice have decreased EAE, which correlates with decreased T_H17 cells in the spinal cord, but when colonized with SFB the severity of EAE is fully restored [12]. Specific T_H17 cells for SFB derived antigens are found in SFB colonized mice, but in the absence of secondary lymphoid organs, nonspecific T_H17 cells are induced [9, 10, 114].

We have previously used the SPF vs. GF mouse model to investigate the impact of the commensal microbiota on adaptive immune cells [2]. In the marrow of GF mice, there were decreased T_H17 cells, $CD4^+IL\text{-}17^+$ cells, and $CD4^+IFN\gamma^+$ cells. In the mLNs of SPF mice, increased $CD4^+$ T-cells, $CD8^+$ T-cells, and $\gamma\delta^+$ T-cells were found [2].

Aim 2: Determine the impact of SFB on commensal gut microbiota osteoimmune response effects.

SFB is a commensal bacterium that adheres to intestinal epithelial cells in the ileum [6]. Characteristic cytokines of helper $CD4^+$ T-cells were assessed to determine the local impact of SFB's presence in the ileum (Fig. 7). MPF mice had increased *Ifnγ* (Fig. 7a) and *Il17* (Fig. 7c) expression in the ileum. The finding that *Il17* was substantially enhanced (50X fold) in the ileum of MPF vs. EF mice is in line with prior reports demonstrating up-regulated *Il17* in the ileums of mice harboring SFB [6, 111].

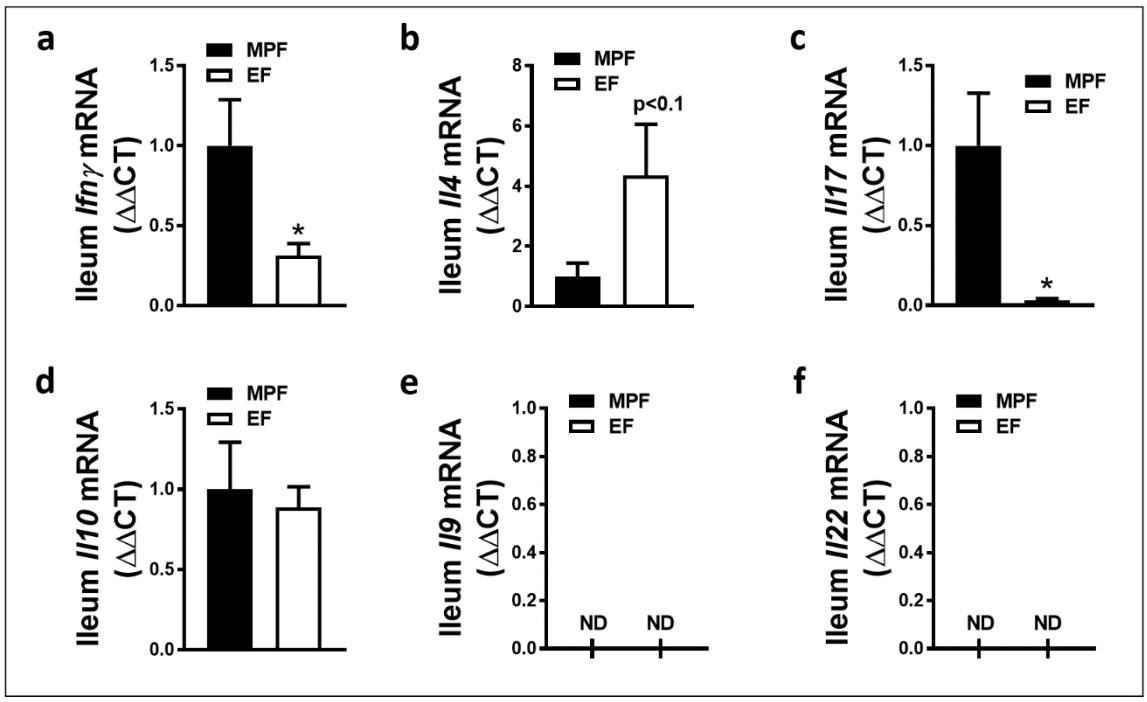

Figure 7: Helper $CD4^+$ T-cell subset gene expression in Ileum. Nine-week-old female MPF vs. EF mice were weighed, euthanized, and ileum isolated for gene expression analysis. qRT-PCR gene expression analysis (n=5/gp): (a) *Ifnγ* mRNA (T_H1 cytokine); (b) *Il4* mRNA (T_H2 cytokine); (c) *Il17* mRNA (T_H17 cytokine); (d) *Il10* mRNA (T_{REG} cytokine) ; (e) *Il9* mRNA (T_H9 cytokine); (f) *Il22* mRNA (T_H22 cytokine). Relative quantification of

mRNA was performed via the comparative C_T method (ΔΔCT); GAPDH was utilized as an internal control gene. Data are reported as mean ± SEM. *p<0.05 vs. MPF.

The mLNs are the gut draining lymph nodes. The small intestine harbors the microbe of interest, SFB, so the mLNs were used to investigate changes of T-cell / B-cell cell populations in the lymph nodes most closely related to SFB's niche. T-cells were further investigated to assess activated and naïve cells (Fig. 8). Decreased helper ($CD3^+CD4^+CD8^-$) T-cells (Fig. 8a) and increased cytotoxic ($CD3^+CD4^-CD8^+$) T-cells (Fig. 8b) were observed in the mLNs of MPF vs. EF mice. No other differences were found in the assayed immune cell populations in the mLNs of MPF vs. EF mice. The gating method for T-cell and B-cell subsets can be seen in the appendix.

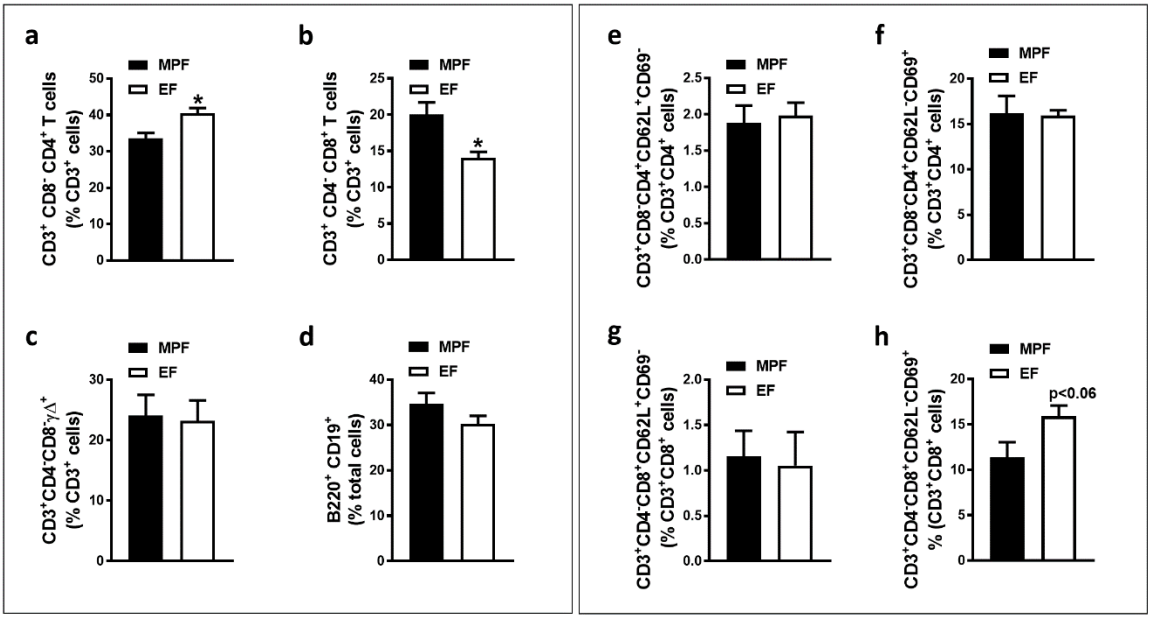

Figure 8: Mesenteric lymph nodes (mLN) T-cell / B-cell subsets. Nine-week-old female MPF & EF mice were euthanized; Cells from the mLN were homogenized and stained (n=5/gp) for flow cytometric analysis. (a-c) T-cell subset composition. (a) $CD3^+CD4^+CD8^-$ (helper T-cells); (b) $CD3^+CD4^-CD8^+$ (cytotoxic T-cells); (c) $CD3^+CD4^-CD8^-\gamma\delta^+$ ($\gamma\delta^+$ T-

cells); Percentages expressed relative to $CD3^+$ cells. (d) Overall B-cells: $B220^+CD19^+$ (B-cells). Percentage expressed relative to total live cells. (e,f) Naïve and activated helper $CD4^+$ T-cells. (e) $CD3^+CD4^+CD62L^+CD69^-$ (Naïve helper $CD4^+$ T-cells); (f) $CD3^+CD4^+CD62L^-CD69^+$ (Activated helper $CD4^+$ T-cells). Percentages expressed relative to total helper $CD3^+CD4^+$ T-cells. (g,h) Naïve and activated cytotoxic $CD8^+$ T-cells. (g) $CD3^+CD8^+CD62L^+CD69^-$ (Naïve cytotoxic $CD8^+$ T-cells); (h) $CD3^+CD8^+CD62L^-CD69^+$ (Activated cytotoxic $CD8^+$ T-cells). Percentages expressed relative to total cytotoxic $CD3^+CD8^+$ T-cells. Data are reported as mean $\pm$ SEM. *$p<0.05$ vs. MPF.

Flow cytometric analysis of helper $CD4^+$ T-cell subsets was performed in mLNs to further delineate different complex microbial compositions impact on gut immunity. (Fig. 9). Helper $CD4^+$ T-cell subset frequencies were similar in the mLNs of MPF vs. EF mice. The gating method used for helper T-cell subsets can be found in the appendix.

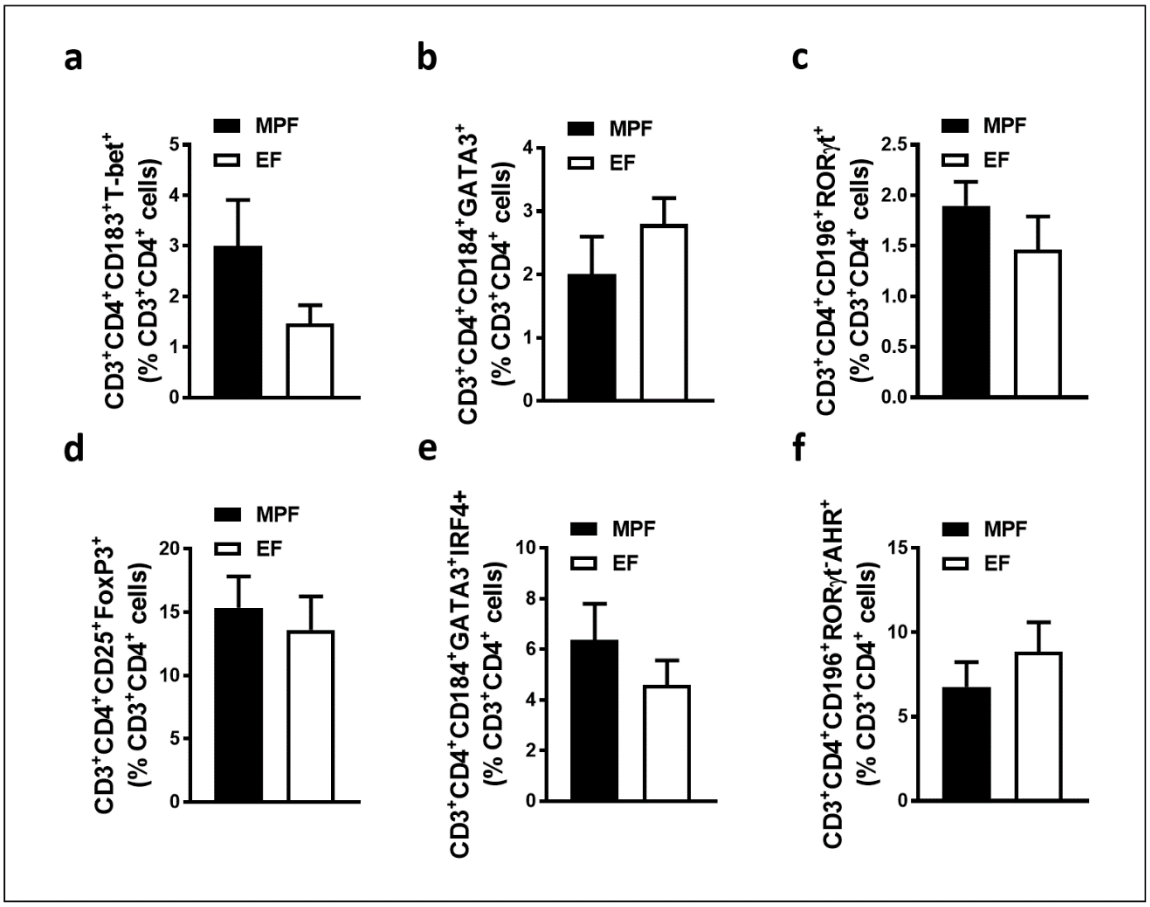

Figure 9: Mesenteric lymph node (mLN) helper $CD4^+$ T-cell subsets. Nine-week-old female MPF & EF mice were euthanized; mLN cells were homogenized and stained (n=5/gp) for flow cytometric analysis. (a-e) Helper $CD4^+$ T-cell subset composition. (a) $CD3^+CD4^+CD183^+$T-bet^+ (T_H1 cells); (b) $CD3^+CD4^+CD184^+GATA3^+$ (T_H2 cells); (c) $CD3^+CD4^+CD196^+RORyt^+$ (T_H17 cells); (d) $CD3^+CD4^+CD25^+FoxP3^+$ (T_{REG} cells); (e) $CD3^+CD4^+CD184^+GATA3^+IRF4^+$ (T_H9 cells); (f) $CD3^+CD4^+CD196^+ROR\gamma t^-AHR^+$ (T_H22 cells). Percentages expressed relative to helper $CD3^+CD4^+$ T-cells. Data are reported as mean ± SEM.

The spleen is a secondary lymphoid organ that contains cell populations of T-cells, B-cells, dendritic cells, and macrophages. B-cells migrate to the spleen to further

differentiate and mature. Because the spleen is a major organ for adaptive immune cell development, changes in immune cell populations were investigated. Flow cytometric analysis was performed on spleen cells to investigate B-cell and T-cell populations. T-cells were further investigated to assess activated and naïve cells populations (Fig. 10). There was no difference in T-cell or B-cell frequencies in the spleens of MPF vs. EF mice.

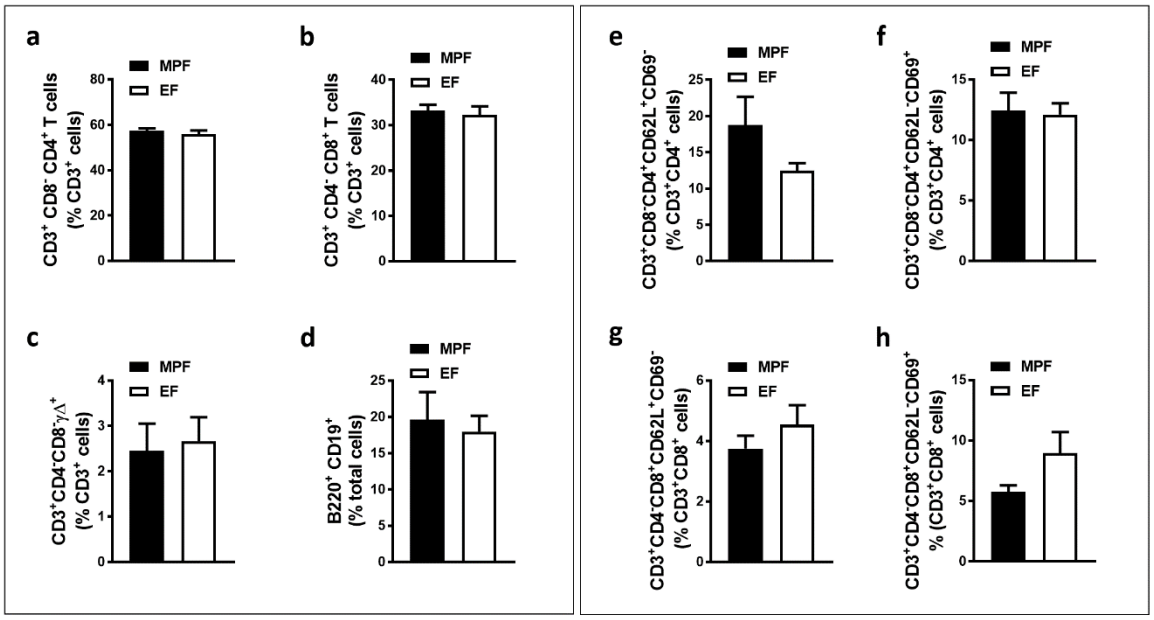

Figure 10: Spleen T-cell/B-cell subsets. Nine-week-old female MPF & EF mice were euthanized; Spleen cells were homogenized and stained (n=5/gp) for flow cytometric analysis. (a-c) T-cell subset composition. (a) $CD3^+CD4^+CD8^-$ (helper T-cells); (b) $CD3^+CD4^-CD8^+$ (cytotoxic T-cells); (c) $CD3^+CD4^-CD8^-\gamma\delta^+$ ($\gamma\delta^+$ T-cells); Percentages expressed relative to $CD3^+$ cells. (d) Overall B-cells. (d) $B220^+CD19^+$ (B-cells). Percentage expressed relative to total live cells. (e,f) Naïve and activated helper $CD4^+$ T-cells. (e) $CD3^+CD4^+CD62L^+CD69^-$ (Naïve helper $CD4^+$ T-cells); (f) $CD3^+CD4^+CD62L^-CD69^+$ (Activated helper $CD4^+$ T-cells). Percentages expressed relative to total helper $CD3^+CD4^+$ T-cells. (g,h) Naïve and activated cytotoxic $CD8^+$ T-cells. (g)

$CD3^+CD8^+CD62L^+CD69^-$ (Naïve cytotoxic $CD8^+$ T-cells); (h) $CD3^+CD8^+CD62L^-CD69^+$ (Activated cytotoxic $CD8^+$ T-cells). Percentages expressed relative to total cytotoxic $CD3^+CD8^+$ T-cells. Data are reported as mean $\pm$ SEM.

Flow cytometric analysis of Helper $CD4^+$ T-cell subsets was carried out in spleen to further discern differences in MPF vs. EF mice systemic immunity (Fig. 11). There were increased T_H1 cells (Fig. 11a) and a trend towards decreased T_H2 cells (Fig. 11b) in the spleens of MPF vs. EF mice. The frequency of T_H17, T_{REG}, T_H9, and T_H22 cells were similar in the spleens of MPF vs. EF mice.

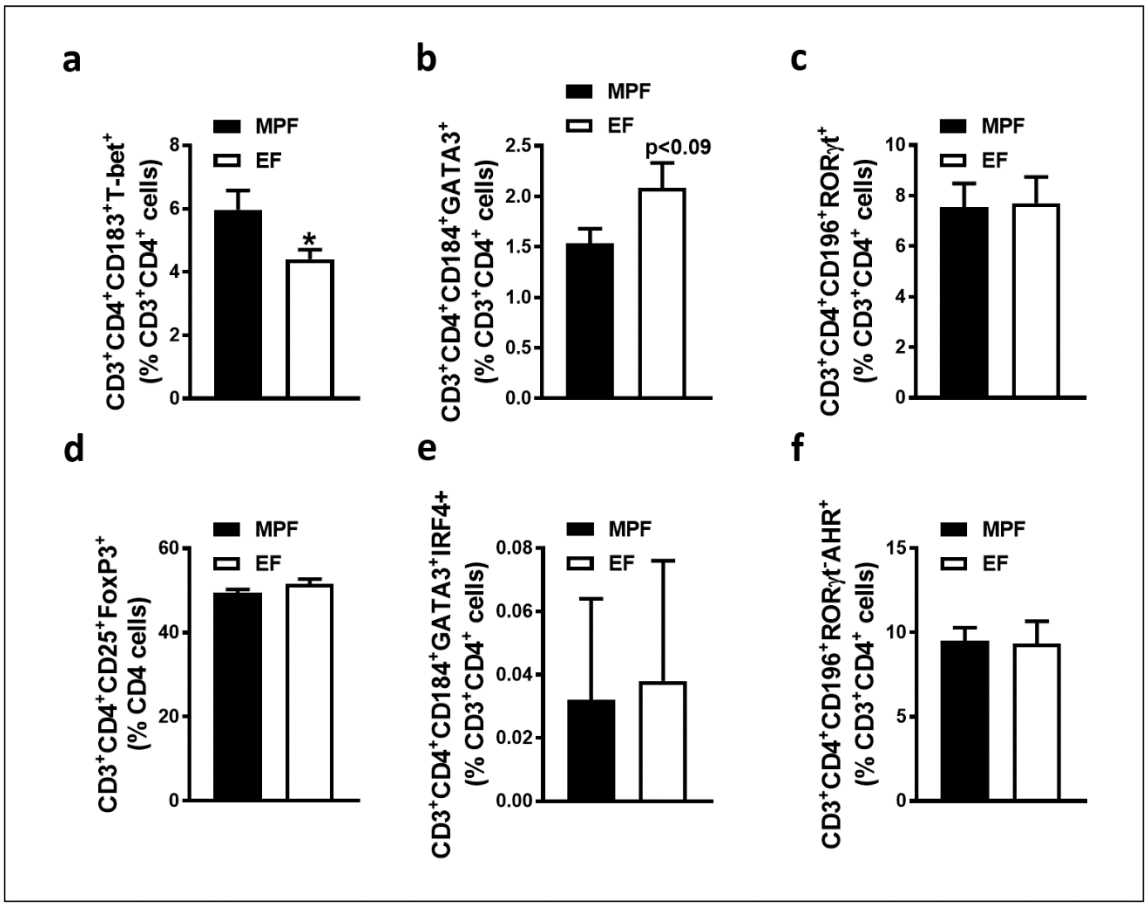

Figure 11: Spleen helper $CD4^+$ T-cell subsets. Nine-week-old female MPF & EF mice were euthanized; spleen cells were homogenized and stained (n=5/gp) for flow cytometric analysis to assess helper T-cell subset composition. (a-e) Helper $CD4^+$ T-cell subset composition. (a) $CD3^+CD4^+CD183^+T\text{-}bet^+$ (T_H1 cells); (b) $CD3^+CD4^+CD184^+GATA3^+$ (T_H2 cells); (c) $CD3^+CD4^+CD196^+RORyt^+$ (T_H17 cells); (d) $CD3^+CD4^+CD25^+FoxP3^+$ (T_{REG} cells); (e) $CD3^+CD4^+CD184^+GATA3^+IRF4^+$ (T_H9 cells); (f) $CD3^+CD4^+CD196^+RORyt^-AHR^+$ (T_H22 cells). Percentages expressed relative to helper $CD3^+CD4^+$ T-cells. Data are reported as mean ± SEM. *p<0.05 vs. MPF.

To further investigate the helper $CD4^+$ T-cell subsets in the spleen, the characteristic cytokines for each helper T-cell subset were assessed via qRT-PCR (Fig.

12). A trend towards an increase in the T_H1 characteristic cytokine, *Ifnγ*, was observed in the spleen of MPF vs. EF mice (Fig. 12a). This finding is in line with the increased T_H1 cell frequency found in the spleen of MPF vs. EF mice (Fig. 11a). The T_H2 characteristic cytokine, *Il4*, was decreased in the spleen of MPF mice (Fig. 12b), which parallels the observed trend towards reduced T_H2 cell frequency in the spleen of MPF vs. EF mice (Fig. 11b).

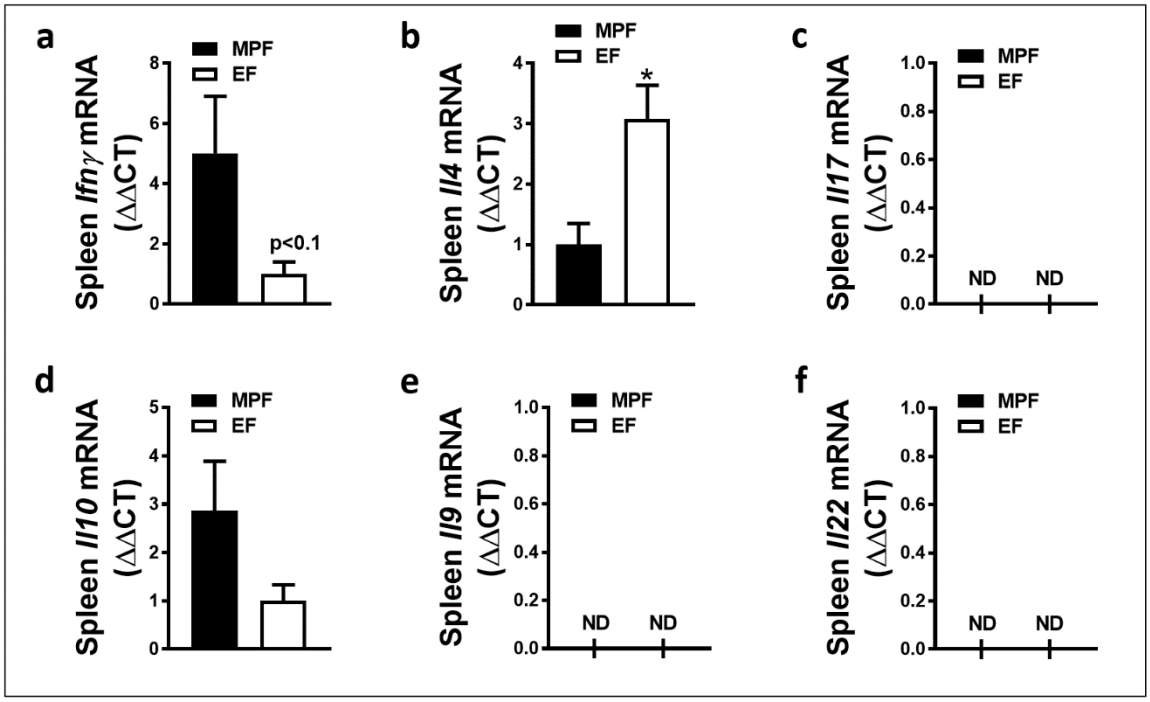

Figure 12: Helper $CD4^+$ T-cell subset gene expression in spleen. Nine-week-old female MPF vs. EF mice were weighed, euthanized, and spleen isolated for gene expression analysis. qRT-PCR gene expression analysis (n=5/gp): (a) *Ifnγ* mRNA (T_H1 cytokine); (b) *Il4* mRNA (T_H2 cytokine); (c) *Il17* mRNA (T_H17 cytokine); (d) *Il10* mRNA (T_{REG} cytokine) ; (e) *Il9* mRNA (T_H9 cytokine); (f) *Il22* mRNA (T_H22 cytokine). Relative quantification of mRNA was performed via the comparative C_T method (ΔΔCT); GAPDH was utilized as an internal control gene. Data are reported as mean ± SEM. *p<0.05 vs. MPF.

Adaptive immune cells originate in the bone marrow. Studies have shown SFB to have effects on inflammatory conditions in the skeleton of arthritic mouse models [115]. T_H17 derived IL17 has been shown to have indirect effects on osteoblasts and osteoclasts [55]. Considering that SFB induced T_H17 mediated immunity has implications at sites distant from the gut, including skeletal joints, flow cytometric analysis was performed to investigate B-cell and T-cell populations in femur bone marrow. T-cells were further investigated by assessing activated and naïve T-cells (Fig. 13). There was a trend towards decreased γδ ($CD3^+CD4^-CD8^-\gamma\delta TCR^+$) T-cells (Fig. 13c) and activated helper $CD4^+$ ($CD3^+CD4^+CD8^-CD62L^-CD69^+$) T-cells (Fig. 13f) in the marrow of MPF vs. EF mice.

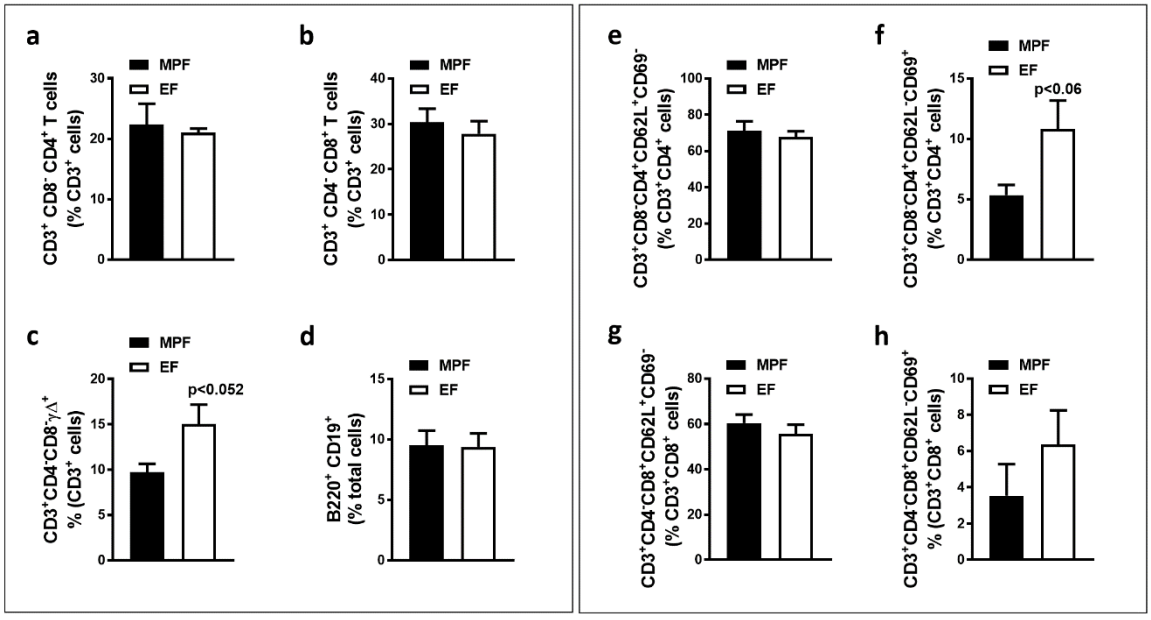

Figure 13: Femur bone marrow T-cell/B-cell subsets. Nine-week-old female MPF & EF mice were euthanized; femur bone marrow cells were flushed, homogenized, and stained (n=5 / gp) for flow cytometric analysis. (a-c) T-cell subset composition. (a) $CD3^+CD4^+CD8^-$ (helper T-cells); (b) $CD3^+CD4^-CD8^+$ (cytotoxic T-cells); (c) $CD3^+CD4^-CD8^-\gamma\delta^+$ ($\gamma\delta^+$ T-cells); Percentages expressed relative to $CD3^+$ cells. (d) Overall B-cells.

(d) $B220^{+}CD19^{+}$ (B-cells). Percentage expressed relative to total live cells. (e,f) Naïve and activated helper $CD4^{+}$ T-cells. (e) $CD3^{+}CD4^{+}CD62L^{+}CD69^{-}$ (Naïve helper $CD4^{+}$ T-cells); (f) $CD3^{+}CD4^{+}CD62L^{-}CD69^{+}$ (Activated helper $CD4^{+}$ T-cells). Percentages expressed relative to total helper $CD3^{+}CD4^{+}$ T-cells. (g,h) Naïve and activated cytotoxic $CD8^{+}$ T-cells. (g) $CD3^{+}CD8^{+}CD62L^{+}CD69^{-}$ (Naïve cytotoxic $CD8^{+}$ T-cells); (h) $CD3^{+}CD8^{+}CD62L^{-}CD69^{+}$ (Activated cytotoxic $CD8^{+}$ T-cells). Percentages expressed relative to total cytotoxic $CD3^{+}CD8^{+}$ T-cells. Data are reported as mean $\pm$ SEM.

SFB's immunomodulatory impact on helper $CD4^{+}$ T-cell subset induction is unknown in bone marrow. Flow cytometric analysis was used to investigate possible SFB induced differences in helper $CD4^{+}$ T-cell subsets in the marrow of MPF vs. EF mice (Fig. 14). The frequencies of helper $CD4^{+}$ T-cell subsets were similar in the marrow MPF vs. EF mice.

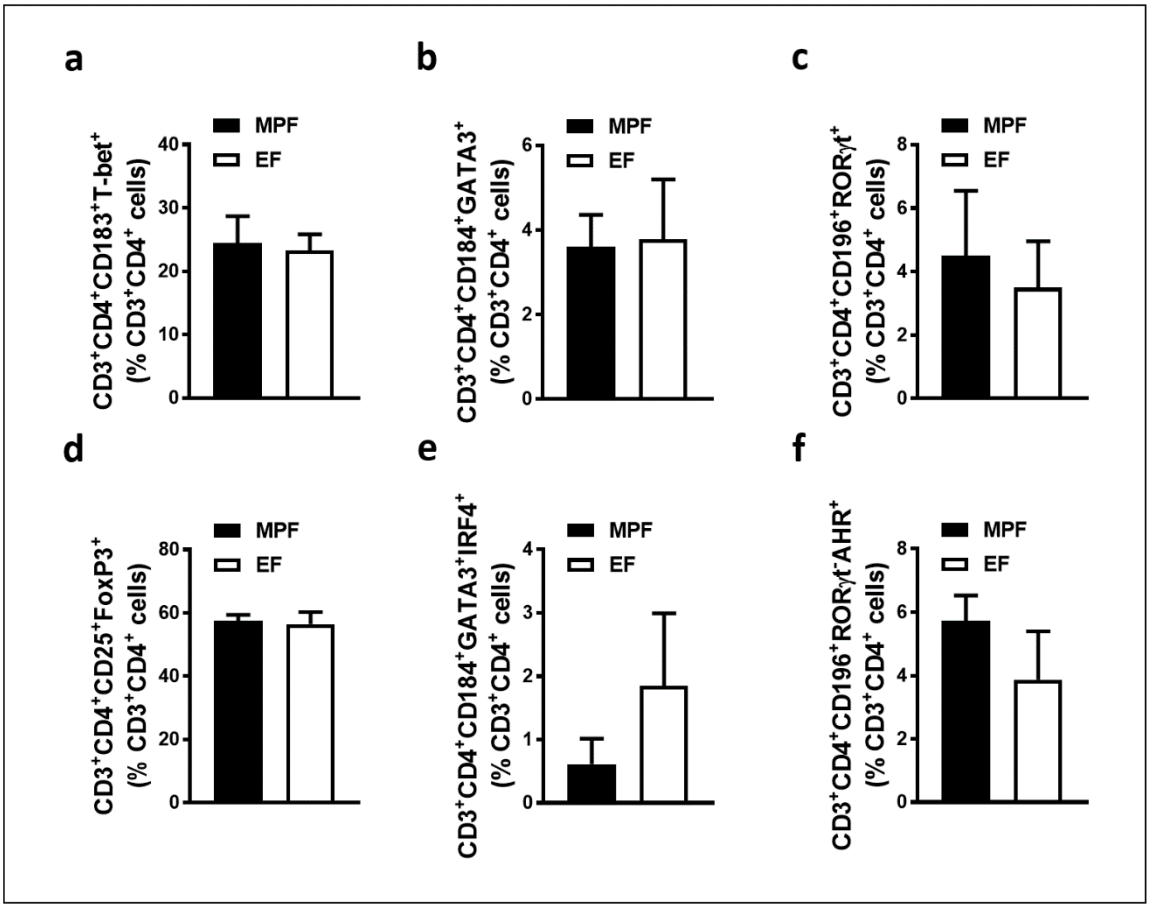

Figure 14: Femur bone marrow helper $CD4^+$ T-cell subsets. Nine-week-old female MPF & EF mice were euthanized; femur bone marrow cells were homogenized and stained (n=5 / gp) for flow cytometric analysis. (a-e) Helper $CD4^+$ T-cell subset composition. (a) $CD3^+CD4^+CD183^+T\text{-}bet^+$ (T_H1 cells); (b) $CD3^+CD4^+CD184^+GATA3^+$ (T_H2 cells); (c) $CD3^+CD4^+CD196^+RORyt^+$ (T_H17 cells); (d) $CD3^+CD4^+CD25^+FoxP3^+$ (T_{REG} cells); (e) $CD3^+CD4^+CD184^+GATA3^+IRF4^+$ (T_H9 cells); (f) $CD3^+CD4^+CD196^+ROR\gamma t^-AHR^+$ (T_H22 cells). Percentages expressed relative to helper $CD3^+CD4^+$ T-cells. Data are reported as mean ± SEM.

Helper T-cell subset characteristic cytokine expression was evaluated in marrow via qRT-PCR analysis, to further assess helper $CD4^+$ T-cell populations (Fig. 15).

Consistent with flow cytometric analysis outcomes (Fig. 14), helper CD4^{+} T-cell subset characteristic cytokine expression findings were similar in the marrow of MPF vs. EF mice.

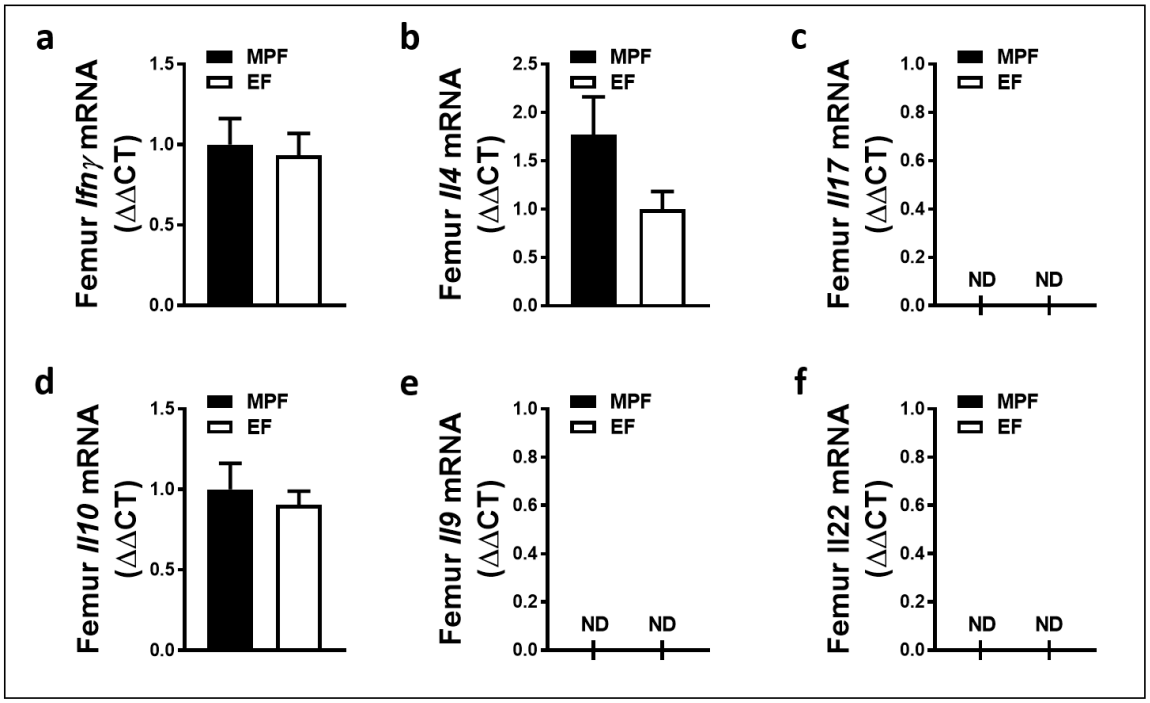

Figure 15: Helper CD4^{+} T-cell subset gene expression in bone marrow. Nine-week-old female MPF vs. EF mice were weighed, euthanized, and bone marrow isolated for gene expression analysis. qRT-PCR gene expression analysis (n=5 / gp): (a) *Ifnγ* mRNA (T_H1 cytokine); (b) *Il4* mRNA (T_H2 cytokine); (c) *Il17* mRNA (T_H17 cytokine); (d) *Il10* mRNA (T_{REG} cytokine); (e) *Il9* mRNA (T_H9 cytokine); (f) *Il22* mRNA (T_H22 cytokine). Relative quantification of mRNA was performed via the comparative C_T method (ΔΔCT); GAPDH was utilized as an internal control gene. Data are reported as mean ± SEM.

Appreciating that the bone marrow cellular composition is highly heterogeneous, and that helper CD4+ T-cells make up roughly 1-2% of total marrow cells, flow cytometric analysis was employed to assess helper CD4+ T-cell cytokine expression.

Bone marrow cells were stimulated, and helper $CD4^+$ T-cell intracellular cytokine expression was evaluated (Fig. 16). Corresponding with flow cytometric transcription factor analysis outcomes (Fig. 14) and marrow gene expression findings (Fig. 15), there were no differences in helper $CD4^+$ T-cell intracellular cytokine expression in the marrow of MPF vs. EF mice.

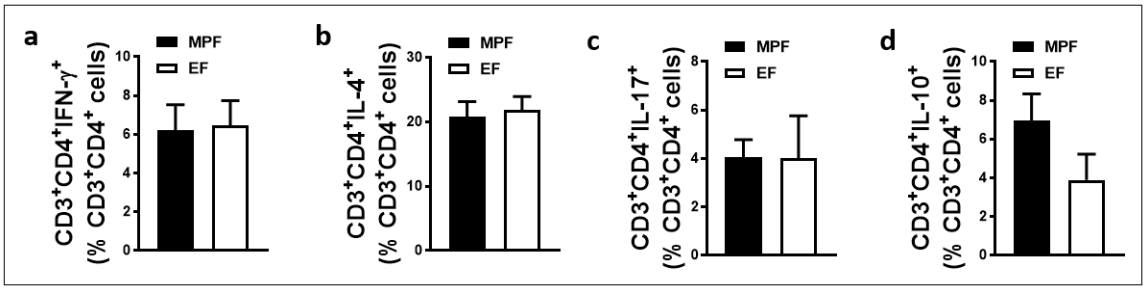

Figure 16: Femoral Marrow Cytokine Stimulation. Nine-week-old MPF & EF mice were euthanized; femoral whole marrow was plated overnight for cytokine activation (eBioscience Cell Stimulation Cocktail, protein transport inhibitors). Cells were isolated and stained (n = 5 / gp) for flow cytometric analysis to assess (a) % $CD3^+CD4^+CD8^-IFN\gamma^+IL4^-IL10^-$ ($CD4^+IFN\gamma^+$) cells, (b) % $CD3^+CD4^+CD8^-IFN\gamma^-IL4^+IL10^-$ ($CD4^+IL4^+$) cells, (c) % $CD3^+CD4^+CD8^-IL17a^+$ ($CD4^+IL17a^+$) cells, (d) % $CD3^+CD4^+CD8^-IFN\gamma^-IL4^-IL10^+$ ($CD4^+IL10^+$) cells. Percentages are expressed relative to $CD3^+CD4^+CD8^-$ cells. Data are reported as mean ± SEM.

CHAPTER 4: CONCLUSIONS AND DISCUSSION

The current study utilized MPF vs. EF mice to investigate differences in commensal microbiota and its implications on immunomodulatory effects. SFB mono-inoculate studies have reported SFB to be host specific with a host specific T_H17 cell response, T_H17 cells increased in the small intestine lamina propria (SI LP), increased IL22 and IL17 production by $CD4^+RORγt^+$ T-cells, increased number of intestinal IgA secreting cells, and higher IgA titers in the intestine and serum [6, 8, 116-119]. The SFB mono-inoculate recapitulates immunologic responses of a complex microbiota, seen in SPF mice, to a full range of CD4+ T-cells like T_H1, T_H2, T_H17, and T_{REG} cells [6, 8]. However, to truly understand how a microbe affects humans the microbe, SFB here, must be studied within a model containing a complex microbiota. The current research study investigated local and distal lymphatic system alterations due to SFB within the healthy gut microbiota. Previously SFB has been reported to influence the helper $CD4^+$ T-cell repertoire and cytokine expression [8, 12, 47]. Seminal research by Ivanov et al. used two groups of SPF mice, one SFB^+, the other SFB^-, and found increased T_H17 cells in the ileum of the mice harboring SFB [6].

The purpose of this study was to determine the influence of SFB on commensal gut microbiota immunomodulatory actions regulating bone modeling in the healthy growing skeleton. The commensal microbiota indirectly impacts bone growth / modeling in health via interactions of immune cells with osteoclasts and osteoblasts [2-4, 95]. Previous research in the Novince lab utilized the SPF vs. GF mouse model to examine commensal gut microbiota immunomodulatory effects on bone remodeling in the healthy young adult skeleton [2]. The current investigation revealed that SFB colonization alters

the commensal gut microbiota's osteoimmune response effects, ultimately having catabolic effects in the healthy growing skeleton.

Interestingly, increased animal weight and tibia length was found in MPF vs. EF mice. A safranin O stain was performed in the proximal tibia growth plate to evaluate endochondral bone formation. Proximal tibia growth plate chondrocyte zone analysis revealed decreased height of the hypertrophic zone in MPF vs. EF mice, and no difference in the proliferative zone or overall height of the growth plate. To investigate the hypertrophic zone of the growth plate, where cartilage is remodeled into bone, Gerber et. al. inhibited vascular endothelial growth factor (VEGF), which led to impaired bone formation, reduced hypertrophic chondrocyte expansion, and decreased blood vessel invasion [100]. They concluded VEGF to mediate vascularization resulting in regulation of the growth plate progression through endochondral ossification via inducing cartilage resorption and bone formation [100]. An investigation using IL6 transgenic mice to model chronic inflammation in the growing skeleton demonstrated impaired growth plate development and epiphyseal ossification [120]. Children with intestinal mucosal inflammation are reported to have an increased risk for growth failure, ending in shorter stature [121]. The endocrine system can contribute to drastic growth retardation as seen in children with defects in IGF1, IGF1R, and IGF2 [122]. It is possible that the increased tibia length and decreased hypertrophic zone in MPF vs. EF mice could be due to decreased VEGF mediated vascularization, decreased growth plate development due to increased inflammation, increased IGF1 expression in MPF vs. EF mice, or a combination of effects.

There is limited literature investigating the impact of commensal microbes on endochondral bone formation. Most studies investigate malnourished children, their gut

microbiota, and longitudinal growth. One study in south India found increased percent relative abundance of Bacteroidetes phylum and enriched inflammatory taxa, *Desulfovibrio* genus and Campylobacterales order, in children with stunted growth, but the control children had more probiotic *Bifidobacterium longum* and *Lactobacillus mucosae* [123]. Another study transplanted the gut microbiota of healthy and malnourished children into GF mice [124]. The microbiota from the healthy children rescued the harmful effects causing stunted growth by the malnourished children's microbiota [124]. The current study is unique because it investigates a healthy host's natural microbiota's effects on growth plate endochondral ossification, and this model could be used to further delineate mechanisms of stunted growth phenotypes due to microbiota.

Micro-CT analysis revealed decreased trabecular bone mineral density, bone volume / tissue volume, and trabecular number in the proximal tibia of MPF vs. EF mice. Since micro-CT analysis did not demonstrate significant differences in cortical bone parameters, subsequent investigations focused on the delineating cellular / molecular mechanism mediating the diminished trabecular bone phenotype found in MPF mice. Differences in trabecular bone parameters may be due to alterations in osteoclastogenesis. Histological sections were stained for tartrate resistance acid phosphatase (TRAP) to investigate osteoclast parameters. Osteoclasts can be identified as $TRAP^{+}$ cells with 3 or more nuclei, lining the bone. Histomorphometric analysis showed an increase in the number of osteoclasts lining the trabecular bone perimeter in MPF vs. EF mice. Increased number of osteoclasts per bone perimeter, if active, could result in decreased trabecular bone phenotype in MPF vs. EF mice.

One study examined the impact of the commensal gut microbiota on cortical bone and reported decreased cortical bone thickness in the presence of the gut microbiota to be dependent on NOD1 and NOD2 signaling [5]. Sjogren et. al. also found decreased cortical bone area in GF vs. Conv. mice [4]. Two studies reported that in SPF / Conv. vs. GF mice, the commensal gut microbiota was associated with decreased trabecular bone area fraction (BA/TA), bone volume fraction (BV/TV), bone mineral density and trabecular number [2, 4]. The current study findings of decreased bone area per tissue area, bone volume per tissue volume, trabecular bone mineral density, and trabecular number in MPF vs. EF mice suggests that SFB alone within the commensal microbiota causes similar decreased trabecular bone phenotypes as seen in SPF / Conv. vs. GF mice. Alterations in osteoclastogenesis contribute to changes in trabecular bone parameters. A SPF vs. GF study found increased osteoclast size, osteoclast / bone interface, eroded perimeter of bone perimeter and osteoclasts on eroded perimeter of bone perimeter [2]. A Conv. vs. GF study found increased number of osteoclast per bone perimeter [4]. The increased number of osteoclasts per bone perimeter in MPF vs. EF mice reveals that less drastic differences in microbial composition (for example, the commensal microbiota with and without SFB), can have similar implications in osteoclastogenesis and trabecular bone parameters.

However, bone modeling / remodeling is mediated through dual osteoclast-osteoblast processes, so osteoblastogenesis needed to be investigated as well. Osteoblast mediated bone mineral matrix formation begins with formation of the organic matrix via secretion of collagen type 1 alpha 1 chain (COL1a1), osteocalcin (OCN), osteopontin (OPN), and proteoglycans [60]. Expression of *Col1a1*, a marker for early osteoblast activity, was decreased in the marrow of MPF vs. EF mice. The expression of *Spp1* (*Opn*) and *Bglap* (*Ocn*), bone mineral matrix proteins which are used as markers

for mature osteoblast activity, were similar in the marrow of MPF vs. EF mice [125]. *Igf1* expression, a pro-osteoblastic signaling factor that induces osteoblast proliferation and maturation, was increased in the marrow of MPF vs. EF mice [58, 64]. Osteoblastic cells express IGF1 in the local marrow environment, but it is important to note that the liver secretes 70% of circulating IGF1 [126]. The enhanced *Col1a1* in the marrow of EF vs. MPF mice implies that EF mice have a pro-osteoblastic phenotype, which potentially is mediated by up-regulated liver-derived IGF1. Future studies are necessary to discern differences in liver-derived IGF1 and circulating IGF-1 levels in MPF vs. EF mice. The decreased trabecular bone parameters may be due to decreased early osteoblast activity in MPF vs. EF marrow and no differences in mature osteoblast activity. When tissues are decalcified for paraffin embedding, the mineralization and osteoblast cellular outcomes of bone are lost or drastically altered. Future studies utilizing methyl methacrylate (MMA) histomorphology will allow for undecalcified tissues to be analyzed, and more extensive histology studies can investigate the osteoblast side of bone homeostasis.

Previous studies in C57BL/6 SPF vs. GF mice have reported an association between the commensal microbiota, decreased osteoblastic function/differentiation potential, increased bone marrow stromal cells' (BMSCs) immunomodulatory actions, and decreased serum IGF1 [2, 3]. These differences are hypothesized to be due to local bone IGF1 suppression in SPF vs. GF mice. Studies with BALB/c and CB6F1 mice reported conflicting findings with increased skeletal growth via augmented liver IGF1 in serum in the presence of commensals [95, 96]. The commensal gut microbiota's ability to influence skeletal tissue derived IGF1 may be influenced by the genetics of the mice studied, suggesting the commensal gut microbiota's effects on IGF1 modulation to be genetically influenced and the cause of phenotypical differences in osteoimmunological

outcomes. The current study utilized C57BL/6, MPF vs. EF mice and found increased *Igf1* expression in marrow correlated with decreased trabecular parameters. However, no osteoblast cellular outcomes were obtained. It should be noted that the difference in *Igf1* expression was very slight and may not be clinically significant. MMA histomorphometry and serum protein studies need to be executed to determine if circulating IGF1 differences are impacting the osteoblastic phenotype.

To further investigate mechanisms mediating the increased number of osteoclasts lining the trabecular bone in MPF vs. EF mice, expression of osteoclast related genes was assessed. Osteoclastogenic studies using inflammatory disease models have shown that inflammatory cytokines indirectly regulate the RANK / RANKL / OPG axis leading to osteoclastogenesis modulation [71, 91, 127-130]. Previous investigations have found the gut microbiota to cause a trend towards an increase in the RANKL / OPG axis in SPF vs. GF mice and increased RANKL in the bone of Conv. vs. GF mice [2, 5]. When RANK on osteoclast lineage cells is stimulated by RANKL, proteins are recruited to translate the transcription factor NFATc1 [103-106]. Activation of the osteoclast differentiation master regulator, NFATc1, drives expression of essential osteoclast genes like TRAP, Cathepsin K, and calcitonin receptor [77, 107-110]. Expression of *Tnfsf11* (RANKL) and *Tnfrsf11b* (OPG), the decoy receptor for RANKL, was similar in the marrow of MPF vs. EF mice. However, the expression of *Nfatc1*, the master regulator of osteoclastogenesis, was increased in the marrow of MPF vs. EF mice which can lead to increased osteoclastogenesis.

Genes related to inflammatory states and microbial responses were augmented in the MPF vs. EF mouse long bone marrow. Specifically, RNA of different components of the TLR4 signaling pathway, *Lbp, Ly96, and Tlr4,* were all up in MPF vs. EF mice. Genetically engineered gene fusion proteins of SFB flagellins have been reported to

activate NFκB via the pattern recognition receptor (PRR), TLR5 response [131]. Flagellin binding to TLR5 on intestinal dendritic cells has been found to induce IgA and T_H17 cell differentiation [132, 133]. It is possible that SFBs induction of TH17 cells and IgA responses is due to its flagella binding to and inducing responses by TLRs. Studies in mice have found that activation of TLR4 expressed on osteoblasts leads to the expression of catabolic factors like RANKL, M-CSF, and other inflammatory cytokines, leading to decreased osteoblast differentiation and increased osteoclast maturation and activity [31-38]. It is possible that the increased TLR4 signaling is contributing to the decrease in early osteoblast activity and increase in number of osteoclast per bone perimeter.

One study examining the role of pattern recognition receptors (PRRs) influenced by the commensal gut microbiota and the impacts in skeletogenesis was executed in TLR5KO vs. C57BL/6 wild type (WT) mice treated with antibiotic vs. untreated [134]. Guss et. al. concluded that antibiotic disruption of the gut microbiota during growth (4-16 weeks old) led to no change in bone cross-sectional geometry but decreased bone mechanical properties determined by decreased femur bending strength [134]. Another important PRR, gut microbiota, and skeletogenesis study used GF vs. Conv. mice with inactivated MYD88 $^{-/-}$, NOD1 $^{-/-}$, or NOD2 $^{-/-}$ [5]. Ohlsson et. al determined the gut microbiota's effects on skeletogenesis, decreased bone mass and increased bone *Tnf* and *Rankl*, to be dependent on NOD1 and NOD2 signaling [5]. Novince et. al. investigated the commensal microbiomes' ability to modulate catabolic effects on skeletogenesis in conjunction with alterations of TLR signaling in the liver [2]. Increased expression of TLR2 signaling components were found in the livers of SPF vs. GF mice [2]. The current study is important in the advancement of research assessing the role of PRRs in response to commensal microbes and the effects on skeletogenesis because

expression of TLR signaling components were looked at in the marrow environment. Further research needs to be done in other microbial murine model systems, like SPF and SFB mono-inoculate vs. GF mice, to determine to what extent the commensals impact on PRRs impacts skeletal tissues.

Another novel finding no known studies have investigated the commensal microbiota with and without SFB, and the impact on IL18 in the marrow. A cytokine that is released in response to TLR4 signaling, *Il18* RNA was expressed at higher levels in the marrow of MPF vs. EF mice [135, 136]. Studies have reported IL18 to inhibit osteoclastogenesis and, when present with TNF, to cause osteoclast apoptosis [137-139]. The number of osteoclasts per bone perimeter was increased and the trabecular parameters were decreased in MPF vs. EF mice, which suggests inefficient inhibition of osteoclastogenesis by IL18 possibly due to osteoclast activity. When IL18 and IL12 are both secreted in response to LPS, they stimulate cells to release IFNγ, which is a potent inflammatory cytokine when released in relatively high amounts [135, 136]. Secreted IFNγ activates cells like macrophages to respond to the microbial fragments, recruits peripheral natural killer cells to the site of infection, and increases the secretion of other chemokines [135].

Recognizing that the field of osteoimmunology has shown that T-cells and B-cells critically regulate osteoclast-osteoblast mediated processes in the developing skeleton, flow cytometric analysis was employed to delineate alterations in these lymphocytic cell populations [51, 52, 54]. The presence of SFB in the ileum has been shown to increase T_H17 / IL-17 mediated gut mucosal immunity, and to have impacts distal from the gut on skeletal processes and other organ systems [6, 140]. Increased *Il17* mRNA expression found in the ileums of MPF vs. EF mice confirms findings of other studies that SFB

colonization enhances TH17 / IL17 mediated immunity in local gut tissues [7, 10, 11]. Studies on disease states like autoimmune arthritis, estrogen depleted menopausal states, and inflammatory bowel disease have shown that up-regulation of Th17 / IL-17 has catabolic effects on bone [109, 161-163]. Investigations on Th17 / IL-17 effects on skeletal development in health, done previously in the Novince lab, found up-regulated Th17 / IL-17 and a decreased bone mass phenotype in SPF compared to GF mice [2]. This suggests the commensal microbiome has catabolic effects on bone in health. Stimulation by IL17 promotes RANKL expression by osteoblasts which increases osteoclastogenesis leading to decreased bone parameters [58, 89].

Most studies on the impact of SFB modulation of the immune system focus on gut immunity, specifically the small intestine lamina propria [6, 8]. Our study agrees with previous reports that the presence of SFB in the murine gut has minimal impact on $CD4^+$ T helper cell subsets in the mLNs and spleen [141]. The mLNs are thought to be a site where $CD4^+$ T-cells differentiate because antigen presenting cells like dendritic cells and macrophages migrate to the mLNs from the gut along with naïve $CD4^+$ T-cells to reach the secondary and tertiary lymphoid organs, like Peyer's patches and SI LP, in the gut [142-146]. However, a study using Jackson B6 mice found SFB induced T_H17 cell differentiation to occur in the SI LP independent of the mLNs, which may explain why there was no difference in T_H17 cell frequency in MPF vs. EF mice mLNs but increased *Il17* mRNA expression in the ileum [141].

Studies investigating the effects of T_H17 cells or IL17 in the bone marrow have mostly been bone in inflammatory disease murine models for rheumatoid arthritis (RA) and inflammatory bowel disease (IBD) [89, 147-149]. Novince et. al. investigated the commensal gut microbiota's impact on the healthy skeleton due to T_H17 / IL17

modulation and found augmented T_H17 / Il17 in marrow and a diminished bone mass phenotype in SPF vs. GF mice [2]. In the current health study, no differences were seen in MPF vs. EF marrow in T_H17 cell frequency, *Il17* mRNA expression, or $CD3^+CD4^+IL17^+$ cells post cell stimulation.

Spleen T_H1 cells were increased, and the characteristic cytokine for T_H1 cells, *Ifnγ,* was trending towards an increase in MPF vs. EF mice. IFNγ has pro-inflammatory effects when secreted in high amounts, and inflammation has been shown to have catabolic effects on bone. IFNγ has been reported to increase fusion of osteoclasts and the resorption activity of fused osteoclasts [150]. In the spleen, there was decreased *Il4* expression, the characteristic cytokine of T_H2 cells, and T_H2 cells were trending towards decreased frequency in MPF vs. EF mice. IL4 inhibits NFκB signaling, which leads to RANKL and TNF induced osteoclastogenesis inhibition [151, 152]. IL4 also decreases the synthesis of pro-inflammatory and osteoclastic genes like TNF, IL1 and IL6 [152, 153]. So, decreased *Il4* expression in MPF vs. EF mice would suggest less osteoclast inhibition by IL4, which is also evident in the decreased trabecular parameters and increased number of osteoclast per bone perimeter in MPF vs. EF mice. In MPF vs. EF mLNs there were increased cytotoxic $CD8^+$ T-cells and decreased helper $CD4^+$ T-cells, but no differences in helper $CD4^+$ T-cell subsets. One study using autoimmune arthritic mouse models to study SFB's impact on the disease found major differences in helper $CD4^+$ T-cell tuning mainly in the gut, but not in the mLNs or spleen, which was also in MPF vs. EF mice, with few helper $CD4^+$ T-cell changes observed at distal sites from the ileum [115]. A study using SFB mono-inoculates and GF mice found increased T_H1, T_H2, T_H17, and T_{REG} immune responses in isolated lamina propria lymphocytes of SFB colonized mice [8]. They also found slight increases in gut $CD25^+FOXP3^+$ T_{REG} cells and IL10-secreting $CD4^+$ T cells in mice harboring SFB, as well as drastically more IL17

producing $CD4^+TCR\alpha\beta^+$ cells [8]. In the current study, a trend towards decreased $\gamma\delta^+$ T-cells and activated helper $CD4^+$ T-cells was seen in the femur marrow of MPF vs. EF mice. Increased T_H17, T_H1, and double positive T-cells have been found in the spinal cords of EAE mice colonized with SFB [12]. However, in the marrow of MPF and EF mice, the frequency of helper CD4+ T-cell subsets was similar with no difference seen after cell stimulation. The cytotoxic $CD8^+$ T-cell subsets and their characteristic cytokines need to be further investigated to determine if changes in their composition is also causing effects in sites far from the ileum like spleen, mLNs, and marrow. Future studies should also investigate the systemic changes in cytokines via serum protein assays.

Bone growth is due to longitudinal endochondral ossification at the growth plate and osteoblast mineralization [154]. This study investigated alterations in the commensal gut microbiota, like the impact of SFB within the commensal gut microbiotas effects on osteoimmunology. The results suggest that even a single gut microbial difference can lead to decreased trabecular bone area per tissue area, bone volume per tissue volume, bone mineral density, and trabecular number as well as increased osteoclast number per bone perimeter. Pro-inflammatory, pro-osteoclastic gene expression, like decreased *Il4,* increased *Nfatc1, Il18, Tlr4, Lbp,* and *Ly96* was evident in MPF vs. EF mice. Both murine models used in this study, MPF and EF, are health models with a healthy gut microbial composition. The impact of SFB on immunity is being researched in many different fields, but research in skeletal growth and development is lacking. Future research needs to be done on how SFB's immunomodulation regulates osteoimmune interactions in healthy skeletal development/growth. The MPF vs. EF model should be utilized to further evaluate osteoblast cellular outcomes via MMA histomorphometry and bone marrow stromal cell Von Kossa, cell expansion, and differentiation potential *in vitro* assays. Osteoclast *in vitro* assays investigating differences in the osteoclast precursor

differentiation potential should also be executed to answer questions about SFB's potential to change pre-osteoclasts differentiation potential and function. Other future investigations should be carried out in SFB mono-inoculate vs. GF mice to delineate the impact SFB alone has on skeletogenesis. This model could be used for *in vitro* assays as well as *in vivo* assays*.* The *in vivo* assays should focus on SFB's immunomodulation in the skeletal tissue and marrow environment. Research has found the commensal microbiota to significantly impact bone growth / remodeling in health and disease [2-4, 53, 85, 94]. However, more research is needed on effects on skeletal processes by the microbe, SFB, in a complex healthy commensal environment. Outcomes from this study imply that limiting specific microbial colonizers, like SFB, post-weaning may be beneficial for maximum bone mass accrual in childhood. Pre-biotics could be administered to children to limit the expansion of microbiota, like SFB, by increasing competition via enhanced growth of other beneficial microorganisms like Bifidobacterium. Patients who are predisposed to diseases associated with low bone mass could benefit from therapeutic interventions via pre-biotics or pro-biotics to decrease microbes that limit bone mass accrual in adolescence to allow for greater bone mass apposition.

REFERENCES

1. Sommer, F. and F. Backhed, *The gut microbiota--masters of host development and physiology.* Nat Rev Microbiol, 2013. **11**(4): p. 227-38.
2. Novince, C.M., et al., *Commensal Gut Microbiota Immunomodulatory Actions in Bone Marrow and Liver have Catabolic Effects on Skeletal Homeostasis in Health.* Sci Rep, 2017. **7**(1): p. 5747.
3. Xiao, E., et al., *Microbiota regulates bone marrow mesenchymal stem cell lineage differentiation and immunomodulation.* Stem Cell Res Ther, 2017. **8**(1): p. 213.
4. Sjogren, K., et al., *The gut microbiota regulates bone mass in mice.* J Bone Miner Res, 2012. **27**(6): p. 1357-67.
5. Ohlsson, C., et al., *Regulation of bone mass by the gut microbiota is dependent on NOD1 and NOD2 signaling.* Cell Immunol, 2017. **317**: p. 55-58.
6. Ivanov, II, et al., *Induction of intestinal Th17 cells by segmented filamentous bacteria.* Cell, 2009. **139**(3): p. 485-98.
7. Talham, G.L., et al., *Segmented filamentous bacteria are potent stimuli of a physiologically normal state of the murine gut mucosal immune system.* Infect Immun, 1999. **67**(4): p. 1992-2000.
8. Gaboriau-Routhiau, V., et al., *The key role of segmented filamentous bacteria in the coordinated maturation of gut helper T cell responses.* Immunity, 2009. **31**(4): p. 677-89.
9. Goto, Y., et al., *Segmented filamentous bacteria antigens presented by intestinal dendritic cells drive mucosal Th17 cell differentiation.* Immunity, 2014. **40**(4): p. 594-607.
10. Yang, Y., et al., *Focused specificity of intestinal TH17 cells towards commensal bacterial antigens.* Nature, 2014. **510**(7503): p. 152-6.
11. Wu, H.J., et al., *Gut-residing segmented filamentous bacteria drive autoimmune arthritis via T helper 17 cells.* Immunity, 2010. **32**(6): p. 815-27.
12. Lee, Y.K., et al., *Proinflammatory T-cell responses to gut microbiota promote experimental autoimmune encephalomyelitis.* Proc Natl Acad Sci U S A, 2011. **108 Suppl 1**: p. 4615-22.
13. Kriegel, M.A., et al., *Naturally transmitted segmented filamentous bacteria segregate with diabetes protection in nonobese diabetic mice.* Proc Natl Acad Sci U S A, 2011. **108**(28): p. 11548-53.
14. Yin, Y., et al., *Comparative analysis of the distribution of segmented filamentous bacteria in humans, mice and chickens.* ISME J, 2013. **7**(3): p. 615-21.
15. Thaiss, C.A., et al., *The microbiome and innate immunity.* Nature, 2016. **535**(7610): p. 65-74.
16. Rakoff-Nahoum, S., et al., *Recognition of commensal microflora by toll-like receptors is required for intestinal homeostasis.* Cell, 2004. **118**(2): p. 229-41.
17. Slack, E., et al., *Innate and adaptive immunity cooperate flexibly to maintain host-microbiota mutualism.* Science, 2009. **325**(5940): p. 617-20.
18. Nigro, G., et al., *The cytosolic bacterial peptidoglycan sensor Nod2 affords stem cell protection and links microbes to gut epithelial regeneration.* Cell Host Microbe, 2014. **15**(6): p. 792-8.
19. Sanos, S.L., et al., *RORgammat and commensal microflora are required for the differentiation of mucosal interleukin 22-producing NKp46+ cells.* Nat Immunol, 2009. **10**(1): p. 83-91.

20. Bouskra, D., et al., *Lymphoid tissue genesis induced by commensals through NOD1 regulates intestinal homeostasis.* Nature, 2008. **456**(7221): p. 507-10.
21. Janssens, S. and R. Beyaert, *Role of Toll-like receptors in pathogen recognition.* Clin Microbiol Rev, 2003. **16**(4): p. 637-46.
22. Janeway, C.A., Jr., *Approaching the asymptote? Evolution and revolution in immunology.* Cold Spring Harb Symp Quant Biol, 1989. **54 Pt 1**: p. 1-13.
23. Murphy K., T.P., Walport M., Janeway C., *Chapter 3: The induced responses of innate immunity*, in *Janeway's immunobiology (8th edition)*. 2012, Garland Science: New York.
24. Gangloff, M., *Different dimerisation mode for TLR4 upon endosomal acidification?* Trends Biochem Sci, 2012. **37**(3): p. 92-8.
25. Akira, S. and K. Takeda, *Functions of toll-like receptors: lessons from KO mice.* C R Biol, 2004. **327**(6): p. 581-9.
26. Akira, S. and K. Takeda, *Toll-like receptor signalling.* Nat Rev Immunol, 2004. **4**(7): p. 499-511.
27. Takeda, K. and S. Akira, *TLR signaling pathways.* Semin Immunol, 2004. **16**(1): p. 3-9.
28. Poltorak, A., et al., *Defective LPS signaling in C3H/HeJ and C57BL/10ScCr mice: mutations in Tlr4 gene.* Science, 1998. **282**(5396): p. 2085-8.
29. Shimazu, R., et al., *MD-2, a molecule that confers lipopolysaccharide responsiveness on Toll-like receptor 4.* J Exp Med, 1999. **189**(11): p. 1777-82.
30. Akira, S., S. Uematsu, and O. Takeuchi, *Pathogen recognition and innate immunity.* Cell, 2006. **124**(4): p. 783-801.
31. Kikuchi, T., et al., *Gene expression of osteoclast differentiation factor is induced by lipopolysaccharide in mouse osteoblasts via Toll-like receptors.* J Immunol, 2001. **166**(5): p. 3574-9.
32. Zou, W., A. Amcheslavsky, and Z. Bar-Shavit, *CpG oligodeoxynucleotides modulate the osteoclastogenic activity of osteoblasts via Toll-like receptor 9.* J Biol Chem, 2003. **278**(19): p. 16732-40.
33. Nemoto, E., et al., *Expression of functional Toll-like receptors and nucleotide-binding oligomerization domain proteins in murine cementoblasts and their upregulation during cell differentiation.* J Periodontal Res, 2008. **43**(5): p. 585-93.
34. Inada, M., et al., *Membrane-bound prostaglandin E synthase-1-mediated prostaglandin E2 production by osteoblast plays a critical role in lipopolysaccharide-induced bone loss associated with inflammation.* J Immunol, 2006. **177**(3): p. 1879-85.
35. Nakao, J., et al., *Low-intensity pulsed ultrasound (LIPUS) inhibits LPS-induced inflammatory responses of osteoblasts through TLR4-MyD88 dissociation.* Bone, 2014. **58**: p. 17-25.
36. Bandow, K., et al., *Molecular mechanisms of the inhibitory effect of lipopolysaccharide (LPS) on osteoblast differentiation.* Biochem Biophys Res Commun, 2010. **402**(4): p. 755-61.
37. Liu, J., et al., *Molecular mechanism of the bifunctional role of lipopolysaccharide in osteoclastogenesis.* J Biol Chem, 2009. **284**(18): p. 12512-23.
38. Itoh, K., et al., *Lipopolysaccharide promotes the survival of osteoclasts via Toll-like receptor 4, but cytokine production of osteoclasts in response to lipopolysaccharide is different from that of macrophages.* J Immunol, 2003. **170**(7): p. 3688-95.

39. Kondo, T., et al., *T cell-dependent acceleration of chemoattractant cytokine gene expression during secondary rejection of allogeneic skin grafts.* Transplantation, 1997. **63**(5): p. 732-42.
40. Hirose, J., et al., *A developing picture of lymphopoiesis in bone marrow.* Immunol Rev, 2002. **189**: p. 28-40.
41. Takahama, Y., *Journey through the thymus: stromal guides for T-cell development and selection.* Nat Rev Immunol, 2006. **6**(2): p. 127-35.
42. Jenkinson, E.J., et al., *The thymus and T-cell commitment: the right niche for Notch?* Nat Rev Immunol, 2006. **6**(7): p. 551-5.
43. Hedrick, S.M., *Thymus lineage commitment: a single switch.* Immunity, 2008. **28**(3): p. 297-9.
44. Alberts B, J.A., Lewis J, et al., *The Adaptive Immune System*, in *Molecular Biology of the Cell. 4th edition*, N.Y.G. Science, Editor. 2002.
45. Raphael, I., et al., *T cell subsets and their signature cytokines in autoimmune and inflammatory diseases.* Cytokine, 2015. **74**(1): p. 5-17.
46. Sun B., Z.Y., *Overview of Orchestration of CD4+ T Cell Subsets in Immune Responses*, in *T Helper Cell Differentiation and Their Function*, I.S.B. (eds), Editor. 2014, Springer, Dordrecht: Advances in Experimental Medicine and Biology. p. 1-13.
47. Belkaid, Y. and O.J. Harrison, *Homeostatic Immunity and the Microbiota.* Immunity, 2017. **46**(4): p. 562-576.
48. Round, J.L. and S.K. Mazmanian, *The gut microbiota shapes intestinal immune responses during health and disease.* Nat Rev Immunol, 2009. **9**(5): p. 313-23.
49. Farkas, A.M., et al., *Induction of Th17 cells by segmented filamentous bacteria in the murine intestine.* J Immunol Methods, 2015. **421**: p. 104-11.
50. Umesaki, Y., et al., *Segmented filamentous bacteria are indigenous intestinal bacteria that activate intraepithelial lymphocytes and induce MHC class II molecules and fucosyl asialo GM1 glycolipids on the small intestinal epithelial cells in the ex-germ-free mouse.* Microbiol Immunol, 1995. **39**(8): p. 555-62.
51. Li, Y., et al., *B cells and T cells are critical for the preservation of bone homeostasis and attainment of peak bone mass in vivo.* Blood, 2007. **109**(9): p. 3839-48.
52. Pacifici, R., *T cells: critical bone regulators in health and disease.* Bone, 2010. **47**(3): p. 461-71.
53. Zaidi, M., *Skeletal remodeling in health and disease.* Nat Med, 2007. **13**(7): p. 791-801.
54. Lorenzo, J., M. Horowitz, and Y. Choi, *Osteoimmunology: interactions of the bone and immune system.* Endocr Rev, 2008. **29**(4): p. 403-40.
55. Takayanagi, H., *Osteoimmunology and the effects of the immune system on bone.* Nat Rev Rheumatol, 2009. **5**(12): p. 667-76.
56. Boyce, B.F. and L. Xing, *Functions of RANKL/RANK/OPG in bone modeling and remodeling.* Arch Biochem Biophys, 2008. **473**(2): p. 139-46.
57. Ducy, P., et al., *Osf2/Cbfa1: a transcriptional activator of osteoblast differentiation.* Cell, 1997. **89**(5): p. 747-54.
58. Nakashima, K., et al., *The novel zinc finger-containing transcription factor osterix is required for osteoblast differentiation and bone formation.* Cell, 2002. **108**(1): p. 17-29.
59. Glass, D.A., 2nd, et al., *Canonical Wnt signaling in differentiated osteoblasts controls osteoclast differentiation.* Dev Cell, 2005. **8**(5): p. 751-64.

60. Florencio-Silva, R., et al., *Biology of Bone Tissue: Structure, Function, and Factors That Influence Bone Cells.* Biomed Res Int, 2015. **2015**: p. 421746.
61. Anderson, H.C., *Matrix vesicles and calcification.* Curr Rheumatol Rep, 2003. **5**(3): p. 222-6.
62. Yoshiko, Y., et al., *Osteoblast autonomous Pi regulation via Pit1 plays a role in bone mineralization.* Mol Cell Biol, 2007. **27**(12): p. 4465-74.
63. Arana-Chavez, V.E., A.M. Soares, and E. Katchburian, *Junctions between early developing osteoblasts of rat calvaria as revealed by freeze-fracture and ultrathin section electron microscopy.* Arch Histol Cytol, 1995. **58**(3): p. 285-92.
64. Celil, A.B. and P.G. Campbell, *BMP-2 and insulin-like growth factor-I mediate Osterix (Osx) expression in human mesenchymal stem cells via the MAPK and protein kinase D signaling pathways.* J Biol Chem, 2005. **280**(36): p. 31353-9.
65. Kimble, R.B., et al., *Estrogen deficiency increases the ability of stromal cells to support murine osteoclastogenesis via an interleukin-1and tumor necrosis factor-mediated stimulation of macrophage colony-stimulating factor production.* J Biol Chem, 1996. **271**(46): p. 28890-7.
66. Kitazawa, R., et al., *Interleukin-1 receptor antagonist and tumor necrosis factor binding protein decrease osteoclast formation and bone resorption in ovariectomized mice.* J Clin Invest, 1994. **94**(6): p. 2397-406.
67. Pacifici, R., et al., *Effect of surgical menopause and estrogen replacement on cytokine release from human blood mononuclear cells.* Proc Natl Acad Sci U S A, 1991. **88**(12): p. 5134-8.
68. Lacey, D.L., et al., *Osteoprotegerin ligand is a cytokine that regulates osteoclast differentiation and activation.* Cell, 1998. **93**(2): p. 165-76.
69. Ash, P., J.F. Loutit, and K.M. Townsend, *Osteoclasts derived from haematopoietic stem cells.* Nature, 1980. **283**(5748): p. 669-70.
70. Walsh, M.C. and Y. Choi, *Biology of the RANKL-RANK-OPG System in Immunity, Bone, and Beyond.* Front Immunol, 2014. **5**: p. 511.
71. Takayanagi, H., et al., *T-cell-mediated regulation of osteoclastogenesis by signalling cross-talk between RANKL and IFN-gamma.* Nature, 2000. **408**(6812): p. 600-5.
72. Yoshida, H., et al., *The murine mutation osteopetrosis is in the coding region of the macrophage colony stimulating factor gene.* Nature, 1990. **345**(6274): p. 442-4.
73. Lagasse, E. and I.L. Weissman, *Enforced expression of Bcl-2 in monocytes rescues macrophages and partially reverses osteopetrosis in op/op mice.* Cell, 1997. **89**(7): p. 1021-31.
74. Simonet, W.S., et al., *Osteoprotegerin: a novel secreted protein involved in the regulation of bone density.* Cell, 1997. **89**(2): p. 309-19.
75. Yasuda, H., et al., *Identity of osteoclastogenesis inhibitory factor (OCIF) and osteoprotegerin (OPG): a mechanism by which OPG/OCIF inhibits osteoclastogenesis in vitro.* Endocrinology, 1998. **139**(3): p. 1329-37.
76. Yasuda, H., et al., *Osteoclast differentiation factor is a ligand for osteoprotegerin/osteoclastogenesis-inhibitory factor and is identical to TRANCE/RANKL.* Proc Natl Acad Sci U S A, 1998. **95**(7): p. 3597-602.
77. Takayanagi, H., et al., *Induction and activation of the transcription factor NFATc1 (NFAT2) integrate RANKL signaling in terminal differentiation of osteoclasts.* Dev Cell, 2002. **3**(6): p. 889-901.
78. Weitzmann, M.N., *Bone and the Immune System.* Toxicol Pathol, 2017. **45**(7): p. 911-924.

79. Nakamura, I. and E. Jimi, *Regulation of osteoclast differentiation and function by interleukin-1.* Vitam Horm, 2006. **74**: p. 357-70.
80. Lu, X., et al., *Transcriptional regulation of the osterix (Osx, Sp7) promoter by tumor necrosis factor identifies disparate effects of mitogen-activated protein kinase and NF kappa B pathways.* J Biol Chem, 2006. **281**(10): p. 6297-306.
81. Lee, S.K., et al., *1,25(OH)2 vitamin D3-stimulated osteoclast formation in spleen-osteoblast cocultures is mediated in part by enhanced IL-1 alpha and receptor activator of NF-kappa B ligand production in osteoblasts.* J Immunol, 2002. **169**(5): p. 2374-80.
82. Polzer, K., et al., *Interleukin-1 is essential for systemic inflammatory bone loss.* Ann Rheum Dis, 2010. **69**(1): p. 284-90.
83. Weitzmann, M.N. and R. Pacifici, *The role of T lymphocytes in bone metabolism.* Immunol Rev, 2005. **208**: p. 154-68.
84. Lacativa, P.G. and M.L. Farias, *Osteoporosis and inflammation.* Arq Bras Endocrinol Metabol, 2010. **54**(2): p. 123-32.
85. Redlich, K. and J.S. Smolen, *Inflammatory bone loss: pathogenesis and therapeutic intervention.* Nat Rev Drug Discov, 2012. **11**(3): p. 234-50.
86. Weitzmann, M.N., et al., *Interleukin-7 stimulates osteoclast formation by up-regulating the T-cell production of soluble osteoclastogenic cytokines.* Blood, 2000. **96**(5): p. 1873-8.
87. Okamoto, K., et al., *Osteoimmunology: The Conceptual Framework Unifying the Immune and Skeletal Systems.* Physiol Rev, 2017. **97**(4): p. 1295-1349.
88. Shen, F., et al., *Cytokines link osteoblasts and inflammation: microarray analysis of interleukin-17- and TNF-alpha-induced genes in bone cells.* J Leukoc Biol, 2005. **77**(3): p. 388-99.
89. Kotake, S., et al., *IL-17 in synovial fluids from patients with rheumatoid arthritis is a potent stimulator of osteoclastogenesis.* J Clin Invest, 1999. **103**(9): p. 1345-52.
90. Van bezooijen, R.L., et al., *Interleukin-17: A new bone acting cytokine in vitro.* J Bone Miner Res, 1999. **14**(9): p. 1513-21.
91. Lubberts, E., et al., *IL-17 promotes bone erosion in murine collagen-induced arthritis through loss of the receptor activator of NF-kappa B ligand/osteoprotegerin balance.* J Immunol, 2003. **170**(5): p. 2655-62.
92. Bouillon, R., et al., *The past 10 years-new hormones, new functions, new endocrine organs.* Nat Rev Endocrinol, 2015. **11**(11): p. 681-6.
93. Zhang, Q., R.C. Riddle, and T.L. Clemens, *Bone and the regulation of global energy balance.* J Intern Med, 2015. **277**(6): p. 681-9.
94. Weitzmann, M.N. and I. Ofotokun, *Physiological and pathophysiological bone turnover - role of the immune system.* Nat Rev Endocrinol, 2016. **12**(9): p. 518-32.
95. Yan, J., et al., *Gut microbiota induce IGF-1 and promote bone formation and growth.* Proc Natl Acad Sci U S A, 2016. **113**(47): p. E7554-E7563.
96. Schwarzer, M., et al., *Lactobacillus plantarum strain maintains growth of infant mice during chronic undernutrition.* Science, 2016. **351**(6275): p. 854-7.
97. Rauch, F., *Bone growth in length and width: the Yin and Yang of bone stability.* J Musculoskelet Neuronal Interact, 2005. **5**(3): p. 194-201.
98. Abad, V., et al., *The role of the resting zone in growth plate chondrogenesis.* Endocrinology, 2002. **143**(5): p. 1851-7.
99. Fazzalari, N.L., et al., *Quantitative analysis of trabecular morphogenesis in the human costochondral junction during the postnatal period in normal subjects.* Anat Rec, 1997. **248**(1): p. 1-12.

100. Gerber, H.P., et al., *VEGF couples hypertrophic cartilage remodeling, ossification and angiogenesis during endochondral bone formation.* Nat Med, 1999. **5**(6): p. 623-8.
101. Dempster, D.W., et al., *Standardized nomenclature, symbols, and units for bone histomorphometry: a 2012 update of the report of the ASBMR Histomorphometry Nomenclature Committee.* J Bone Miner Res, 2013. **28**(1): p. 2-17.
102. Novince, C.M., et al., *Proteoglycan 4: a dynamic regulator of skeletogenesis and parathyroid hormone skeletal anabolism.* J Bone Miner Res, 2012. **27**(1): p. 11-25.
103. Asagiri, M., et al., *Autoamplification of NFATc1 expression determines its essential role in bone homeostasis.* J Exp Med, 2005. **202**(9): p. 1261-9.
104. Matsuo, K., et al., *Nuclear factor of activated T-cells (NFAT) rescues osteoclastogenesis in precursors lacking c-Fos.* J Biol Chem, 2004. **279**(25): p. 26475-80.
105. Cao, H., et al., *Activating transcription factor 4 regulates osteoclast differentiation in mice.* J Clin Invest, 2010. **120**(8): p. 2755-66.
106. Maruyama, K., et al., *The transcription factor Jdp2 controls bone homeostasis and antibacterial immunity by regulating osteoclast and neutrophil differentiation.* Immunity, 2012. **37**(6): p. 1024-36.
107. Hirotani, H., et al., *The calcineurin/nuclear factor of activated T cells signaling pathway regulates osteoclastogenesis in RAW264.7 cells.* J Biol Chem, 2004. **279**(14): p. 13984-92.
108. Matsumoto, M., et al., *Essential role of p38 mitogen-activated protein kinase in cathepsin K gene expression during osteoclastogenesis through association of NFATc1 and PU.1.* J Biol Chem, 2004. **279**(44): p. 45969-79.
109. Kim, K., et al., *Nuclear factor of activated T cells c1 induces osteoclast-associated receptor gene expression during tumor necrosis factor-related activation-induced cytokine-mediated osteoclastogenesis.* J Biol Chem, 2005. **280**(42): p. 35209-16.
110. Kim, Y., et al., *Contribution of nuclear factor of activated T cells c1 to the transcriptional control of immunoreceptor osteoclast-associated receptor but not triggering receptor expressed by myeloid cells-2 during osteoclastogenesis.* J Biol Chem, 2005. **280**(38): p. 32905-13.
111. Ivanov, II, et al., *Specific microbiota direct the differentiation of IL-17-producing T-helper cells in the mucosa of the small intestine.* Cell Host Microbe, 2008. **4**(4): p. 337-49.
112. Qiu, J., et al., *Group 3 innate lymphoid cells inhibit T-cell-mediated intestinal inflammation through aryl hydrocarbon receptor signaling and regulation of microflora.* Immunity, 2013. **39**(2): p. 386-99.
113. Stepankova, R., et al., *Segmented filamentous bacteria in a defined bacterial cocktail induce intestinal inflammation in SCID mice reconstituted with CD45RBhigh CD4+ T cells.* Inflamm Bowel Dis, 2007. **13**(10): p. 1202-11.
114. Lecuyer, E., et al., *Segmented filamentous bacterium uses secondary and tertiary lymphoid tissues to induce gut IgA and specific T helper 17 cell responses.* Immunity, 2014. **40**(4): p. 608-20.
115. Chappert, P., *Role of SFB in autoimmune arthritis: an example of regulation of autoreactive T cell sensitivity in the gut.* Gut Microbes, 2014. **5**(2): p. 259-64.
116. Atarashi, K., et al., *Th17 Cell Induction by Adhesion of Microbes to Intestinal Epithelial Cells.* Cell, 2015. **163**(2): p. 367-80.

117. Ericsson, A.C., et al., *Segmented filamentous bacteria: commensal microbes with potential effects on research.* Comp Med, 2014. **64**(2): p. 90-8.
118. Klaasen, H.L., et al., *Apathogenic, intestinal, segmented, filamentous bacteria stimulate the mucosal immune system of mice.* Infect Immun, 1993. **61**(1): p. 303-6.
119. Umesaki, Y., et al., *Differential roles of segmented filamentous bacteria and clostridia in development of the intestinal immune system.* Infect Immun, 1999. **67**(7): p. 3504-11.
120. De Benedetti, F., et al., *Impaired skeletal development in interleukin-6-transgenic mice: a model for the impact of chronic inflammation on the growing skeletal system.* Arthritis Rheum, 2006. **54**(11): p. 3551-63.
121. Pichler, J., et al., *Growth and bone health in pediatric intestinal failure patients receiving long-term parenteral nutrition.* Am J Clin Nutr, 2013. **97**(6): p. 1260-9.
122. Wit, J.M. and C. Camacho-Hubner, *Endocrine regulation of longitudinal bone growth.* Endocr Dev, 2011. **21**: p. 30-41.
123. Dinh, D.M., et al., *Longitudinal Analysis of the Intestinal Microbiota in Persistently Stunted Young Children in South India.* PLoS One, 2016. **11**(5): p. e0155405.
124. Blanton, L.V., et al., *Gut bacteria that prevent growth impairments transmitted by microbiota from malnourished children.* Science, 2016. **351**(6275).
125. Ducy, P. and G. Karsenty, *Two distinct osteoblast-specific cis-acting elements control expression of a mouse osteocalcin gene.* Mol Cell Biol, 1995. **15**(4): p. 1858-69.
126. Sjogren, K., et al., *Effects of liver-derived insulin-like growth factor I on bone metabolism in mice.* J Bone Miner Res, 2002. **17**(11): p. 1977-87.
127. Koenders, M.I., et al., *Blocking of interleukin-17 during reactivation of experimental arthritis prevents joint inflammation and bone erosion by decreasing RANKL and interleukin-1.* Am J Pathol, 2005. **167**(1): p. 141-9.
128. Swain, S.L., *T cell subsets and the recognition of MHC class.* Immunol Rev, 1983. **74**: p. 129-42.
129. Pettit, A.R., et al., *TRANCE/RANKL knockout mice are protected from bone erosion in a serum transfer model of arthritis.* Am J Pathol, 2001. **159**(5): p. 1689-99.
130. Kim, K.W., et al., *Interleukin-22 promotes osteoclastogenesis in rheumatoid arthritis through induction of RANKL in human synovial fibroblasts.* Arthritis Rheum, 2012. **64**(4): p. 1015-23.
131. Kuwahara, T., et al., *The lifestyle of the segmented filamentous bacterium: a non-culturable gut-associated immunostimulating microbe inferred by whole-genome sequencing.* DNA Res, 2011. **18**(4): p. 291-303.
132. Uematsu, S., et al., *Regulation of humoral and cellular gut immunity by lamina propria dendritic cells expressing Toll-like receptor 5.* Nat Immunol, 2008. **9**(7): p. 769-76.
133. Uematsu, S. and S. Akira, *Immune responses of TLR5(+) lamina propria dendritic cells in enterobacterial infection.* J Gastroenterol, 2009. **44**(8): p. 803-11.
134. Guss, J.D., et al., *Alterations to the Gut Microbiome Impair Bone Strength and Tissue Material Properties.* J Bone Miner Res, 2017. **32**(6): p. 1343-1353.
135. Kaplanski, G., *Interleukin-18: Biological properties and role in disease pathogenesis.* Immunol Rev, 2018. **281**(1): p. 138-153.

136. Nakanishi, K., et al., *Interleukin-18 is a unique cytokine that stimulates both Th1 and Th2 responses depending on its cytokine milieu.* Cytokine Growth Factor Rev, 2001. **12**(1): p. 53-72.
137. Udagawa, N., et al., *Interleukin-18 (interferon-gamma-inducing factor) is produced by osteoblasts and acts via granulocyte/macrophage colony-stimulating factor and not via interferon-gamma to inhibit osteoclast formation.* J Exp Med, 1997. **185**(6): p. 1005-12.
138. Kitaura, H., et al., *IL-18 induces apoptosis of adherent bone marrow cells in TNF-alpha mediated osteoclast formation in synergy with IL-12.* Immunol Lett, 2006. **107**(1): p. 22-31.
139. Morita, Y., et al., *IL-18 inhibits TNF-alpha-induced osteoclastogenesis possibly via a T cell-independent mechanism in synergy with IL-12 in vivo.* Calcif Tissue Int, 2010. **86**(3): p. 242-8.
140. Burgess, S.L., et al., *Bone marrow dendritic cells from mice with an altered microbiota provide interleukin 17A-dependent protection against Entamoeba histolytica colitis.* MBio, 2014. **5**(6): p. e01817.
141. Geem, D., et al., *Specific microbiota-induced intestinal Th17 differentiation requires MHC class II but not GALT and mesenteric lymph nodes.* J Immunol, 2014. **193**(1): p. 431-8.
142. Coombes, J.L. and F. Powrie, *Dendritic cells in intestinal immune regulation.* Nat Rev Immunol, 2008. **8**(6): p. 435-46.
143. Johansson-Lindbom, B. and W.W. Agace, *Generation of gut-homing T cells and their localization to the small intestinal mucosa.* Immunol Rev, 2007. **215**: p. 226-42.
144. Johansson-Lindbom, B., et al., *Functional specialization of gut CD103+ dendritic cells in the regulation of tissue-selective T cell homing.* J Exp Med, 2005. **202**(8): p. 1063-73.
145. Johansson-Lindbom, B., et al., *Selective generation of gut tropic T cells in gut-associated lymphoid tissue (GALT): requirement for GALT dendritic cells and adjuvant.* J Exp Med, 2003. **198**(6): p. 963-9.
146. Mora, J.R., et al., *Selective imprinting of gut-homing T cells by Peyer's patch dendritic cells.* Nature, 2003. **424**(6944): p. 88-93.
147. Ciucci, T., et al., *Bone marrow Th17 TNFalpha cells induce osteoclast differentiation, and link bone destruction to IBD.* Gut, 2015. **64**(7): p. 1072-81.
148. Halvorsen, E.H., et al., *Interleukin-15 induces interleukin-17 production by synovial T cell lines from patients with rheumatoid arthritis.* Scand J Immunol, 2011. **73**(3): p. 243-9.
149. Hueber, A.J., et al., *Mast cells express IL-17A in rheumatoid arthritis synovium.* J Immunol, 2010. **184**(7): p. 3336-40.
150. Kim, J.W., et al., *Effect of interferon-gamma on the fusion of mononuclear osteoclasts into bone-resorbing osteoclasts.* BMB Rep, 2012. **45**(5): p. 281-6.
151. Wei, S., et al., *Interleukin-4 reversibly inhibits osteoclastogenesis via inhibition of NF-kappa B and mitogen-activated protein kinase signaling.* J Biol Chem, 2002. **277**(8): p. 6622-30.
152. Amarasekara, D.S., et al., *Regulation of Osteoclast Differentiation by Cytokine Networks.* Immune Netw, 2018. **18**(1): p. e8.
153. te Velde, A.A., et al., *Interleukin-4 (IL-4) inhibits secretion of IL-1 beta, tumor necrosis factor alpha, and IL-6 by human monocytes.* Blood, 1990. **76**(7): p. 1392-7.

154. Pines, M. and S. Hurwitz, *The role of the growth plate in longitudinal bone growth.* Poult Sci, 1991. **70**(8): p. 1806-14.

APPENDIX

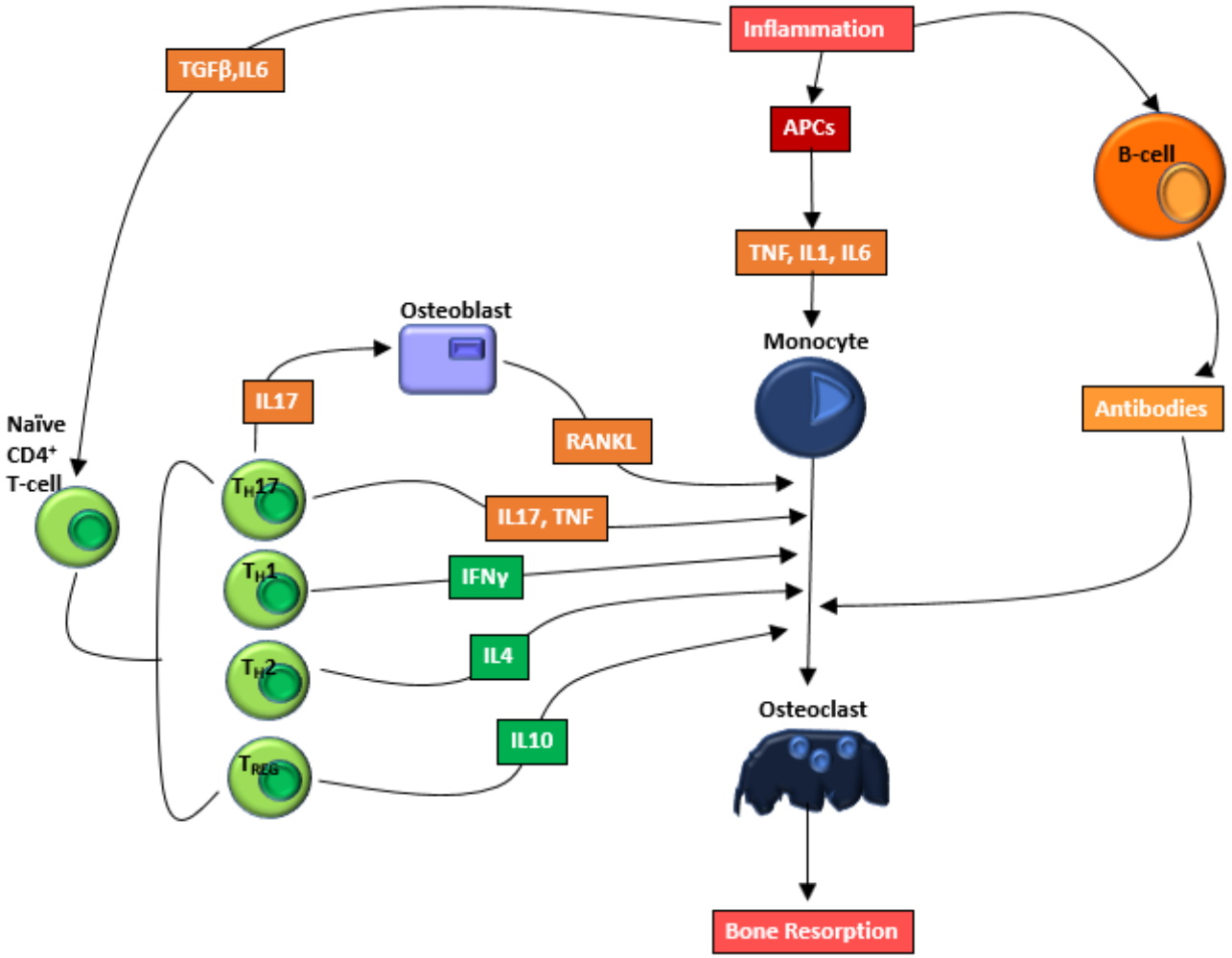
Inflammation
TGFβ,IL6
APCs
B-cell
TNF, IL1, IL6
Osteoblast
Monocyte
IL17
RANKL
Antibodies
Naïve
CD4+
T-cell
TH17
IL17, TNF
TH1
IFNγ
IL4
TH2
IL10
TREG
Osteoclast
Bone Resorption

Appendix Figure A.1: Interactions of immune cells and bone cells. In state of inflammation immune cell released cytokines mediate bone resorption through interactions with osteoclasts and osteoblasts. B-cells and T-cells are activated by antigen presenting cells (APCs) like dendritic cells. Osteoblasts produce RANKL, T-cells produce pro-osteoclastogenic cytokines like, IL17 and TNF, and anti-osteoclastogenic cytokines like, IFNγ, IL4, and IL10.

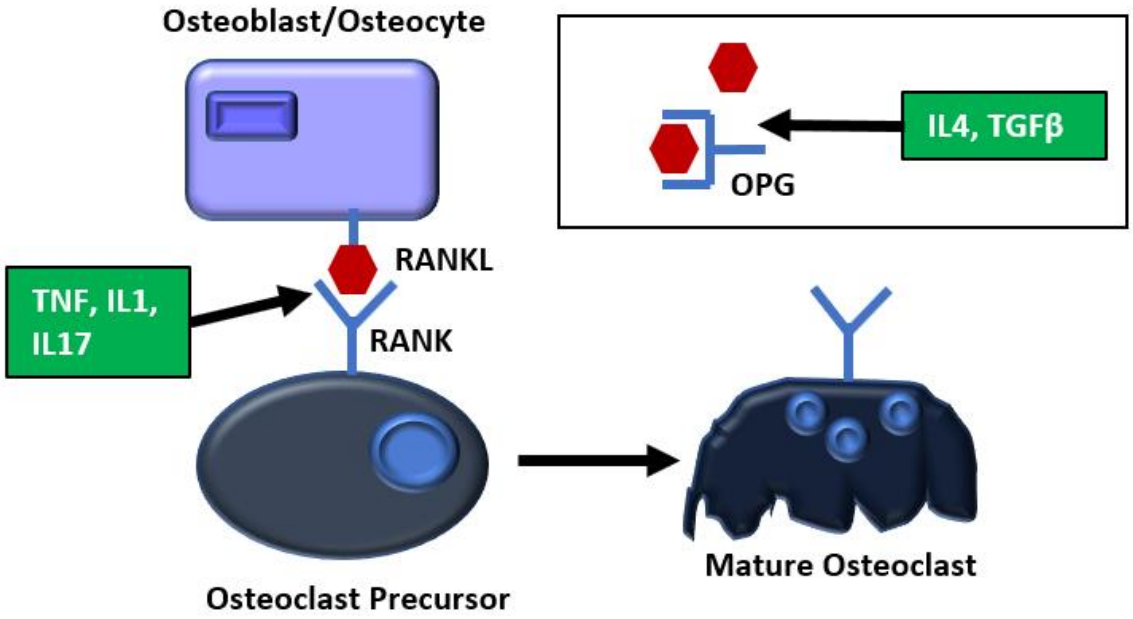

Appendix Figure A.2: RANKL-Mediated Osteoclastogenesis. Osteoclast maturation and function is driven by RANKL, either free or expressed by osteoblasts, binding to and signaling through RANK expressed on osteoclast precursors and mature osteoclasts. OPG is the decoy receptor for RANKL and inhibits osteoclastogenesis when it sequesters RANKL. IL1, IL17, and TNF enhance RANKL-mediated osteoclastogenesis. IL4 and TGFβ inhibit osteoclastogenesis through enhanced OPG regulation.

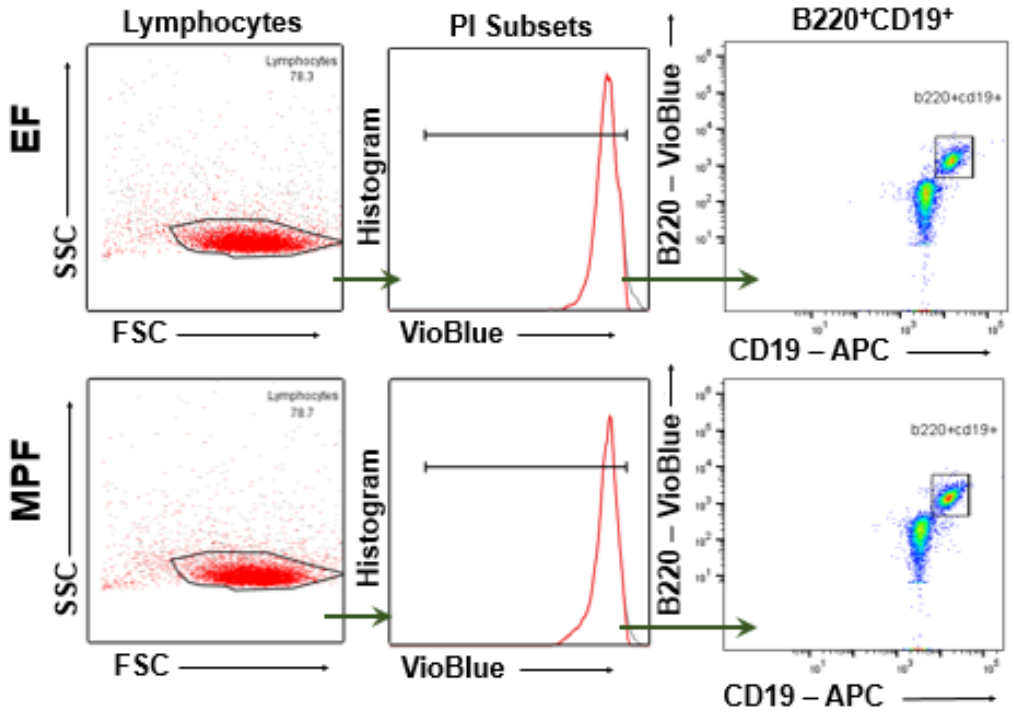

Appendix Figure A.3: Gating Strategy for B-cells. Nine-week-old female MPF and EF mice were euthanized; specimens harvested for analysis. Representative gating of flow cytometric analysis for ($B220^{+}CD19^{+}$) B-cells in mesenteric lymph nodes (mLNs); n=5/gp.

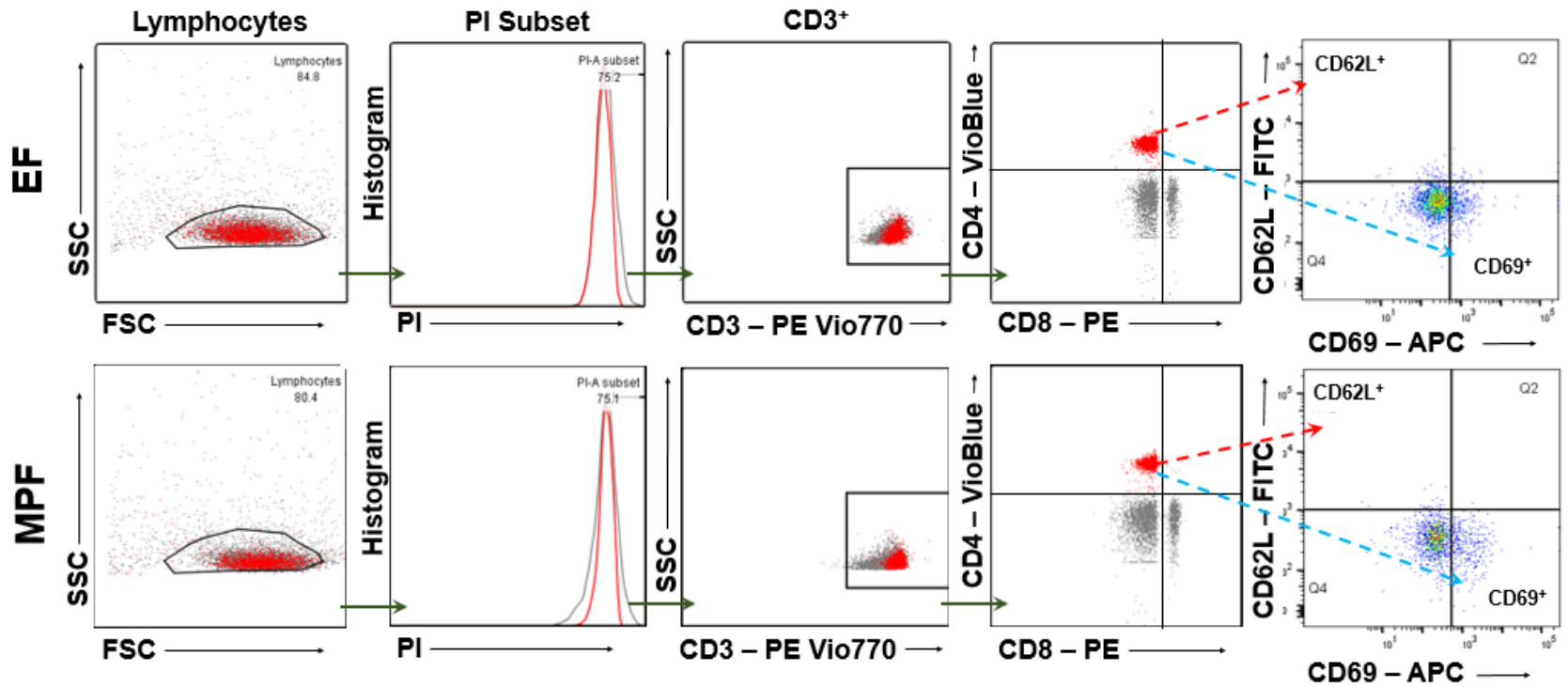

Appendix Figure A.4: Gating Strategy for Activated / Naïve Helper T-cells. Nine-week-old female MPF and EF mice were euthanized; specimens harvested for analysis. Representative gating of flow cytometric analysis for naïve ($CD3^+CD8^-CD4^+CD62L^+CD69^-$)(red arrows) and activated ($CD3^+CD8^-CD4^+CD62L^-CD69^+$)(blue arrows) T-cells in mesenteric lymph nodes (mLNs); n=5/gp.

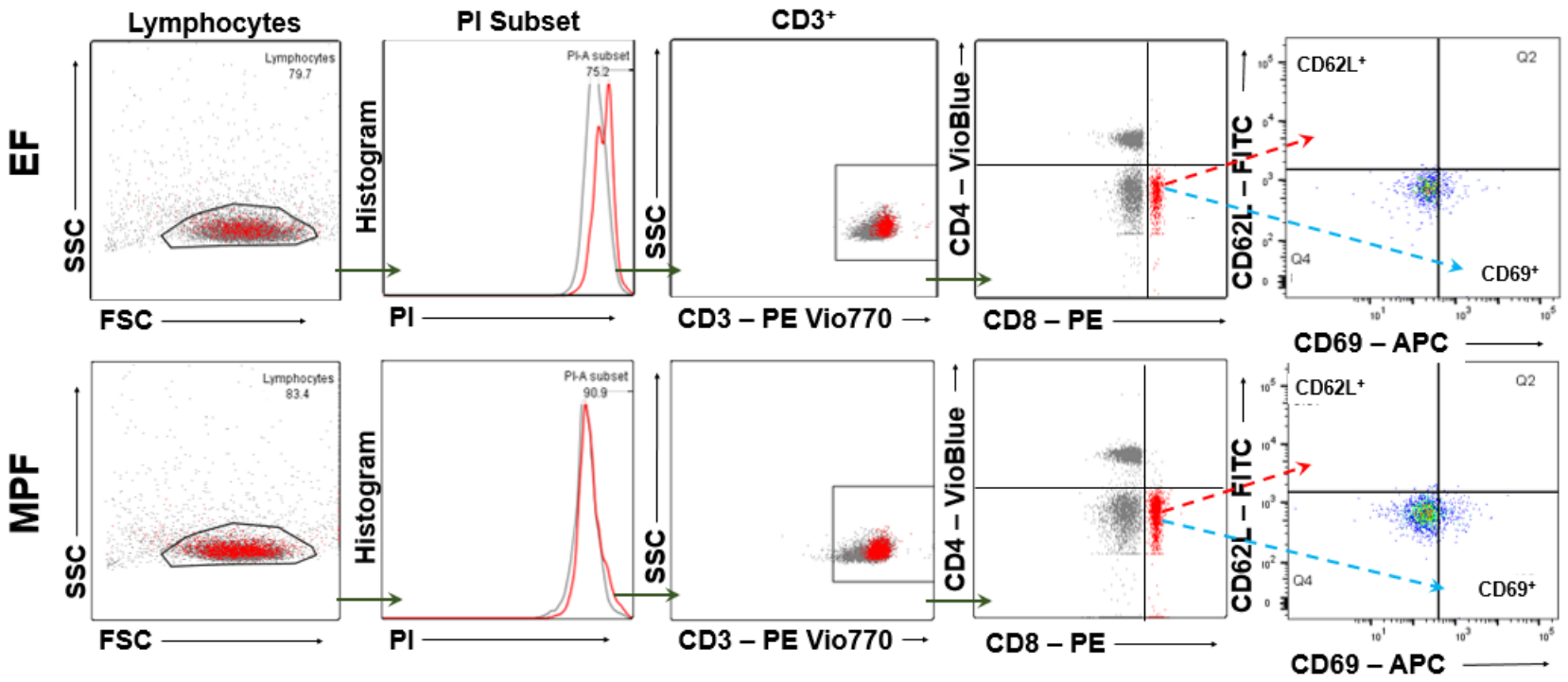

Appendix Figure A.5: Gating Strategy for Activated / Naïve Cytotoxic T-cells. Nine-week-old female MPF and EF mice were euthanized; specimens harvested for analysis. Representative gating of flow cytometric analysis for naïve ($CD3^+CD8^+CD4^-CD62L^+CD69^-$)(red arrows) and activated ($CD3^+CD8^+CD4^-CD62L^-CD69^+$)(blue arrows) T-cells in mesenteric lymph nodes (mLNs); n=5/gp.

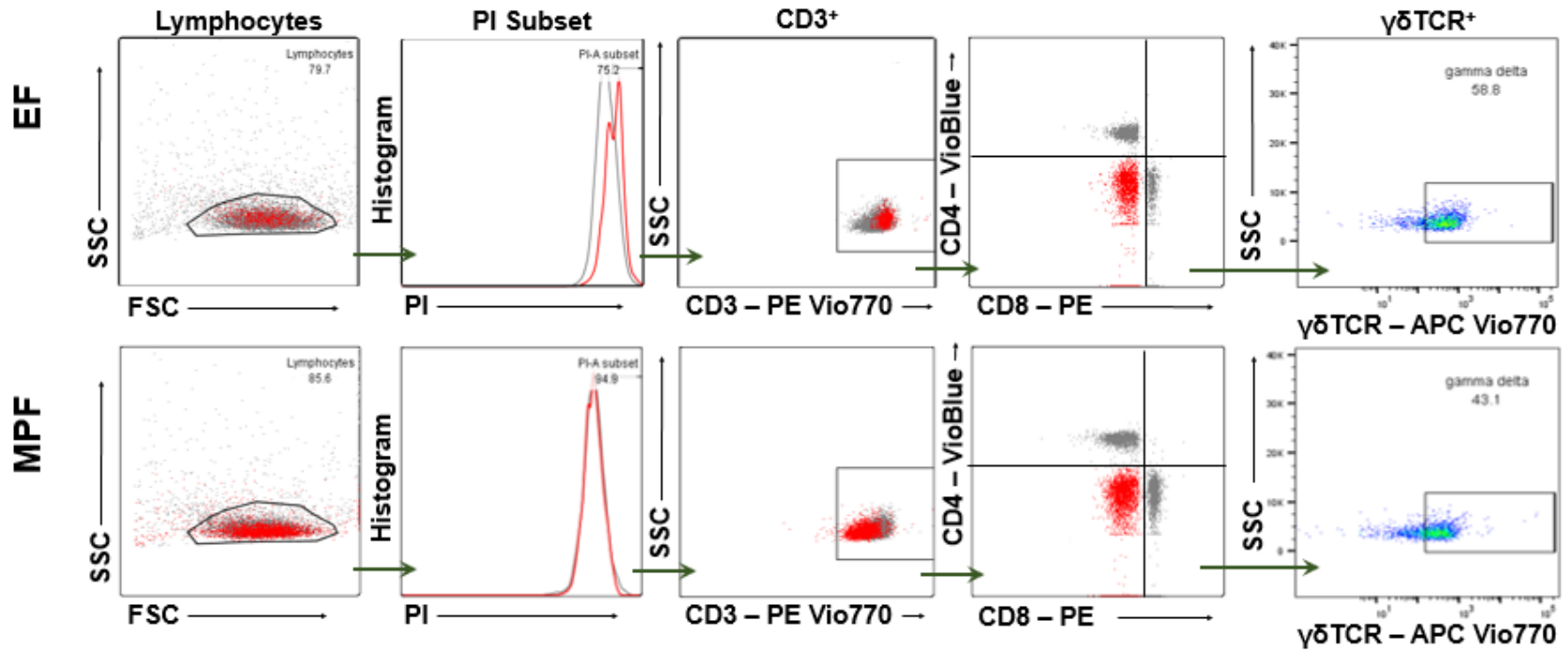

Appendix Figure A.6: Gating Strategy for γδ T-cells. Nine-week-old female MPF and EF mice were euthanized; specimens harvested for analysis. Representative gating of flow cytometric analysis for ($CD3^+CD8^-CD4^-\gamma\delta TCR^+$) T-cells in mesenteric lymph nodes (mLNs); n=5/gp.

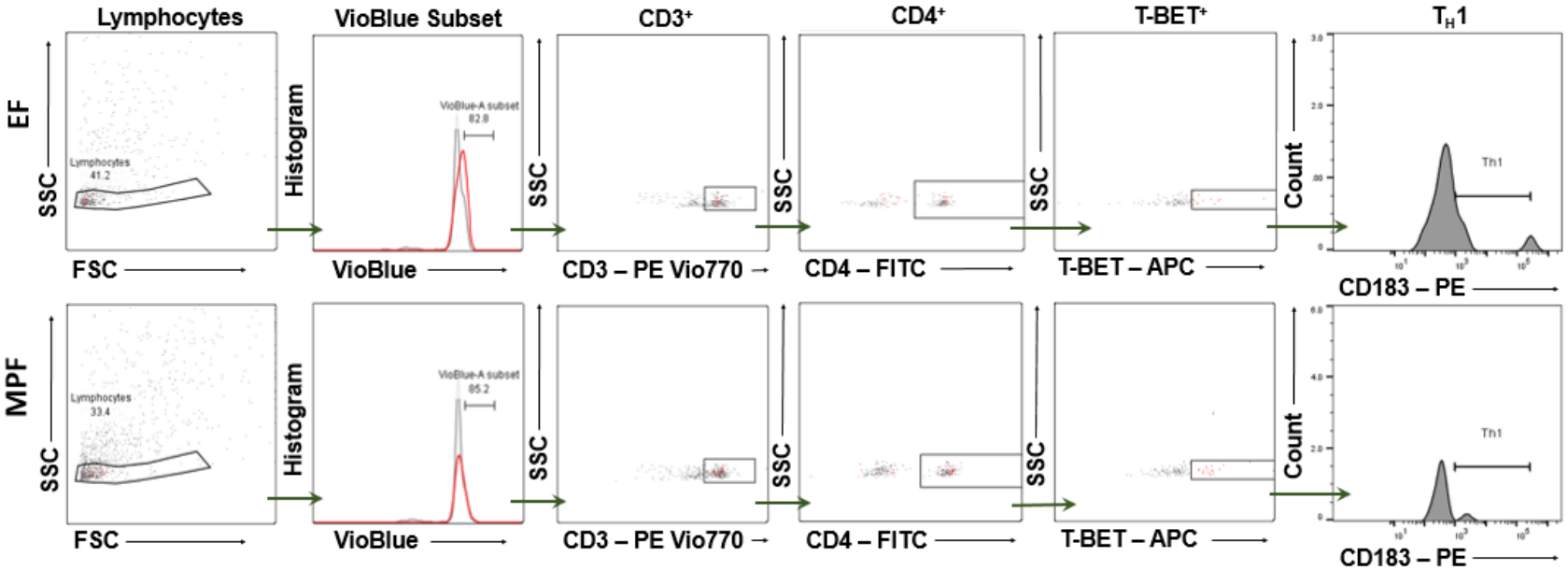

Appendix Figure A.7: Gating Strategy for T_H1 cells. Nine-week-old female MPF and EF mice were euthanized; specimens harvested for analysis. Representative gating of flow cytometric analysis for ($CD3^+CD4^+CD183^+T\text{-}BET^+$) T_H1 cells in mesenteric lymph nodes (mLNs); n=5/gp.

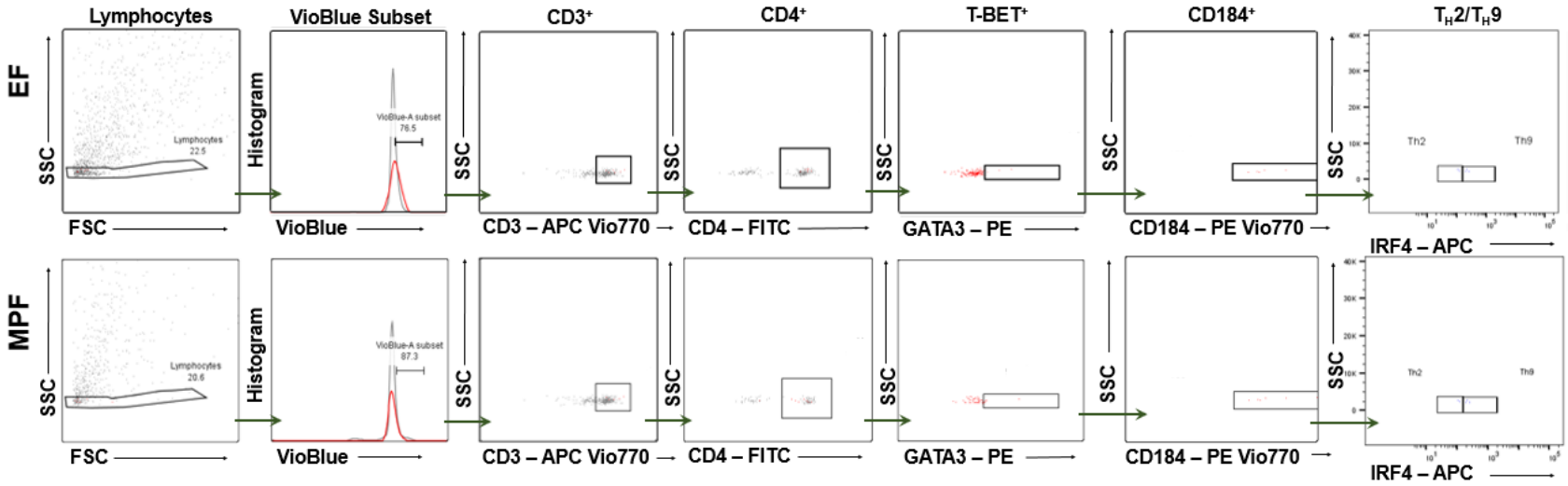

Appendix Figure A.8: Gating Strategy for T_H2 and T_H9 cells. Nine-week-old female MPF and EF mice were euthanized; specimens harvested for analysis. Representative gating of flow cytometric analysis for ($CD3^+CD4^+CD184^+GATA3^+IRF4^-$) T_H2 cells and($CD3^+CD4^+CD184^+GATA3^+IRF4^+$) T_H9 cells in mesenteric lymph nodes (mLNs); n=5/gp.

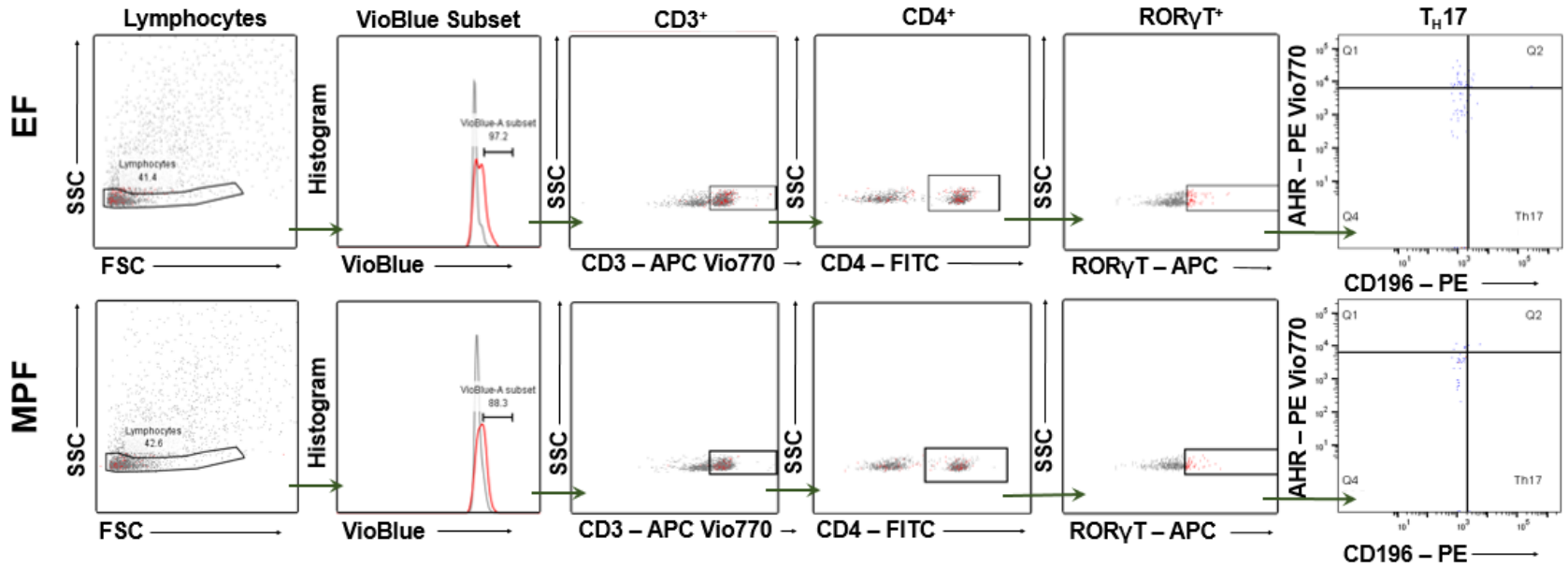

Appendix Figure A.9: Gating Strategy for T_H17 cells. Nine-week-old female MPF and EF mice were euthanized; specimens harvested for analysis. Representative gating of flow cytometric analysis for ($CD3^+CD4^+CD196^+$ $ROR\gamma T^+AHR^-$) T_H17 cells in mesenteric lymph nodes (mLNs); n=5/gp.

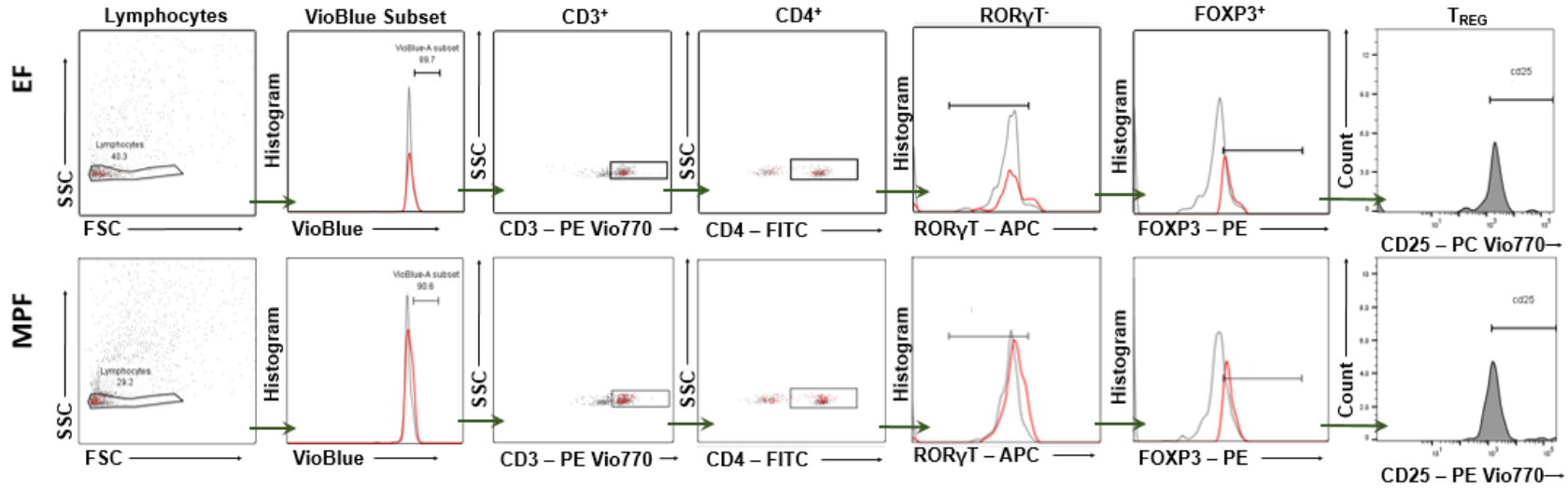

Appendix Figure A.10: Gating Strategy for T_{REG} cells. Nine-week-old female MPF and EF mice were euthanized; specimens harvested for analysis. Representative gating of flow cytometric analysis for ($CD3^+CD4^+CD25^+FOXP3^+ROR\gamma T^-$) T_{REG} cells in mesenteric lymph nodes (mLNs); n=5/gp.

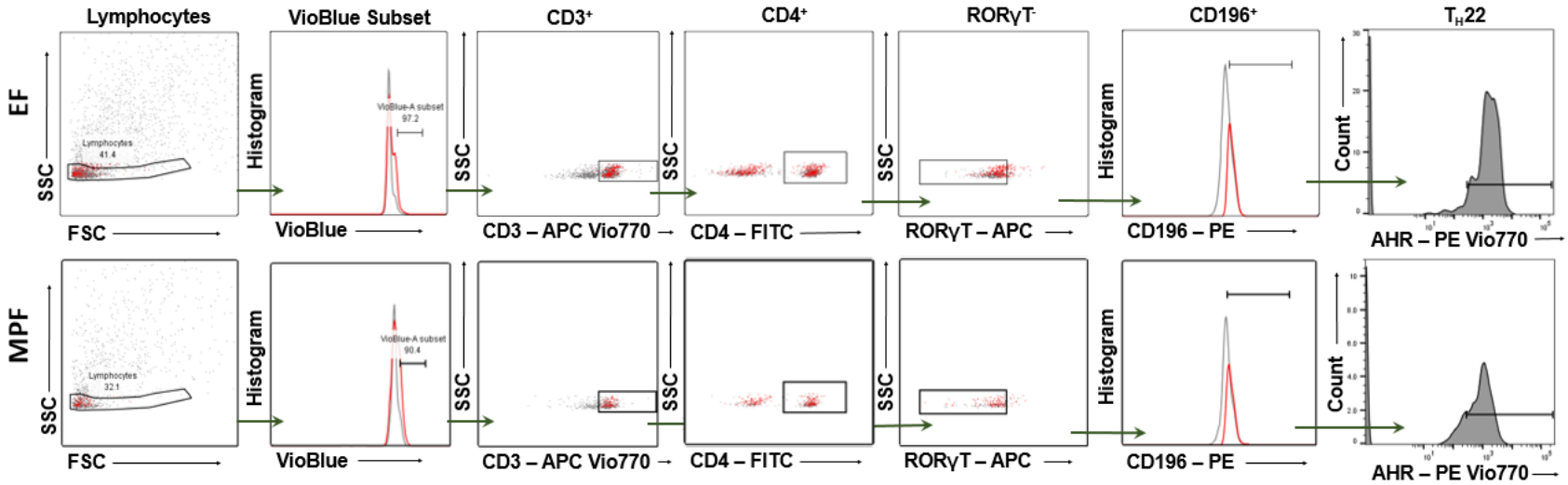

Appendix Figure A.11: Gating Strategy for T_H22 cells. Nine-week-old female MPF and EF mice were euthanized; specimens harvested for analysis. Representative gating of flow cytometric analysis for ($CD3^+CD4^+ROR\gamma T^-CD196^+AHR^+$) T_H22 cells in mesenteric lymph nodes (mLNs); n=5/gp.

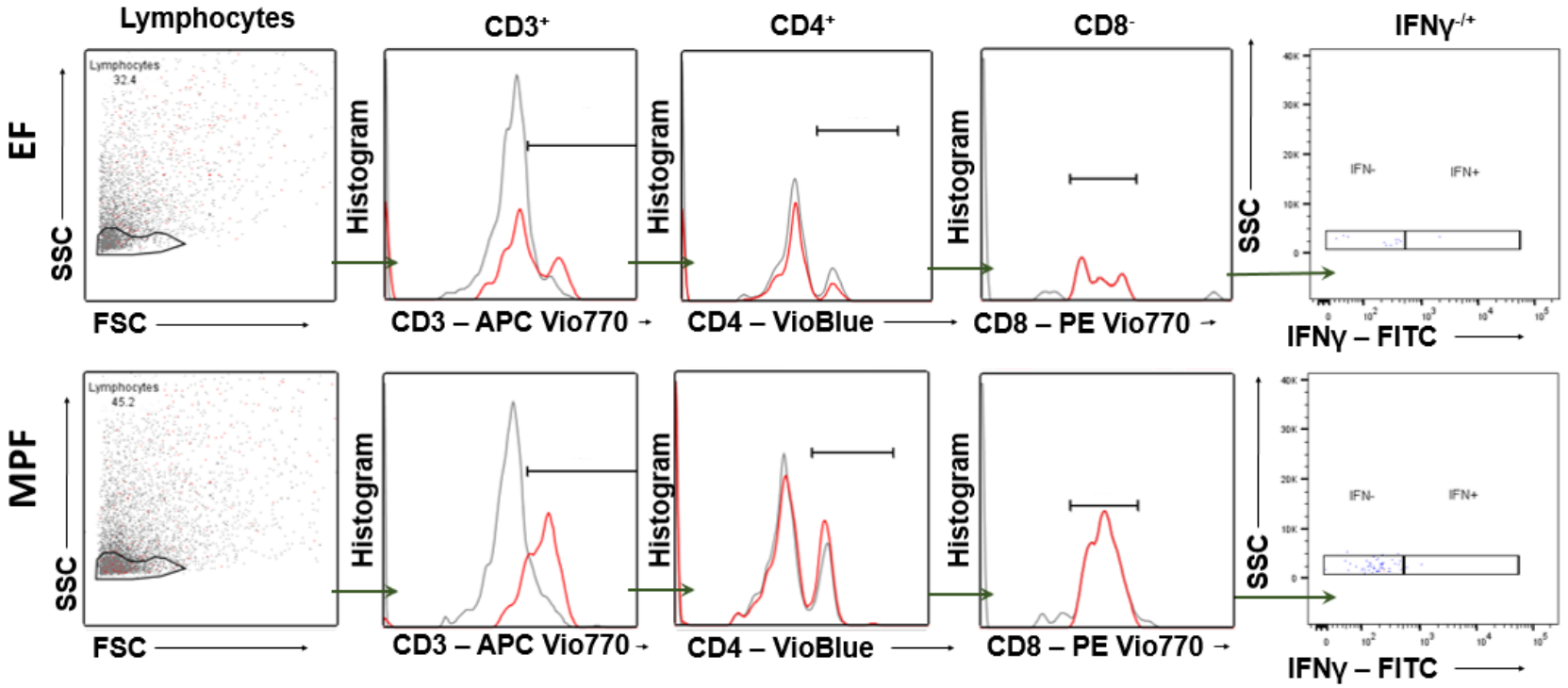

Appendix Figure A.12: Gating Strategy for $CD3^+CD4^+IFN\gamma^+$ cells. Nine-week-old female MPF and EF mice were euthanized; specimens harvested for analysis. Representative gating of flow cytometric analysis for intracellular cytokine analysis of ($CD3^+CD4^+CD8^-IFN\gamma^+$) T_H1 cells in femoral bone marrow; n=5/gp.

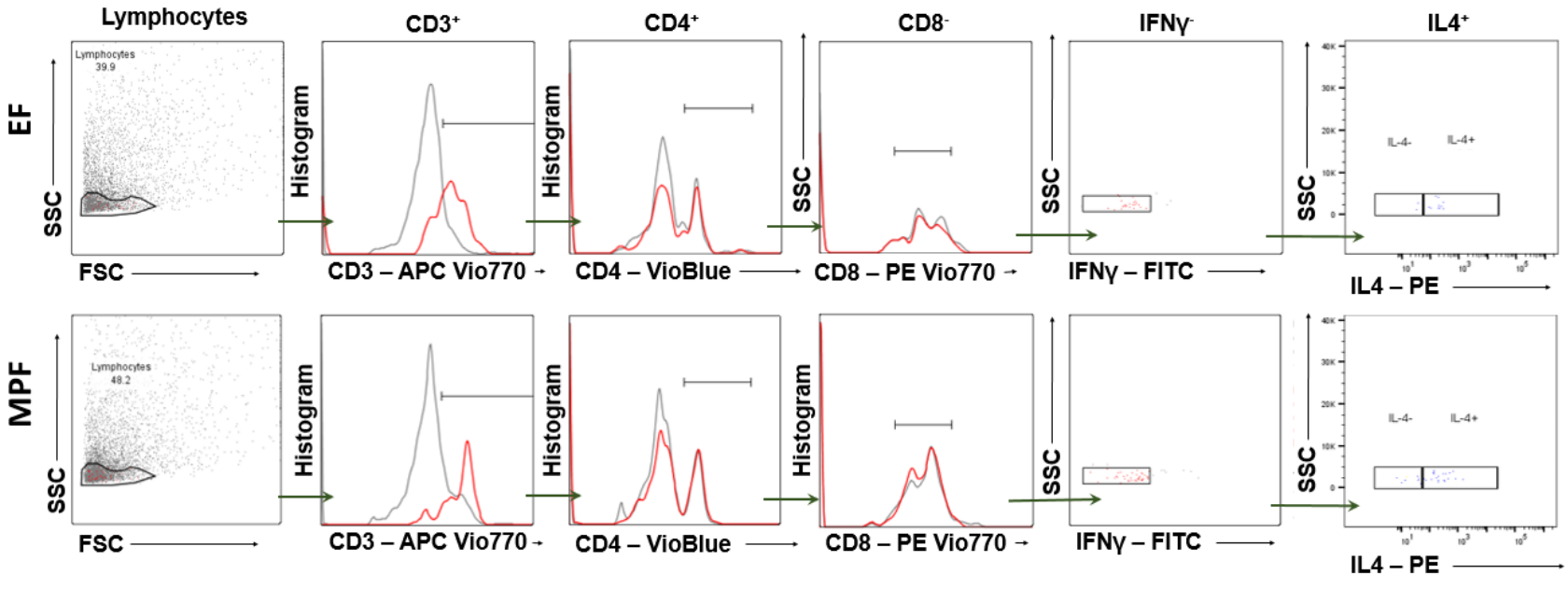

Appendix Figure A.13: Gating Strategy for $CD3^+CD4^+IL4^+$ cells. Nine-week-old female MPF and EF mice were euthanized; specimens harvested for analysis. Representative gating of flow cytometric analysis for intracellular cytokine analysis of ($CD3^+CD4^+CD8^-IFN\gamma^-IL4^+$) T_H2 cells in femoral bone marrow; n=5/gp.

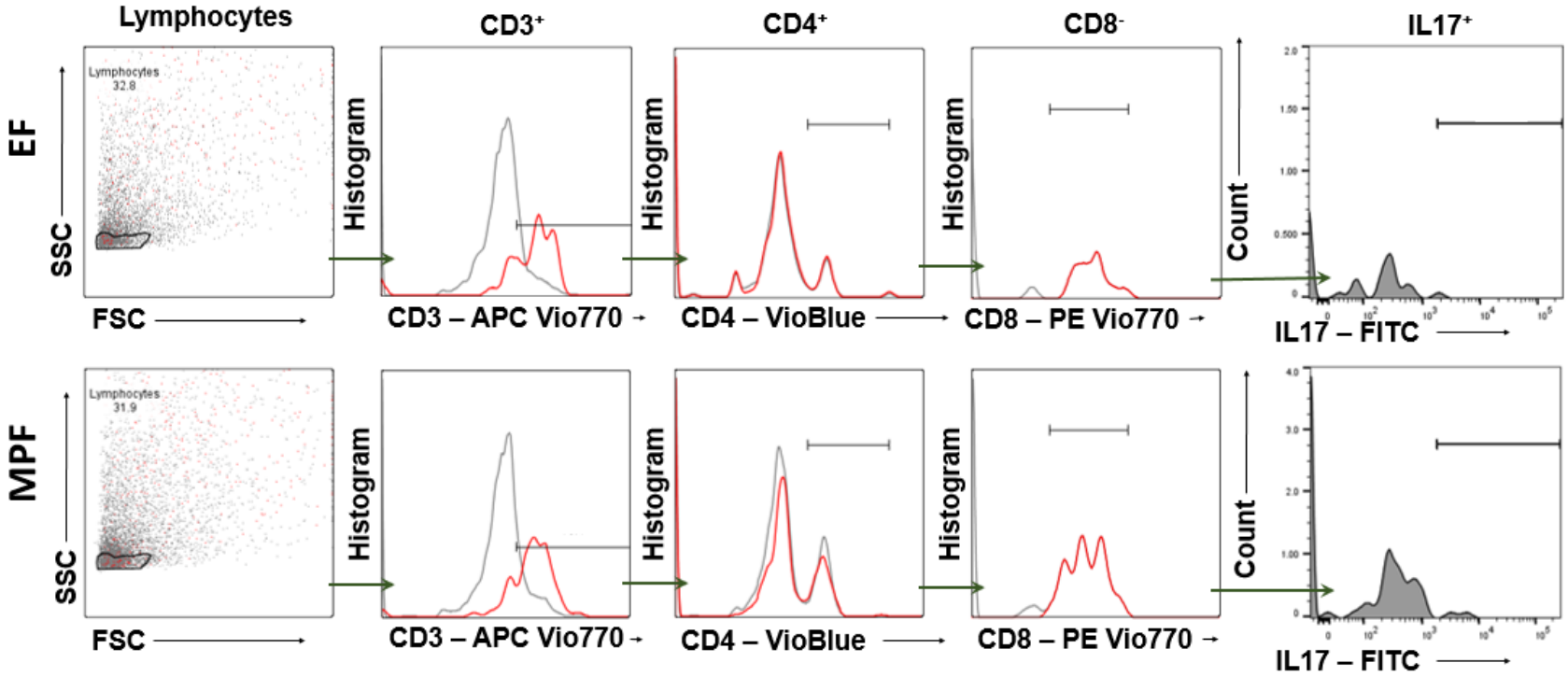

Appendix Figure A.14: Gating Strategy for $CD3^+CD4^+IL17^+$ cells. Nine-week-old female MPF and EF mice were euthanized; specimens harvested for analysis. Representative gating of flow cytometric analysis for intracellular cytokine analysis of ($CD3^+CD4^+CD8^-IL17^+$) T_H17 cells in femoral bone marrow; n=5/gp.

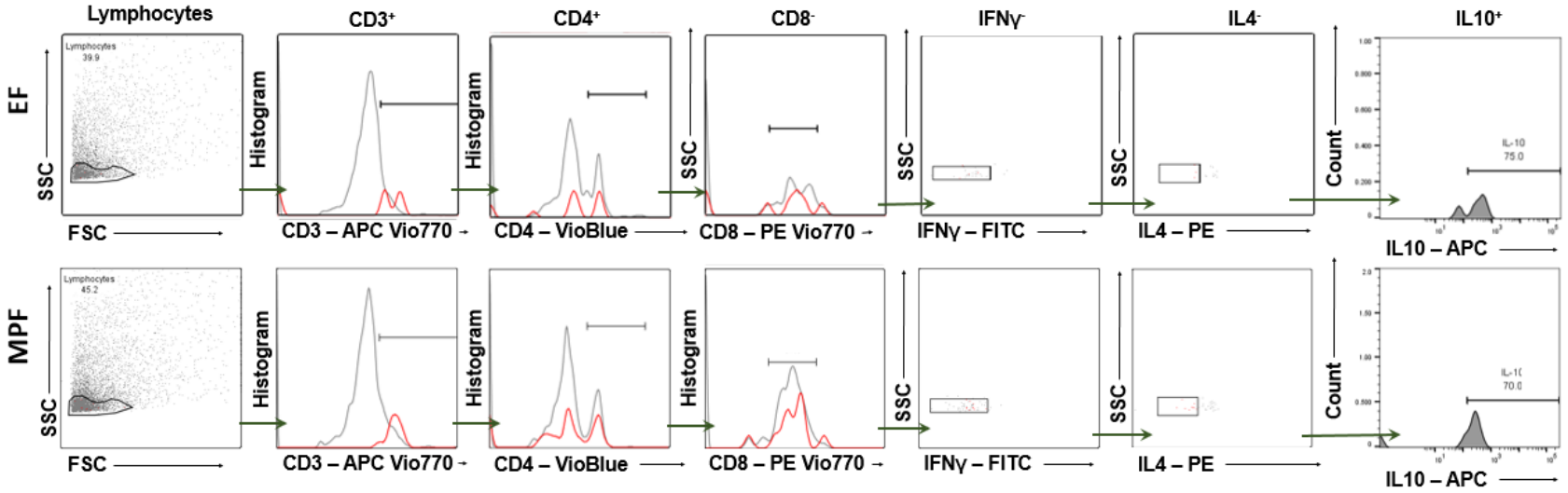

Appendix Figure A.15: Gating Strategy for $CD3^+CD4^+IL10^+$ cells. Nine-week-old female MPF and EF mice were euthanized; specimens harvested for analysis. Representative gating of flow cytometric analysis for intracellular cytokine analysis of ($CD3^+CD4^+CD8^-IFN\gamma^-IL4^-IL10^+$) T_{REG} cells in femoral bone marrow; n=5/gp.

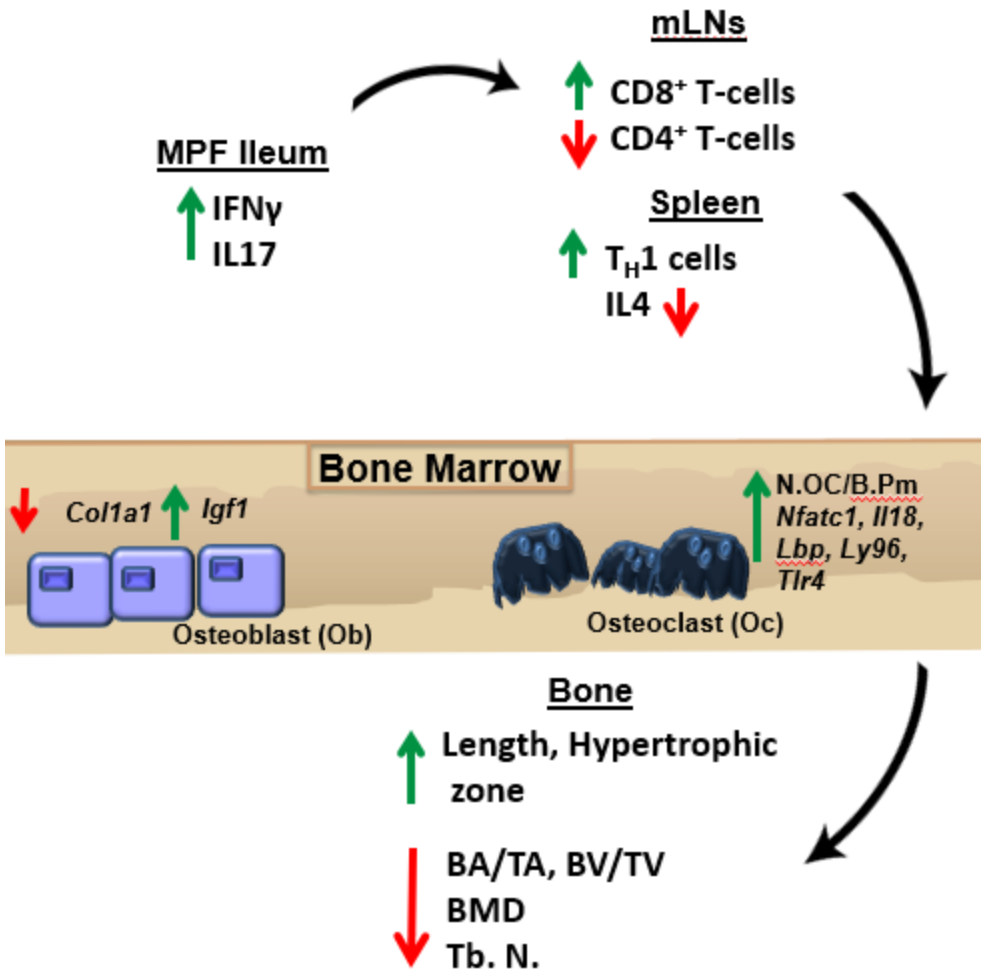

Appendix Figure A.16: Schematic summarizing study findings MPF vs. EF.